SAPIENZA
UNIVERSITÀ DI ROMA

FACOLTÀ DI INGEGNERIA DELL'INFORMAZIONE, INFORMATICA E STATISTICA

Corso di Laurea Magistrale in Ingegneria Elettronica

Ultra-broadband mobile networks: evaluation of massive MIMO and multi-carrier aggregation performances in LTE-Advanced

Relatrice
Prof.ssa Maria-Gabriella Di Benedetto

Correlatori
Ing. Andrea Castellani
Ing. Pamela Sciarratta Armani Campanella
TIM

Candidato
Marco Neri

Anno Accademico 2016 - 2017

A Filippo, la mia ispirazione

Acknowledgements

First and foremost, I want to thank my advisor, Mrs. Maria-Gabriella Di Benedetto for her encouragement, backing and guidance in carrying out this thesis. She gave me the chance to develop it at TIM allowing me to delve into topics that are at the forefront of technology and to get into the business reality, still too far from the academic world.

This work would have never been possible without the help of my co-advisors, Andrea and Pamela, whose guidelines and suggestions have been fundamental during the six months spent together. Thanks also to Camillo and Pietro that have been willing to help me with the troubles I encountered, always with a smile on their faces. I express my gratitude to Tommaso and the whole *ns-3* community for having solved some of my problems with the simulator. Special thanks to Renzo, Nicola and the to the lab guys that made me feel a part of their group from the very beginning.

Last six months were definitely intense and my family had to stand my anxieties, indecisions and some moments of impatience. Despite this, they never made me feel guilty and they have always been by my side, indulging my needs and my moods, like they have always done for the last 24 years. To my Mom and Dad, to Fede, to Grandma Mirella and to all my relatives, my unconditioned fondness and my eternal gratitude. My thanks go, moreover, to my inspiration Filippo, to whom I dedicate this thesis.

Thanks to my "αλήθειες φίλοι", a branch of my family, whose affinity and help have never been called into question. Thanks also to all those friends, that make me feel at home, wherever I am.

Finally, a special thanks to my travel companions, Claudio and Marco. We spent six incredible months together, working shoulder to shoulder. It has been an amazing adventure thanks to their company. I will miss working with those nuts!

Grazie,

Ringraziamenti

Prima di tutto vorrei ringraziare la mia Relatrice, la professoressa Maria-Gabriella Di Benedetto, per l'incoraggiamento, il supporto e la guida nello svolgimento di questa tesi e per avermi dato la possibilità di svilupparla all'interno della TIM, permettendomi di approfondire argomenti all'avanguardia e conoscere una realtà, quella aziendale, ancora troppo lontana dal mondo universitario.

Tale lavoro non sarebbe stato possibile senza l'aiuto dei miei Correlatori, Andrea e Pamela, le cui linee guida e suggerimenti sono stati fondamentali nei sei mesi passati insieme. Prezioso è stato anche l'aiuto di Camillo e Pietro, che sono stati sempre disponibili nel darmi una mano a risolvere i problemi incontrati, sempre con il sorriso. Grazie anche a Tommaso e a tutta la comunità *ns-3* per l'aiuto con il simulatore. Un ringraziamento particolare va poi a Renzo, Nicola e ai ragazzi del laboratorio, che mi hanno fatto sentire parte di un gruppo sin dal primo giorno.

Gli ultimi sei mesi sono stati decisamente intensi e la mia famiglia ha dovuto sopportare le mie ansie, le indecisioni e qualche momento di impazienza. Nonostante ciò, non me l'hanno mai fatto pesare e, anzi, sono stati sempre al mio fianco, assecondando le mie necessità e i miei stati d'animo, come sempre da 24 anni a questa parte. A Mamma e Papà, a Fede, a Nonna Mirella e a tutta la banda vanno il mio incondizionato affetto e la mia eterna gratitudine. La mia riconoscenza va, inoltre, alla mia fonte di ispirazione, Filippo, a cui è dedicata questa tesi.

Grazie ai miei "αλήθειες φίλοι", ormai un ramo della famiglia, la cui vicinanza e aiuto non sono mai in discussione. Grazie anche a tutti quegli amici che, indipendentemente da dove mi trovi, mi fanno sempre sentire come se fossi a casa.

Infine, un ringraziamento speciale va ai compagni di viaggio, Claudio e Marco, con cui abbiamo passato sei mesi incredibili, spalla a spalla. È stata una fantastica avventura, soprattutto grazie alla loro compagnia. Mi mancherà lavorare con quei due pazzi!

Grazie,

Abstract

LTE-Advanced networks are spreading widely across the world and they are continuing to evolve as new device features are being released to move towards the peak data rates introduced by 3GPP Release 11, 12 and 13. Mobile network Operators are looking for technologies that guarantee better performances but they have to deal with limitations due to commercial devices' RF components that prevent the Operator from exploiting such technologies at their best.

Then, they are \

The aim of this thesis was to study the LTE-Advanced system in order to figure out which would be the best deployment strategy. For this scope, we used a network simulator first born for LTE and we adapted it to last LTE-A features. We analyzed a dense urban scenario and deduced the system performance in terms of throughput and we evaluated the performances of MIMO 4x4 and Carrier Aggregation. A set of conclusions is derived from the comparison between the system simulations and real measures made on commercial devices.

Abstract [IT]

I sistemi LTE-Advanced sono in via di diffusione in tutto il mondo e continuano ad evolversi con l'inserimento di nuove funzionalità che permettano il raggiungimento dei target fissati dalle Release 11, 12 e 13 del 3GPP. Gli Operatori mobili sono alla ricerca di tecnologie che garantiscano migliori performance ma si stanno scontrando con delle limitazioni dovute ai componenti RF dei device commerciali. Tali limitazioni impediscono di coniugare le tecnologie che puntano all'aumento dello spettro e quelle che garantiscono una migliore efficienza spettrale.

Fin quando tali limitazioni non saranno superate, gli Operatori dovranno agire secondo un compromesso e stanno cercando di capire in quale direzione muoversi ed investire.

Lo scopo di questa tesi è quello di studiare il sistema LTE-A nella sua interezza per capire quale sia la miglior scelta di deployment dal punto di vista dell'Operatore. Per questo fine, abbiamo utilizzato un simulatore di rete, nato per il sistema LTE a lo abbiamo adattato includendo le ultime funzionalità rilasciate. Abbiamo analizzato uno scenario urbano densamente popolato ed estratto dalle simulazioni la prestazione del sistema dal punto di vista del throughput smaltito e valutato le performance del MIMO 4x4 e della Carrier Aggregation.

Infine, abbiamo tratto delle conclusioni e dato dei suggerimenti, sfruttando anche il paragone tra i risultati delle simulazioni e delle misure reali fatte su nuovi device commerciali.

Table of contents

List of the Abbreviations

1G	First Generation
2G	Second Generation
3G	Third Generation
3GPP	Third Generation Partnership Project
4G	Fourth Generation
ABS	Almost Blank Subframes
AM	Acknowledged Mode
AMC	Adaptive Modulation and Coding
API	Application Programming Interface
BER	Bit Error Rate
BLER	Block Error Rate
BS	Base Station
CA	Carrier Aggregation
CB	Coordinated Beamforming
CCS	Cross-Carrier Scheduling
CDF	Cumulative Density Function
CDMA	Code Division Multiple Access
CL	Closed Loop
CM	Connection Management
CoMP	Coordinated Multi Point
CP	Cyclic Prefix
CQI	Channel Quality Indicator
CS	Coordinated Scheduling
DL	DownLink
DL-SCH	DownLink Shared Channel
DPS	Dynamic Point Selection
DRB	Data Radio Bearer
EARFCN	EUTRA Absolute Radio-Frequency Channel Number
eICIC	Enhanced Inter-Cell Interference Coordination
eNB	eNodeB
EPC	Evolved Packet Core
EPS	Evolved Packet System
ESM	EPS Session Management
E-UTRA	Evolved Universal Terrestrial Access
E-UTRAN	Evolved Universal Terrestrial Access Network
FDD	Frequency Division Duplexing
GSM	Global System for Mobile Communications
HARQ	Hybrid Automatic ReQuest
HetNet	Heterogeneous Networks

HSPA	High Speed Packet Access
ICMP	Internet Control Message Protocol
IP	Internet Protocol
ITU	International Telecommunication Union
JP	Joint Processing
LAA	Licensed Assisted Access
LoS	Line of Sight
LSM	Link-to-System Mapping
LTE	Long Term Evolution
LTE-A	LTE-Advanced
MAC	Medium Access Control
MCS	Modulation and Coding Scheme
MIB	Master Information Block
MIESM	Mutual Information Effective SINR Mapping
MIMO	Multiple Input Multiple Output
MM	Mobility Management
MU-MIMO	Multi-User MIMO
NAS	Non-Access Stratum
NLoS	Non-Line of Sight
NPRB	Number of PRB
OFDM	Orthogonal Frequency Division Multiplexing
OFDMA	Orthogonal Frequency Division Multiple Access
OL	Open Loop
PAPR	Peak-to-Average Power Ratio
PCC	Principal Component Carrier
PCRF	Policy and Charging Rules Function
PDCP	Packet Data Convergence Protocol
PDF	Probability Density Function
PDN	Packet Data Network
PDSCH	Physical Downlink Shared Channel
PDU	Protocol Data Unit
PF	Proportional Fair
PGW	Packet GateWay
PHY	Physical Layer
PRACH	Physical Random-Access Channel
PRB	Physical Resource Block
PS	Packet Switch
PSC	Primary Serving Cell
PUCCH	Physical Uplink Control Channel
PUSCH	Physical Uplink Shared Channel

QAM	Quadrature Amplitude Modulation
QoS	Quality of Service
QPSK	Quadrature Phase-Shift Keying
QXDM	Qualcomm eXtensible Diagnostic Monitor
RAT	Radio Access Technology
RBG	Resource Block Group
RBS	Radio Base Station
RE	Resource Element
RLC	Radio Link Control
RNC	Radio Network Controller
RNTI	Radio Network Temporary Identifier
ROHC	Robust Header Compression
RRC	Radio Resource Control
RSRP	Reference Signal Received Power
S&W	Stop & Wait
SAE	System Architecture Evolution
SCC	Secondary Component Carrier
SC-FDMA	Single Carrier Frequency Division Multiple Access
SCS	called Single Carrier-Scheduling
SGW	Serving Gateway
SIB	System Information Block
SINR	Signal-to-Noise Ratio
SISO	Single Input Single Output
SON	Self-Organizing Networks
SRB	Signaling Radio Bearer
SRS	Sounding Reference Signal
TBS	Transport Block Size
TCP	Transmission Control Protocol
TDD	Time Division Duplexing
TM	Transmission Mode
TP	Throughput
TR	Technical Report
TS	Technical Specification
TSG RAN	Technical Specification Group Radio Access Network
TTI	Transmission Time Interval
UDP	User Datagram Protocol
UE	User Equipment
UL	UpLink
UM	Unacknowledged Mode
UMTS	Universal Mobile Telecommunications System

Introduction

Context and objectives

Nowadays we live in a world where mobile communications are used by most of the world population since they have become more affordable. In 2016, there were about 7.5 billion subscribers worldwide and they are supposed to reach 8.9 billion in 2022, according to some forecasts (Ericsson Mobility Report, November 2016). The spread of mobile technologies all around the world led to the birth of global standard-developing organizations such as the Third Generation Partnership Project (3GPP).

Mobile communication technologies are divided into generations:

- 1G was the analog mobile radio system, first introduced in 1980s for wireless telephone technology;
- 2G is the first digital mobile system, launched in 1991, based on GSM and CDMA. This technology difficultly handles complex data such as videos;
- 3G was introduced in 2000s. It's based on UMTS and has higher data transmission speed. The big challenge was to build the infrastructure for 3G and fees were very expensive at the beginning;
- 4G refers to the Long Term Evolution (LTE), started in late 2000s. It provides very high transmission speed but requires a more complex hardware.

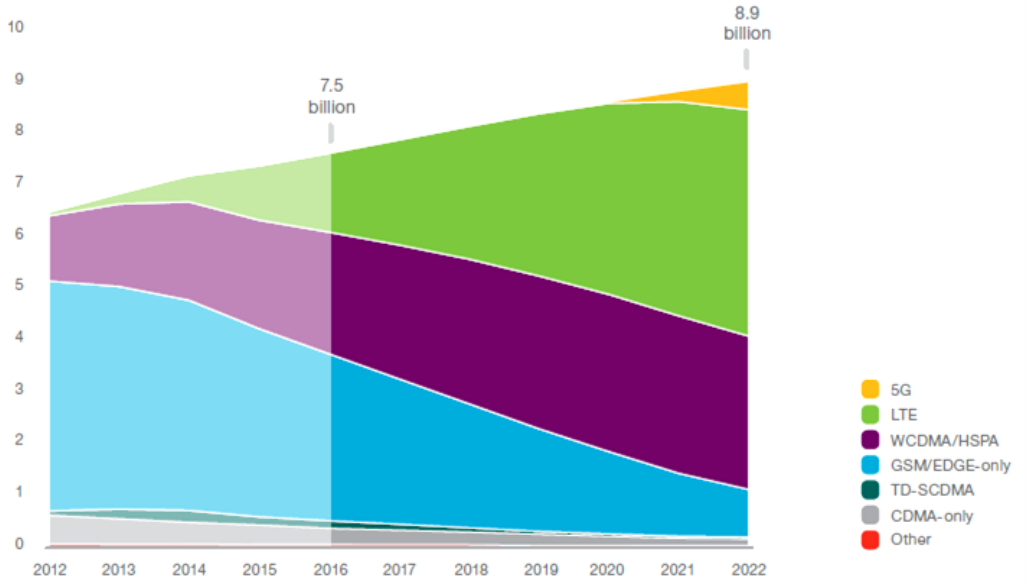

Figure 1.1 Mobile subscribers per technology (Ericsson Mobility Report, November 2016)

From the figure above we can see how LTE is becoming the market dominant technology and it will be so for at least 10 years, even after the upcoming of 5G. By 2022, LTE subscribers are predicted to be 4.6 billion, more than the half of the whole mobile subscriptions. This demand pushes LTE Data Rates to new limits. However, LTE as it was first intended in Release 8 could guarantee at maximum a downlink data rate of 300Mbps (even though typical maximum data rate for early devices was no more than 150 Mbps). This limit has been overtaken with the birth of LTE Advanced (LTE-A), first introduced in Release 10, that was frozen by 3GPP in April 2011. New commercially available LTE capabilities provide greater spectral efficiency and allow to reach the milestone data rate of 1Gbps using 60 MHz of spectrum. These capabilities, which will be discussed more accurately further in this work, are:

- 3~4 Component Carrier Aggregation over licensed or unlicensed bands;
- 256 Quadrature Amplitude Modulation (256QAM);
- 4x4 Multiple Input Multiple Output (4X4 MIMO).

Commercial LTE-A devices are growing throughout the world and Operators are upgrading mobile networks with Category 16 implementations that will support up to 1Gbps data rates. Typically, this target data rate is not fully achievable so far because of Operators spectrum fragmentation and commercial devices limitation due to RF components (mainly transceivers). In fact, the maximum number of downlink antenna ports managed by current commercial devices is 8. This number can be exploited in diverse ways, either using MIMO 4x4 on two aggregated bands, or using MIMO 4x4 on one band and MIMO 2x2 on two bands. In this way, the theoretical maximum throughput is about 800 Mbps. When this constraint will be overcome, devices will be able to also support MIMO 8x8 and above to guarantee the target peak data rata for next generation technologies.

Two possible approaches open up. The first based on bandwidth broadening and the second on the improvement of the spectral efficiency. At the moment, mobile Operators are trying to figure out which approach or combination of approaches is the best in terms of performance and costs.

The aim of this work is to analyze every single capability among those just presented, for a given outdoor scenario, to study the advantages that each one gives in terms of throughput and the deployment strategies. We also try to determine the capacity of a real LTE network composed of five sites in a dense urban scenario.

Nowadays, video accounts for 50% of mobile data traffic while in 2022 the percentage will rise to 75%. For this reason, we focused our simulations on a high-quality video sharing, that requires a minimum user throughput of 12 Mbps.

This study was carried on with a network simulator and the results were compared with real measures taken in collaboration with TIM on new commercial devices.

The fundamentals of LTE and of LTE-A are described in Chapters 1 and 2as well as the features and the innovations introduced by the latter. The scenario is described in Chapter 3 with some while Chapter 4 is focused on the Network Simulator NS3 that has been used as platform for the simulations whose implementations and results are described in Chapter 5. Chapter 6 presents real measurements and the validation of the simulated results. Finally, in Chapter 7 main results of this thesis are summarized and likely future works to be done are exposed.

1 LTE

1.1 Background

With Long Term Evolution, we refer to a specific technology born in the first decade of 2000s as the evolution of the UMTS. The first steps towards the standardization started in December 2004. Several motivations brought to the birth of this Study Item within the 3GPP:

- Need to ensure the continuity of competitiveness of the 3G system for the future
- User demand for higher data rates and Quality of Service (QoS)
- Packet Switch (PS) optimized system
- Continued demand for cost reduction
- Low complexity

In particular, in 3GPP Technical Report TR 25.913 "*Requirements for Evolved UTRA (E-UTRA) and Evolved UTRAN (E-UTRAN)*" the goals and the minimum requirements for this technology are exposed:

- Efficient support for PS and Real-Time services
- Peak data rate up to 150Mbps in Downlink (DL) and 75Mbps in Uplink (UL) based on MIMO 2x2 and 20MHz bandwidth with 64QAM. These values correspond to a peak spectral efficiency of 7.5bps/Hz in DL and 3.75bps/Hz in UL. As comparison, note that UMTS Release 6 provides a peak data rate of 14.4Mbps in DL and 11Mbps in UL based on Single Antenna transmission on 5MHz.
- Higher average user throughput per MHz
- Higher spectral efficiency
- Lower latency: ~ 10ms
- Possibility to work both on paired (FDD) and unpaired (TDD) bands
- Bandwidth scalability: LTE can work on a flexible bandwidth from 1.4 to 20MHz.

1.2 LTE System Architecture

LTE architecture is called Evolved Packet System (EPS). It encompasses the Evolved UMTS Terrestrial Radio Access Network (E-UTRAN) and the Evolved Packet Core (EPC). The latter takes care of all the non-radio aspects and is also named System Architecture Evolution (SAE). Figure 1.2 represents the simplified architecture of EPS: the links correspond to the main logic interfaces that are at the IP protocol.

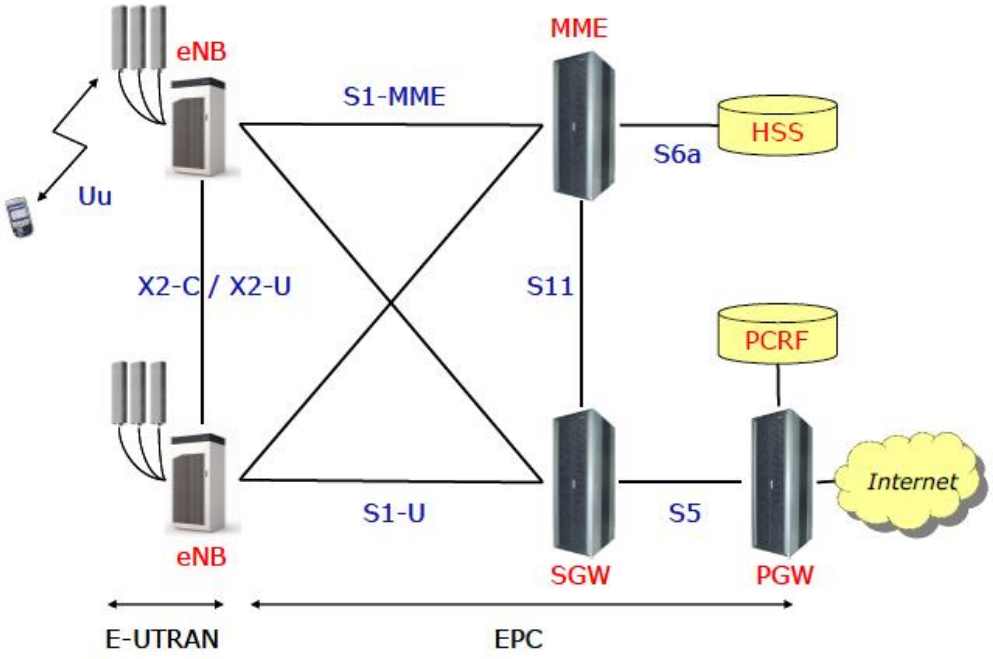

Figure 1.2 EPS architecture

E-UTRAN handles the radio communication between the mobile and the EPC and consists of a single component, the eNodeB (eNB). It is responsible mainly of two functions:

- The eNB sends and receives radio transmissions to all the mobiles using the analogue and digital signal processing functions of the LTE air interface
- The eNB controls the low-level operation of all its mobiles, by sending them signaling messages such as handover commands

Unlike UMTS or GSM, there isn't a radio controller as the Radio Network Controller (RNC): in fact, eNB is the combination of NodeB and RNC, fulfilling both roles. A eNB can also be connected to nearby base stations by the X2 interface which manages the handover procedure between two nodes without losing data. Each eNB connects with the EPC by means of the S1 interface: the Standard distinguishes between S1-MME and

S1-U. The former links the eNB and Mobility Management Entity while the latter is responsible of the data flow between eNB and Serving Gateway (SGW). SGW and MME are mutually linked by S11 interface, whilst interface S5 links SGW and Packet Data Network Gateway (PGW). Here, we briefly describe the functions exploited by the nodes included in the EPC:

- MME is the control node that handles the Non-Access Stratum (NAS) signaling from and to UE. It oversees the Mobility Management (MM) and of Connection Management (CN). Moreover, it is in charge of Session Management (SM) through ESM protocol. This protocol instantiates the logic connections between UE and PDN.
- IP packets from and towards the eNBs pass through the SGW whose function is to anchor the user plane data in case of mobility among different nodes.
- PGW is the access to external Packet Data Networks (PDN): a UE can have several connections towards multiple PGW in order to reach multiple PDNs. Moreover, PGW assigns the IP addresses to the devices.
- Home Subscriber Server (HSS) contains subscription data and possible roaming access restrictions. It also holds information on the PDN to which the user equipment can attach.
- Policy and Charging Rules Function (PCRF) is the network element that oversees the Policy and Charging Control (PCC). It determines the services management in terms of QoS and communicates the relative parameters to the PGW that configures the appropriate data bearers.

1.3 LTE Radio Interface

Figure 1.3 shows the radio interface protocol stack. In the next section, we will focus on the physical layer while here we will give an overview of the levels above:

- Radio Resource Control RRC
- Packet Data Convergence Protocol PDCP
- Radio Link Control RLC
- Medium Access Control MAC

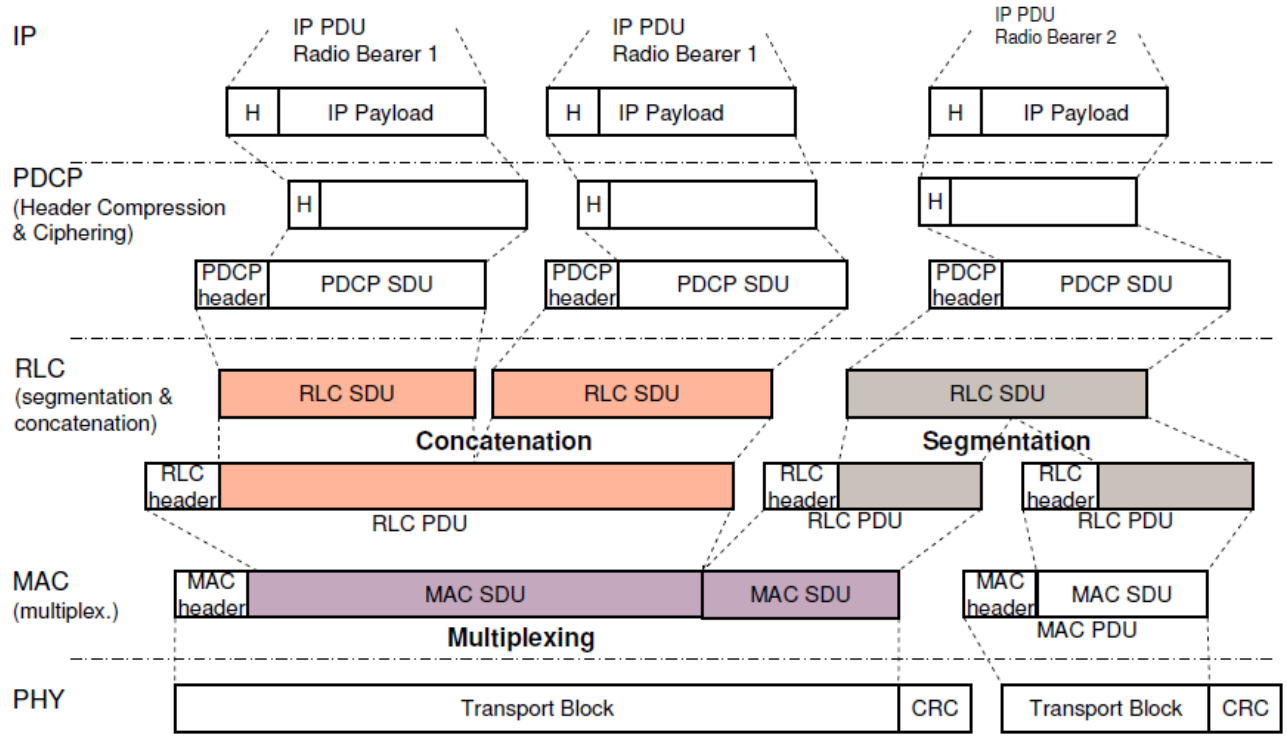

Figure 1.3 LTE Protocol Stack (*3GPP*)

1.3.1 Radio Resource Control

As for UMTS, RRC is used on the Air Interface. This level is responsible for the signaling between UE and eNB and exists at the IP level. It is mainly used for the management of radio resources and for the configuration of lower levels. In LTE, there are only two states for the mobile devices: RRC_IDLE and RRC_CONNECTED. The former mode has the lowest energy consumption: the UE monitors the paging channels, acquires the System Information, measures the adjacent cells and makes the cell selection/reselection. In the latter mode, the UE can exchange data with the core and monitors the downlink channels to determine whether he should receive packets.

The main functionalities carried out by the RRC are:

- *Broadcast of the System Information*: within this information the User Equipment finds the parameters needed to access the radio network. These messages are structured as blocks named System Information Blocks (SIB) each of which contains a limited number of information. The principal SIB is the Master Information Block (MIB) which reports i.e. the system frequency bandwidth, the

configuration of some channels. It is mapped in the frequency domain and it is transmitted every 40ms. Other SIBs are defined in 3GPP TS 36.331:

  - SIB1 is transmitted every 80ms and reports the information to access a cell. Moreover, it provides the scheduling of the other SIBs
  - SIB2 includes the information on the radio configuration of common channels and signals (PRACH, PDSCH, PUCCH, PUSCH, SRS)
  - SIB3 contains information to regulate the Cell Re-selection both inter-frequency and intra-frequency. It also holds the s-IntraSearch parameter, corresponding to the threshold over which the UE can decide not to make intra-frequency measures.
  - SIB4 encompasses specific information to govern the Cell Re-selection in case of intra-LTE intra-frequency
  - SIB5 reports specific information to carry out the Cell Re-selection in case of intra-LTE inter-frequency
  - SIB6 and SIB7 include specific information to control the Cell Re-selection for inter-RAT respectively towards UTRAN and GERAN

  Other SIBs (8-13) are used for precise scopes, like the search for home eNB.

- *Paging*: its aim is mainly to awake a UE in IDLE mode, to notify the arrival of incoming calls
  or of an update of the System Information.
- *UE Cell Selection and Re-selection*: when in IDLE mode, the UE selects a suitable cell and camps to it. Differently from older technologies, in LTE, the eNB can provide the UE with a specific priority for the frequency layers within or outside the technology. If the UE camps to the highest priority cell (or frequency) it doesn't make further measures until the signal level of the serving cell is higher than a threshold value. On the contrary, if it attached to a low-level
  cell (or frequency) he must make measures searching for a higher priority cell.
- *RRC Connection Establishment*: with this procedure, it is possible to assign radio resources to

the UE. Once the procedure is completed, the UE is in CONNECTED mode.

- *Measurement Control and Reporting*: this function comprehends the procedures through which the eNB makes the UE start one or more measures.

1.3.2 Packet Data Convergence Protocol

This protocol furnishes to higher levels the so-called Radio Bearer. In particular, it provides the RRC Control Plane with the Signaling Radio Bearer (SRB) and the RRC User Plane with the Data Radio Bearer (DRB). The main functionalities of the PDCP are:

- *Sequence PDU Numbering*
- *Header Compression*: in order to compress the protocol overhead, it is used the Robust Header Compression (ROHC) so that the transmission efficiency improves
- *Integrity Protection* for signaling messages

1.3.3 Radio Link Control

RLC can be set in three ways: Acknowledged Mode (AM), Unacknowledged Mode (UM) and Transparent Mode (TM). In AM, the RLC delivers PDU to higher levels without errors. It uses ACK/NACK with specific "Status Report" PDUs. On the contrary, UM doesn't call for the ACK/NACK and consequently there aren't retransmissions: even if the PDU is received with errors, it is however delivered to the upper level. Finally, in TM there aren't overheads so that it allows neither retransmission nor error recognition. Its only aim it to buffer the PDUs to be transmitted.

Although the RLC is capable of handling transmission errors, error-free delivery is in most cases handled by the MAC-based Hybrid Automatic ReQuest protocol (HARQ). Then, the double retransmission mechanism might seem redundant. Nonetheless, sometimes the HARQ retransmissions can fail and the RLC layer ensures the correct transmission.

1.3.4 Medium Access Control

MAC layer carries out the following three actions:

- Multiplexing of PDUs coming from upper levels into a physical Transport Block

- HARQ: the retransmission protocol used by MAC is the N-channel Stop&Wait. In general, in the S&W protocol, the transmitter sends each PDU only after the acknowledgement of the occurred transmission by the receiver. Then, it might be subject to a deadlock situation. To prevent it, LTE has introduced the N-channel variant (with N=8), to parallelize up to 8 processes operating in independent manner.
- Radio resources Dynamic Scheduling: as in HSPA, in LTE there are shared channels that are regulated by MAC. Notably, MAC scheduler determines the UE that can be served during the i-th Transmission Time Interval (TTI) which corresponds to 1ms.

During each TTI the eNB scheduler considers the physical radio environment per UE. They report the perceived quality to decide which Modulation and Coding Scheme (MCS) to use. Then, it assigns the priority amongst the UE and finally, informs them of allocated radio resources. The eNB schedules both on the downlink and on the uplink.

1.4 Physical layer

The PHY layer is a highly efficient mean of transferring both data and control information between an eNB and a UE. This layer employs technologies that are new in mobile applications with respect to UMTS. In this section, we will give an overview of these novelties introduced by LTE.

1.4.1 Multiple Access Techniques

3G telecommunications use the code division access technique. Each UE is given one or more codes to transmit or receive. In the frequency domain, a fixed band portion is assigned to each user. The transition from UMTS to LTE led to the usage of different multiple access techniques: the Orthogonal Frequency Division Multiple Access (OFDMA) on the downlink and the Single Carrier Frequency Division Multiple Access (SC-FDMA) on the uplink. OFDM is a multi-carrier technology that subdivides the bandwidth into a multitude of mutually orthogonal narrowband subcarriers. Multiple users can share these subcarriers. Since the OFDMA leads to high Peak-to-Average Power

Ratio, it requires expensive power amplifiers that would lead to highly expensive devices. Hence, in UL LTE provides for the SC-FDMA that guarantees a low PAPR and lower costs.

1.4.1.1 OFDMA

This technique is based on Orthogonal Frequency Division Multiplexing (OFDM), that uses a very high number of carriers to transport the information from and to the UE. Each carrier is closely spaced with a subcarrier spacing Δf = 15kHz. The higher the number of carriers is, the better is the instantaneous capacity assigned to a single user.

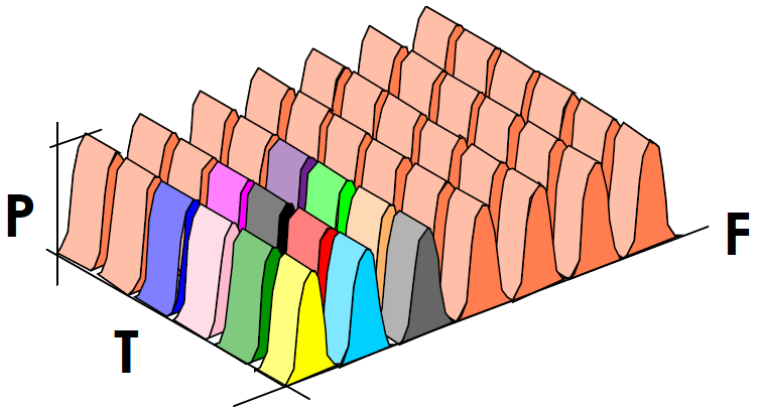

Figure 1.4 OFDMA in LTE

In order to guarantee the orthogonality, the symbol time (which is the inverse of the subcarrier spacing) is $1/\Delta f$ = 66.7μs. Figure 1.7 shows that the tails of the adjacent carriers are next to zero value.

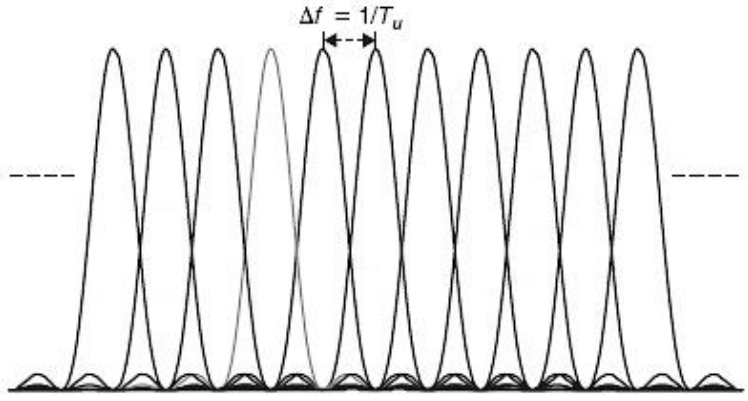

Figure 1.5 OFDM carriers overlapping

To avoid Inter-Symbol Interference (ISI), LTE employs the Cyclic Prefix Insertion: it consists in enlarging the OFDM symbol duration by inserting a prefix that corresponds to the final part of the symbol. This is represented in figure 1.8 where it is also evident

how a part of the previous symbol overlies the CP of the following one. Orthogonality is however granted if the maximum delay spread between principal path and the signal replications is less than the duration of the prefix.

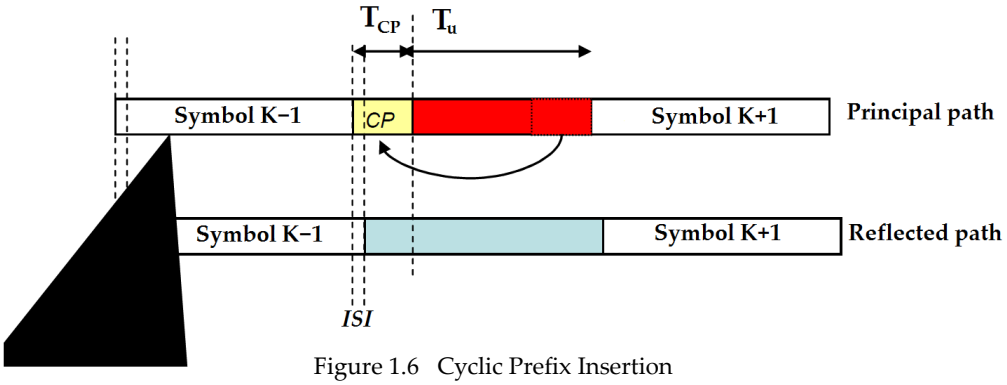

Figure 1.6 Cyclic Prefix Insertion

In OFDM, each subcarrier can have a different modulation scheme corresponding to a specific transmission speed. It is selected in accordance with SINR level. First LTE releases envisage the usage of Quadrature Phase-Shift Keying (QPSK), 16-Phase Quadrature Amplitude Modulation (16QAM) and 64-State Quadrature Amplitude Modulation (64QAM). Higher modulation orders have more bits per symbol and guarantee higher data rates but they are less robust to noise.

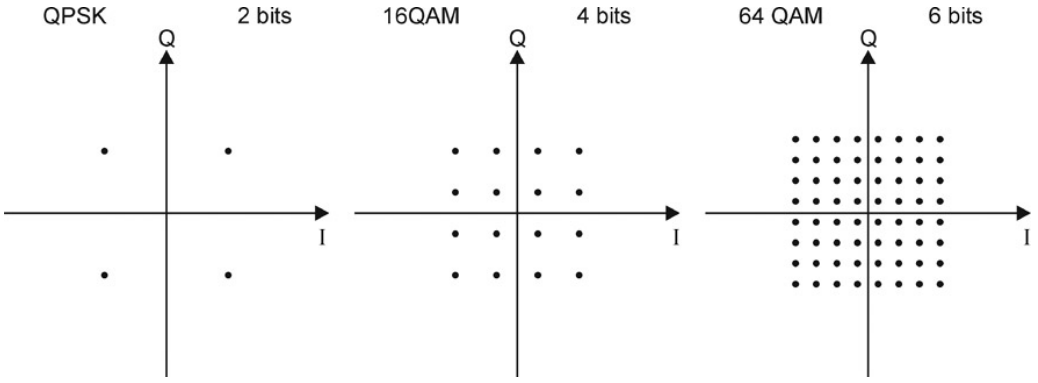

Figure 1.7 Modulation schemes for LTE

1.4.1.2 SC-FDMA

Unlike OFDMA, this technique provides for a serial data transmission instead of the parallel one. Here, the symbols are no more univocally associated to N subcarriers. The aim is to spread the information of the N modulation symbols over the N subcarriers, obtaining de facto a unique carrier. The spreading helps to reduce the PAPR since the single subcarriers are no more individually modulated. The difference is clear in figure 1.8.

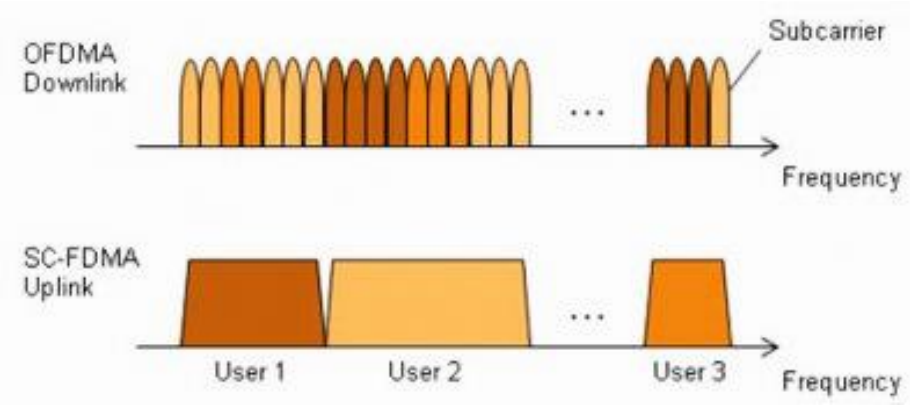

Figure 1.8 OFDMA and SC-FDMA (*3GPP*)

1.4.2 Frame Structure

According the duplexing mode used, there are two frame structure types for E-UTRA: with Frequency Division Duplexing (FDD) it is used the frame structure Type 1 while frame structure Type 2 is for Time Division Duplexing (TDD) mode.

In FDD, both uplink and downlink transmissions are structured as frames that last 10ms (Type 1 frame). Each frame is divided in 10 subframes each of which has a 1ms duration. In turn, each subframe is split in two 0.5ms slots. Then, in each frame there are 20 slots. Then, each time slot is made of several OFDM symbols: if a Normal Cyclic Prefix is used, there are 7 symbols; otherwise, in case of Extended Cyclic Prefix, there 6 of them. We will study networks that provide for Normal Cyclic Prefixes. In the frequency domain, each slot corresponds to 180kHz divided in 12 sub-carriers, 15kHz each. The ensemble of the frequency resources and symbols is called Physical Resource Block (PRB), which then contains 84 Resource Elements RE. This structure is shown in figure 1.9 while in table 1.1 you can find the maximum number of PRB that can be assigned to each UE.

Bandwidth [MHz]	1.4	3	5	10	15	20
Number of PRB	6	15	25	50	75	100

Table 1.1 Maximum NPRB as a function of the system bandwidth

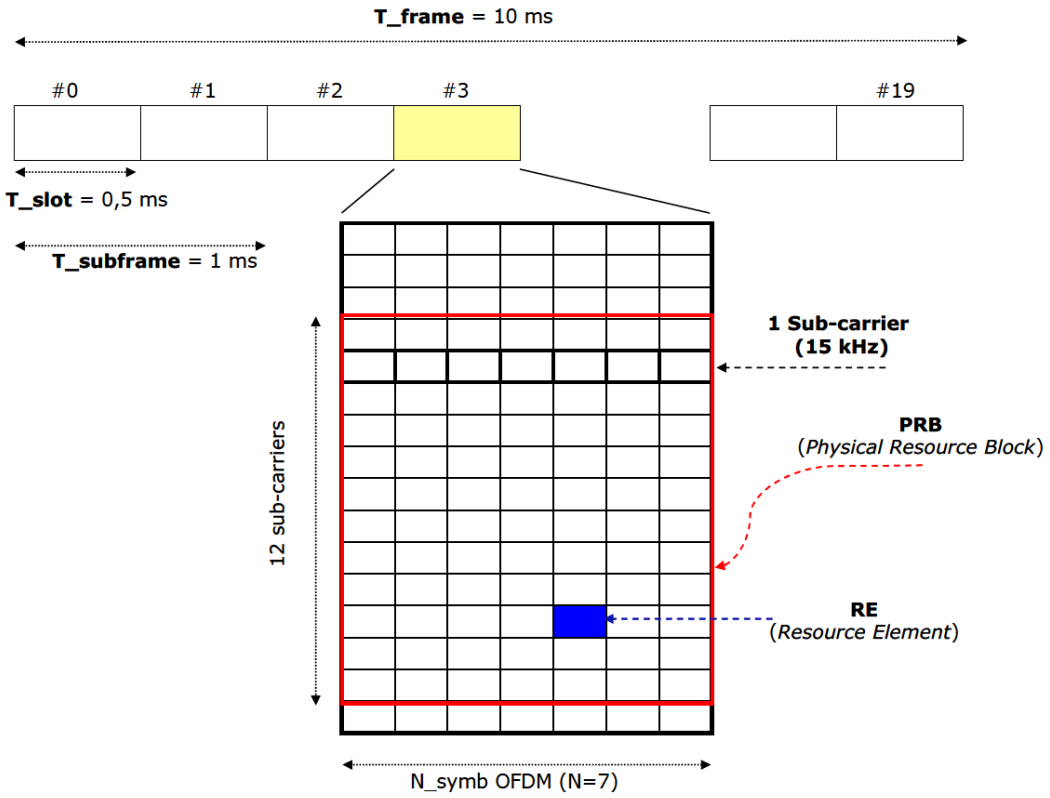

Figure 1.9 Frame Structure in FDD

Each RE includes the information about the modulation order. Each symbol has a duration of 66.7μs, as seen before, and this is a consequence of the subcarrier spacing value of 15 kHz. The length of the CP is variable: it is about 5.2μs for the first symbol and about 4.7μs for the other six symbols, leading to an overall duration of (5.2+66.7) + (4.7*66.7) * 6 = 71.9 + 428.4μs = 0.5ms.

1.5 Multiple Input Multiple Output

MIMO is a technique that helps to achieve improvements in spectral efficiency and in data rate. It consists in the use of multiple antennas in both transmission and reception.

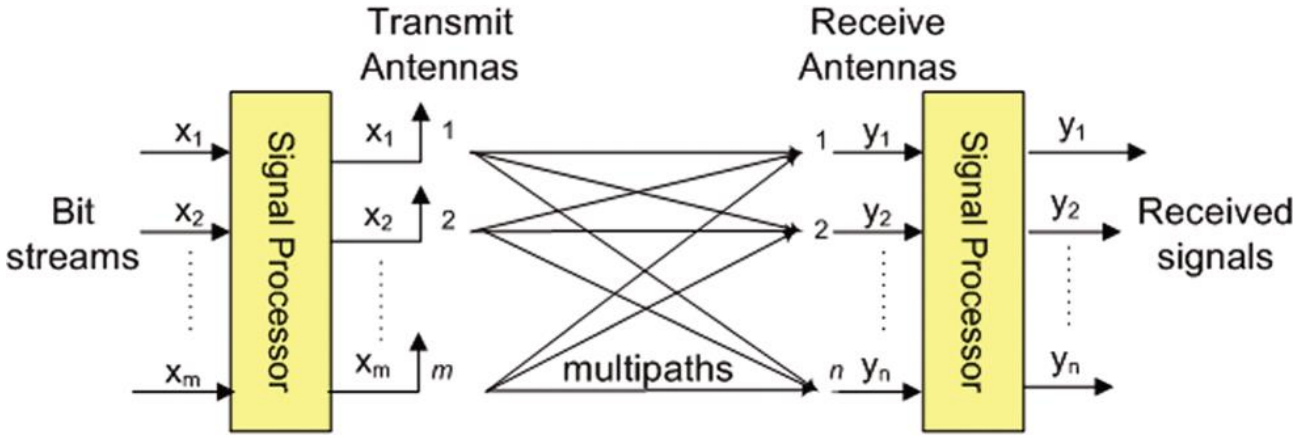

Figure 1.10 MIMO

To transmit independent streams, MIMO uses spatial multiplexing. The amount of data received by each antenna is defined *layer*; it means that the LTE throughput increases linearly with the number of layers.

The first LTE Release supported only MIMO 2x2 because of the difficulties in implementing it onto devices: in fact, a higher number of antennas leads to a higher power consumption and bigger dimensions. Release 8 provided several transmission modes:

Transmission Mode	Downlink Transmission Scheme
Mode 1	Single Antenna Port
Mode 2	Transmit Diversity
Mode 3	Open-Loop Spatial Multiplexing
Mode 4	Closed-Loop Spatial Multiplexing
Mode 5	Multi-User MIMO
Mode 6	Closed-Loop Rank-1 Spatial Multiplexing
Mode 7	Single Antenna Port Beamforming

Table 1.2 LTE Transmission Modes (*3GPP*)

The main difference between Open and Closed Loop is the feedback that the UE sends to the eNB. Then, in Modes 3 and 6 there is an overhead.

1.6 Resources Scheduling

Time/frequency resources scheduling is carried out by the eNB; it allocates them according to the quality feedback CQI sent by the device. The scheduling is organized on a TTI base: the eNB assigns an integer number *K* of PRBs that, in the frequency domain, is equivalent to *K* * 180kHz.

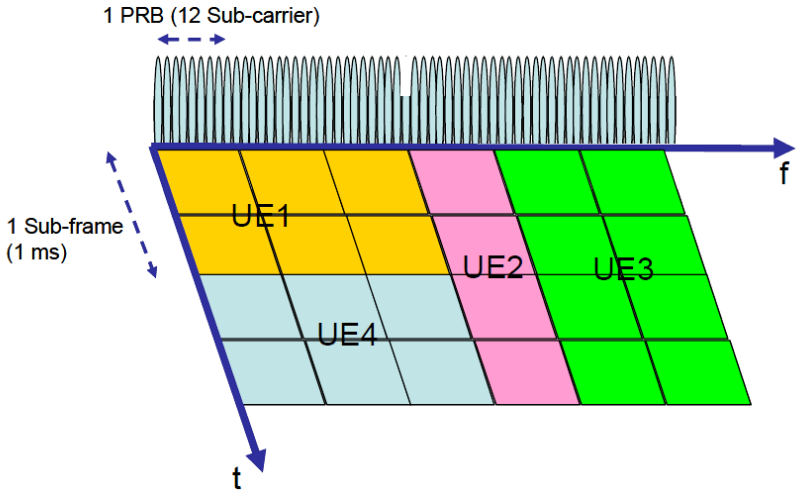

Figure 1.11 Dynamic Scheduling Example

Several scheduling algorithms can be implemented in LTE and the most common are Round Robin (RR), Proportional Fair (PF) and Best CQI.

1.6.1 Round Robin Scheduler

RR algorithm allows the UE to access the resources in circular order, giving every user an equal opportunity to access the shared resources. Since it is a channel blind algorithm, its maximum throughput is worse than that other algorithms can offer. On the contrary, it provides for a great fairness and a good bandwidth utilization and is used mostly in scenarios that do not require high speed.

1.6.2 Proportional Fair Scheduler

At the beginning, PF scheduler was proposed as an alternative to max-min scheduler. This technique offers a tradeoff between the maximum average throughput and the user fairness. It works by scheduling the user when the instantaneous channel quality is high with respect to its condition over time. PF scheduling achieves multi-user diversity by scheduling high channel quality during different time slots.

1.6.3 Best CQI Scheduler

This algorithm is designed to give priority to those UE having the best channel conditions. Then, it offers a high throughput to the users that are near the Base Station whereas those that are located at the cell edge have less probability of getting access to the shared resources.

1.7 LTE UE Categories

The development of each technology is usually carried out to fulfill the requests made by Markets, each of which is interested in different specific requirements and priorities. Too many distinct categories would force a highly complex network that must manage many features. Then, 3GPP decided to define within Release 8, five categories, whose principal features are reported in the figure in the next page.

Category		1	2	3	4	5
Peak rate Mbps	DL	10	50	100	150	300
	UL	5	25	50	50	75
Capability for physical functionalities						
RF bandwidth		20MHz				
Modulation	DL	QPSK, 16QAM, 64QAM				
	UL	QPSK, 16QAM				QPSK, 16QAM, 64QAM
Multi-antenna						
2 Rx diversity		Assumed in performance requirements.				
2x2 MIMO		Not supported	Mandatory			
4x4 MIMO		Not supported				Mandatory

Figure 1.12 LTE Categories in Release 8 (*3GPP*)

1.8 Frequency Allocation

In TS 36.104, 3GPP defines the bands over which LTE is designed to operate. Some bands are FDD, some are TDD and others are indicated as FDD/CA; these can be used only as aggregated bands since they are unpaired, that is to say that they work only on downlink or uplink.

Band	Duplex Mode	Uplink (MHz)	Downlink (MHz)
1	FDD	1920 – 1980	2110 – 2170
2	FDD	1850 – 1910	1930 – 1990
3	FDD	1710 – 1785	1805 – 1880
4	FDD	1710 – 1755	2100 – 2155
5	FDD	824 – 849	869 – 894
6	FDD	830 – 840	875 – 885
7	FDD	2500 – 2570	2620 – 2690
8	FDD	880 – 915	925 – 960
9	FDD	1749.9 – 1784.9	1844.9 – 1879.9
10	FDD	1710 – 1770	2100 – 2170
11	FDD	1427.9 – 1447.9	1475.9 – 1495.9
12	FDD	699 – 716	729 – 746
13	FDD	777 – 787	746 – 756
14	FDD	788 – 798	758 – 768
17	FDD	704 – 716	734 – 746
18	FDD	815 – 830	860 – 875
19	FDD	830 – 845	875 – 890
20	FDD	832 – 862	791 – 821
21	FDD	1477.9 – 1462.9	1495.9 – 1510.9
22	FDD	3410 – 3490	3510 – 3590
23	FDD	2000 – 2020	2180 – 2200
24	FDD	1626.5 – 1660.5	1525 – 1559

25	FDD	1850 – 1915	1930 – 1995
26	FDD	814 – 849	859 – 894
27	FDD	807 – 824	852 – 869
28	FDD	703 – 748	758 – 803
29	FDD / CA		717 – 728
30	FDD	2305 – 2315	2350 – 2360
31	FDD	452.5 – 457.5	462.5 – 467.5
32	FDD / CA		1452 – 1496
33	TDD	1900 – 1920	1900 – 1920
34	TDD	2010 – 2025	2010 – 2025
35	TDD	1850 – 1910	
36	TDD		1930 – 1990
37	TDD	1910 – 1930	1910 – 1930
38	TDD	2570 – 2620	2570 – 2620
39	TDD	1880 – 1920	1880 – 1920
40	TDD	2300 – 2400	2300 – 2400
41	TDD	2496 – 2690	2496 – 2690
42	TDD	3400 – 3600	3400 – 3600
43	TDD	3600 – 3800	3600 – 3800
44	TDD	703 – 803	703 – 803
45	TDD	1447 – 1467	1447 – 1467
46	TDD	5150 – 5925	5150 – 5925
65	FDD	1920 – 2010	2110 – 2200
66	FDD	1710 – 1780	2110 – 2200
67	FDD / CA		738 – 758
68	FDD	698 – 729	753 – 758
69	FDD / CA		2570 – 2620
70	FDD	1695 – 1710	1995 – 2020

Table 1.3 LTE frequency bands from 3GPP TS 36.104

In the table above, we highlighted the frequencies that are used in Europe and, more specifically in Italy. Bands 3, 7 and 20 can be used as principal carrier while Band 32 (commercially named L Band) is an unpaired band and can be used only in aggregation with others.

The LTE spectrum is divided among mobile Operators. The division is shown in figure 1.13. Note that each square corresponds to 5MHz in DL and UL.

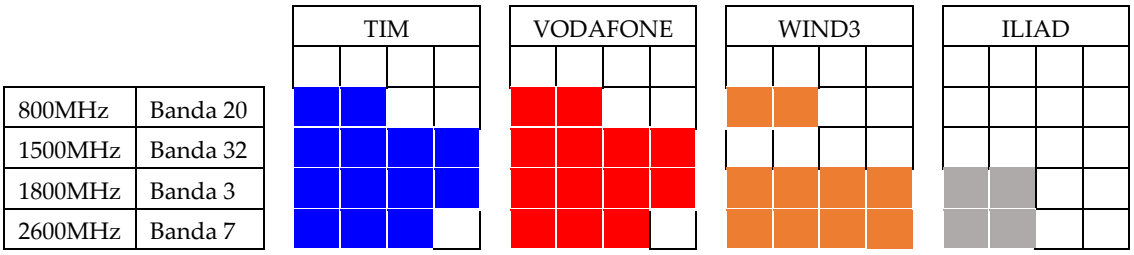

Figure 1.13 Spectrum division among the Operators in Italy

2 LTE-Advanced

2.1 Beyond Release 8

Following the freeze of Release 8, 3GPP started working on a further evolution of LTE, to be defined in Release 10, in order to guarantee to this technology the worldwide leadership among mobile networks. In May 2008, 3GPP defined the bases of the so-called LTE-Advanced in TR 36.913 "*Requirements for further advancements for Evolved Universal Terrestrial Radio Access (E-UTRA) LTE-Advanced*":

- Backward compatibility of LTE-A Release 10 with the LTE systems in Release 8
- Target peak data rate of 1Gbps in DL and 500Mbps in UL based on MIMO 4x4 and 64QAM on a 100MHz spectrum
- Capability to aggregate more spectrum (Carrier Aggregation) up to 100MHz

Further improvements have been introduced by Release 12 such as the higher order modulation 256QAM. This led to a peak data rate of 3Gbps with a spectral efficiency up to 30bps/Hz with MIMO 8x8. Moreover, Release 13 introduced the possibility to aggregate up to 32 carrier components even among different spectrum types.

2.2 Enhancements for LTE-Advanced

The improved Carrier Aggregation, MIMO and 256QAM are not the only novelties introduced in LTE-A. In fact, further enhancements have been developed and the most significant are the deployment of Heterogeneous Networks (HetNets) to increase capacity with Enhanced Inter-Cell Interference Coordination (eICIC) and Coordinated Multi Point (CoMP) technique and the evolution towards Self Organizing Networks (SON).

2.2.1 Carrier Aggregation

CA allows to increase the peak data rate by concatenating several bands in order to transmit on a wider bandwidth, up to 100MHz. Moreover, it leads to a more flexible handling of the frequencies in heterogeneous scenarios. Carrier aggregation supports both contiguous and non-contiguous spectrum as well as asymmetric bandwidth for

FDD. This technology requires the sharing of baseband between the nodes that work on the involved frequencies.

CA is also the base for a further development of LTE-A: in fact, this feature allows also the concatenation of different spectrum types, as shown in figure 2.1. Since mobile network Operators deal with limited licensed bands, they are seeking for the development of LTE Licensed Assisted Access (LAA) that aggregates a 60MHz band in the 5GHz spectrum of Wi-Fi. Then, both Operators and Industries are carrying on studies on this technology that would guarantee both an increase of the data rate and the possibility to transmit on a wider spectrum.

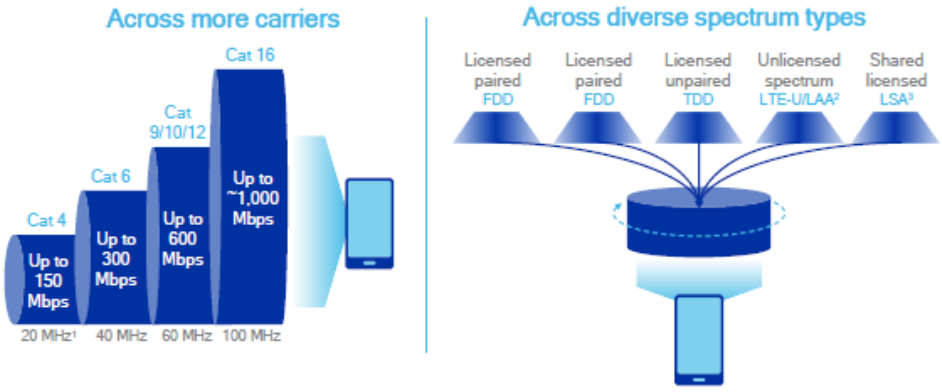

Figure 2.1 Carrier Aggregation modes (*Qualcomm*)

When CA is used, there are several serving cells, one for each component carrier (CC). The coverage of each cell may differ, according to the pathloss. Then, the RRC connection is only handled by the Primary Serving Cell (PSC) served by the Primary Component Carrier (PCC). All the other component carriers are defined as Secondary Component Carrier (SCC): they can be removed when required, while the PSC is changed only at handover.

With refer to scheduling, there are two main alternatives for CA: resources can be either scheduled on the same carrier unawarely of the other frequencies scheduling or simultaneously across the multiple frequencies. The former technique is called Single Carrier-Scheduling (SCS) and the latter is named Cross-Carrier Scheduling (CCS). In real networks, CCS is not used yet and SCS is the only current algorithm.

2.2.2 Enhanced Multi-Antenna Techniques

MIMO schemes for DL in LTE provide for up to 4 layers. In Release 10, these have been extended to up to 8 layers. It is very difficult to implement such a complex radio interface on a device; in fact, nowadays there are few devices that can implement MIMO 4x4, while devices with 8 antennas are still being studied. It is important to underline that MIMO 4x4 is not very robust with respect to noise and requires high SINRs.

Apart from the number of antennas, novelties have been introduced with *active antennas* based on the *digital beamforming*: it allows to focalize the signal between UE and eNB so that also the useful signal increases with respect to the interference. Moreover, the introduction of Multi-User MIMO (MU-MIMO), led to an increase of spectral efficiency: it consists in sending information towards different users over the same resources. With active antennas, it is possible to create several cells, both horizontally and vertically (*cell-splitting*), so that the system capacity augments for equal bandwidth. For instance, figure 2.2 shows the case of vertical sectorization that allows to double the number of cells created by a single plant.

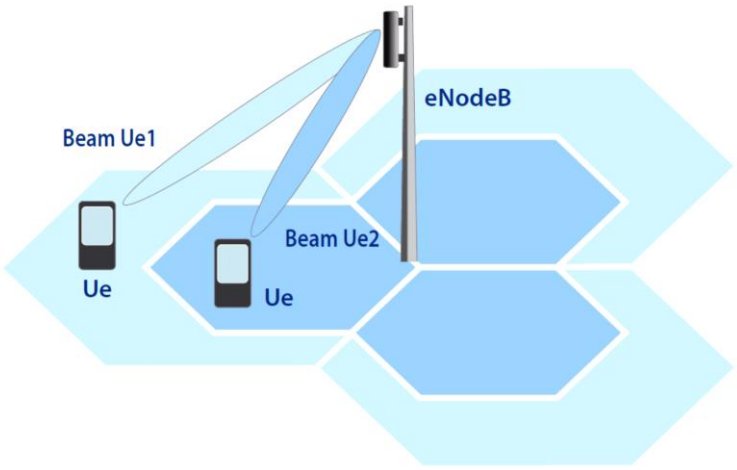

Figure 2.2 Example of active antennas usage

Another technique introduced with LTE-A, in Release 11, is the CoMP. The signal is transmitted and received by multiple coordinating points, increasing the useful signal level and decreasing the interference. It requires the base-band processing to be shared by the coordinated plants. There are three techniques:

- Coordinated Scheduling (CS) or Coordinated Beamforming (CB): transmitting points coordinate in order to maximize the received useful signal and to reduce the interference with other users.

- Dynamic Point Selection (DPS): the most suitable transmission point is selected instantaneously to optimize system performances.
- Joint Processing (JP): in DL, each device receives from several transmitting points and the signal recombination increases the signal quality.

Finally, Release 12 introduced new Transmission Modes in addition to those in table 1.2: TM8, TM9 and TM10. They support the transmission on up to 8 layers and on Antenna Ports 7 and 8.

2.2.3 Heterogeneous Networks

To guarantee a uniform experience to the UE within a cell, it was necessary to change the topology of traditional sites. To expand the network without encountering very high costs, the Operators must act in a more flexible way: they are building up an advanced heterogeneous topology of networks. A network becomes heterogeneous with the utilization of diverse types of base station introducing low power small cells (micro-, pico-, femto-cells, relay nodes) that can solve problems of coverage holes in areas covered only by macro eNBs, increasing the capacity in hot spots. The placement of small cells is easier than that of macro ones but Operators must deal with an increasing intercell interference. In HetNets, there are advanced strategies to coordinate the base stations to optimize the interference management. One of these is the Enhanced Inter-Cell Interference Coordination (eICIC) that uses Almost Blank Subframes (ABS) to minimize the interference due to macro cells.

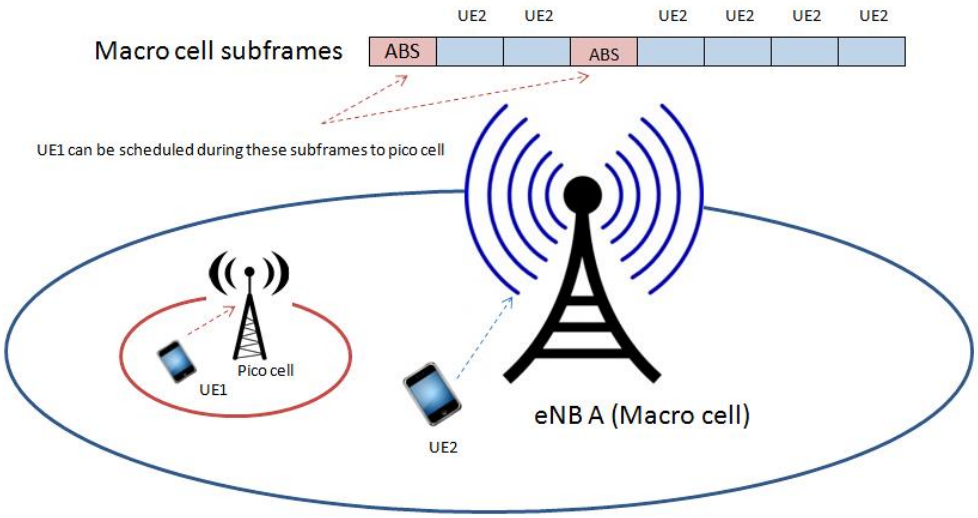

Figure 2.3 eICIC with ABS

The blank subframes do not contain data but only control channel and cell reference signals. During the ABS, the macro cell does not transmit so that the pico-cell can serve the most interfered users.

2.3 LTE-Advanced UE Categories

As well as LTE UE Categories, LTE-A ones are defined in 3GPP's TS 36.306. Release 11 introduced three new Categories: 6, 7, 8. These included the new features just released for commercial devices. The last Release defines new Categories, up to Cat19. At the moment of writing, on a few of the latest commercial devices belong to Cat16 and can theoretically achieve up to 1Gbps DL data rate. Actually, because of the spectrum fragmentation, the maximum theoretical throughput is about 700Mbps. Below, we report an extract of Table 4.1A-1 from TS 36.306 V.14.2.0, updated to March 2017.

UE DL Category	Maximum number of DL-SCH transport block bits received within a TTI	Maximum number of bits of a DL-SCH transport block received within a TTI	Total number of soft channel bits	Maximum number of supported layers for spatial multiplexing in DL
DL Category 6	301504	149776 (4 layers, 64QAM) 75376 (2 layers, 64QAM)	3654144	2 or 4
DL Category 7	301504	149776 (4 layers, 64QAM) 75376 (2 layers, 64QAM)	3654144	2 or 4
DL Category 9	452256	149776 (4 layers, 64QAM) 75376 (2 layers, 64QAM)	5481216	2 or 4
DL Category 10	452256	149776 (4 layers, 64QAM) 75376 (2 layers, 64QAM)	5481216	2 or 4

DL Category 11	603008	149776 (4 layers, 64QAM) 195816 (4 layers, 256QAM) 75376 (2 layers, 64QAM) 97896 (2 layers, 256QAM)	7308288	2 or 4
DL Category 12	603008	149776 (4 layers, 64QAM) 195816 (4 layers, 256QAM) 75376 (2 layers, 64QAM) 97896 (2 layers, 256QAM)	7308288	2 or 4
DL Category 13	391632	195816 (4 layers, 256QAM) 97896 (2 layers, 256QAM)	3654144	2 or 4
DL Category 14	3916560	391656 (8 layers, 256QAM)	47431680	8
DL Category 15	749856-798800	149776 (4 layers, 64QAM) 195816 (4 layers, 256QAM) 75376 (2 layers, 64QAM) 97896 (2 layers, 256QAM)	9744384	2 or 4
DL Category 16	978960 -1051360	149776 (4 layers, 64QAM) 195816 (4 layers, 256QAM) 75376 (2 layers, 64QAM) 97896 (2 layers, 256QAM)	12789504	2 or 4
DL Category 17	25065984	391656 (8 layers, 256QAM)	303562752	8
DL Category 18	1174752-1206016	[299856 (8 layers, 64QAM) 391656 (8 layers, 256QAM) 149776 (4 layers, 64QAM) 195816 (4 layers, 256QAM) 75376 (2 layers, 64QAM) 97896 (2 layers, 256QAM)	14616576	2 or 4 [or 8]
DL Category 19	1566336 -1658272	[299856 (8 layers, 64QAM) 391656 (8 layers, 256QAM) 149776 (4 layers, 64QAM) 195816 (4 layers, 256QAM) 75376 (2 layers, 64QAM) 97896 (2 layers, 256QAM)	19488768	2 or 4 [or 8]

Table 2.1 Extract of 3GPP Table 4.1A-1 from Release 36.306

3 Scenario

3.1 Case Study

We will consider five sites in a realistic neighborhood to represent a dense urban scenario. Each site is characterized by three sectors and an average radius of 550m, leading to a 0.9km^2 coverage.

Figure 3.1 Site location and beams directions

Our study considers the employment of antennas transmitting with a Radio Base Station (RBS) output power of 43 dBm for each radio branch. These antennas are multi-array and can work at all the frequencies needed to do the carrier aggregation over four bands: 800MHz, 1500MHz, 1800MHz and 2600MHz. These are also well-prepared for different MIMO applications.

Since it is a dense urban scenario, we expect around 500/1000 users per site. Of course, each one has distinctive characteristics which need to be parameterized:

- Location;
- Mobility, with the following user distribution:
    - Fixed - 60%;
    - Walking 3km/h - 25%;
    - Car 30km/h - 15%;

- Device category, according to which we determine the capabilities of each user:
  - Category 6 supports 64QAM, MIMO 2X2 and Carrier Aggregation over 2 bands;
  - Category 11 supports 256QAM, MIMO 2x2 and Carrier Aggregation over 3 bands;
  - Category 16 supports 256QAM, MIMO 4x4 and Carrier Aggregation over 4 bands.

3.2 Analytical description

Since we are interested in evaluating the overall system throughput, we first need to identify the parameters that can influence it. At first glance, we can say that these are mainly the spectral efficiency and the Number of Physical Resource Blocks, which in turn depend on the Channel Quality Indicator and then on the received power. A schematization is given in figure 3.3. Here, one can distinguish also some elements referring to probability density functions: in fact, our treatise tries to analyze the whole network from a statistic perspective in order to give description of the propagation phenomena without loss of generality. There are also other parameters who are fixed or, anyway, considered constant. Note that the following consideration will be made on a single site.

First, the transmitted power is fixed as well as the transmission and reception gains are determined. The number and the category of the user equipment are supposed to be known.

The first assumption we make is to consider the user's position probability density function as if it was uniform: we assign to each point of the site the same probability to be occupied by a user equipment, both along the radius and the angles. Doing that we assume the position to be a uniform random variable.

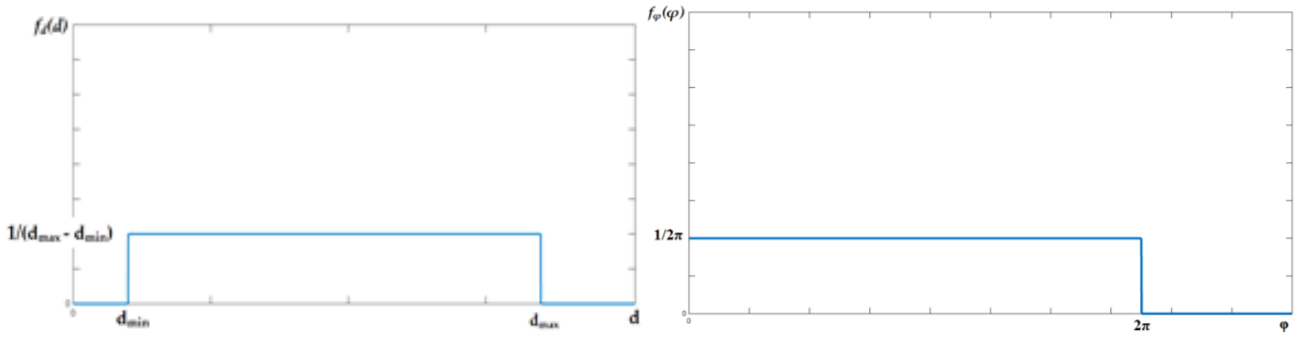

Figure 3.2 Probability distribution along the radius (left) and the angle (right)

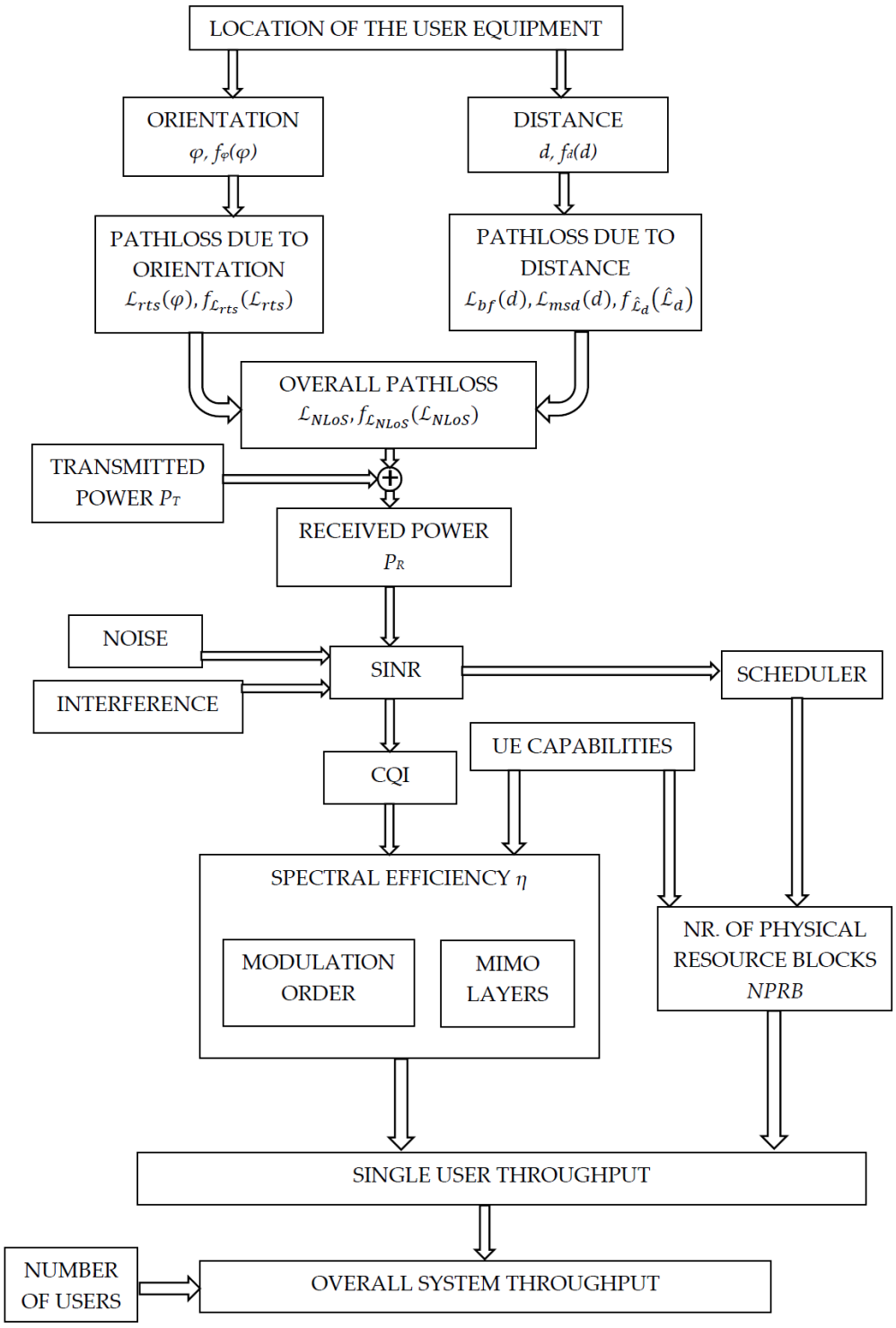

Figure 3.3 Flow chart of the evaluation of the overall throughput

The power received by each user is determined as follows:

$$P_{R_{dB}} = P_{T_{dB}} - A_{dB} \tag{3.1}$$

where $P_{R_{dB}}$ is the received power by the UE, $P_{T_{dB}}$ is the RBS transmit power and A_{dB} is the attenuation.

To evaluate the attenuation in a complex scenario like the one we are keen to study we will refer to the ITU Recommendation ITU-R P.1411-8, "*Propagation data and prediction methods for the planning of short-range outdoor radiocommunication systems and radio local area networks in the frequency range 300 MHz to 100 GHz*". This recommendation provides guidance on outdoor short range (less than 1km) for both line-of-sights (LoS) and non-line-of-sight (NLoS) environments. In particular, we are interested in the over rooftop propagation described in section 4.2.

Signals can arrive at the device by diffraction mechanisms or by multipath that could be the result of a combination of diffraction and reflection mechanisms.

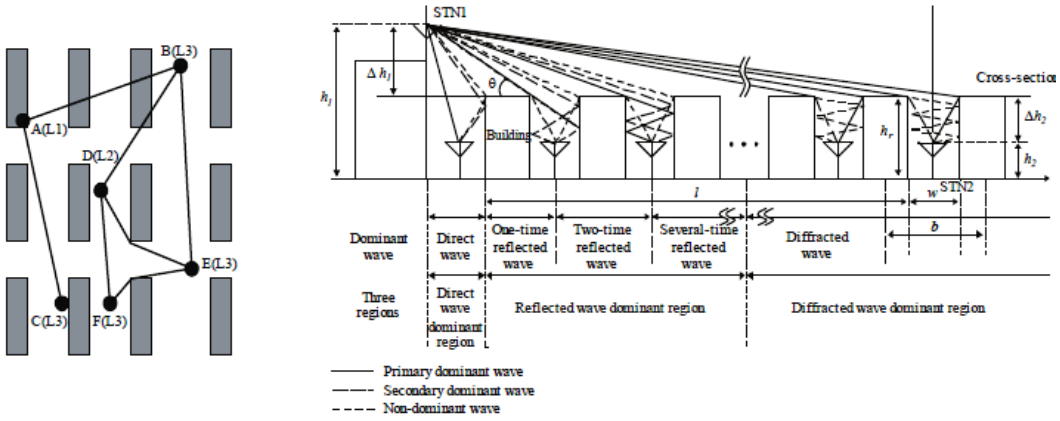

Figure 3.4 Typical propagation situation in urban areas (left) and NLoS case (right) (ITU-R P. 1411-01/02)

This model is defined for paths A to B and D to B, as depicted in figure 3.4 and is valid within the followings:

- h_1 (height of the eNB, that is the antenna electrical center): 4 to 50m;
- h_2 (height of the UE): 1 to 3m;
- f (frequency): 800 to 5000MHz;
- d (distance): 20 to 5000m, even if this recommendation is intended for distances up to 1km.

Note that we can use this model since we assume that all the roof-tops heights differ only by an amount less than the first Fresnel-zone radius over a path of length *l*. The loss between isotropic antennas is expressed as the sum of free-space loss L_{bf}, the diffraction loss from roof-top to street L_{rts} and the reduction due to multiple screen diffraction L_{msd}. The first two terms are independent of the RBS antenna height, while the third depends on it. In general, we have:

$$L_{NLoS} = \begin{cases} L_{bf} + L_{rts} + L_{msd} & \text{for} \quad L_{rts} + L_{msd} > 0 \\ L_{bf} & \text{for} \quad L_{rts} + L_{msd} \leq 0 \end{cases} \tag{3.2}$$

The free-space loss is given by:

$$L_{bf} = 32.4 + 20\log(d/1000) + 20\log(f) \tag{3.3}$$

where d is the path length in meters and f is the frequency in MHz.

The diffraction loss describes the coupling of the wave that propagates along the multiple-screen path into the street. It considers the street width w and orientation with respect to the direct path φ:

$$L_{rts} = -8.2 - 10\log(w) + 10\log(f) + 20\log(\Delta h_2) + L_{ori} \tag{3.4}$$

L_{ori} is the street orientation correction factor, which considers the effects of roof-top-to-street-diffraction into streets that are not perpendicular to the direction of propagation:

$$L_{ori} = \begin{cases} -10 + 0.54\varphi & \text{for} \quad 0° \leq \varphi < 35° \\ 2.5 + 0.075(\varphi - 35) & \text{for} \quad 35° \leq \varphi < 55° \\ 4.0 - 0.114(\varphi - 55) & \text{for} \quad 55° \leq \varphi < 90° \end{cases} \tag{3.5}$$

where $\Delta h_2 = h_r - h_2$ and h_r is the average height of buildings. Note that since each site is divided in three sectors, the maximum φ is 60°.

L_{ori} takes into account the roof-top-to-street diffraction for those streets that are not perpendicular to the direction of propagation.

The multiple screen diffraction loss depends on the antenna height relative to the building heights and on the incidence angle. The criterion for grazing incidence is the so called "settled field distance" d_s:

$$d_s = \frac{\lambda d^2}{\Delta h_1^2} \tag{3.6}$$

where $\Delta h_1 = h_1 - h_r$.

For the calculation of L_{msd}, d_s is compared to the distance l over which the buildings extend. The procedure described below is used to remove any discontinuity between the models used when the length of the building is greater or less than d_s.

$$L_{msd} = \begin{cases} -\tanh\left(\frac{\log(d) - \log(d_{bp})}{\chi}\right) \cdot (L1_{msd}(d) - L_{mid}) + L_{mid} & \text{for } l > d_s \text{ and } dh_{bp} > 0 \\ tanh\left(\frac{log(d) - log(d_{bp})}{\chi}\right) \cdot (L2_{msd}(d) - L_{mid}) + L_{mid} & \text{for } l \leq d_s \text{ and } dh_{bp} > 0 \\ L2_{msd}(d) & \text{for } dh_{bp} = 0 \\ L1_{msd}(d) - \tanh\left(\frac{\log(d) - \log(d_{bp})}{\zeta}\right) \cdot (L_{upp} - L_{mid}) - L_{upp} + L_{mid} & \text{for } l > d_s \text{ and } dh_{bp} < 0 \\ L2_{msd}(d) + tanh\left(\frac{log(d) - log(d_{bp})}{\zeta}\right) \cdot (L_{mid} - L_{low}) + L_{mid} - L_{low} & \text{for } l \leq d_s \text{ and } dh_{bp} < 0 \end{cases} \quad (3.7)$$

where

$$dh_{bp} = L_{upp} - L_{low}$$
$$\zeta = (L_{upp} - L_{low}) \cdot \upsilon$$
$$L_{mid} = \frac{L_{upp} + L_{low}}{2}$$
$$L_{upp} = L1_{mid}(d_{bp})$$
$$L_{low} = L2(d_{bp})$$
$$d_{bp} = |\Delta h_1| \sqrt{\frac{1}{\lambda}}$$
$$\upsilon = 0.0417$$
$$\chi = 0.1$$

With refer to (3.7), since we are in a dense urban environment, the building extension l can be considered infinite so that we take into account only those terms with $l > d_s$.

Furthermore, the individual model losses are defined as follows:

- Calculation of $L1_{msd}$ for $l > d_s$

$$L1_{msd}(d) = L_{bsh} + k_a + k_d \log\left(\frac{d}{1000}\right) + k_f \log(f) - 9\log(b) \quad (3.8)$$

where L_{bsh} is a loss term that depends on the antenna height

$$L_{bsh} = \begin{cases} -18\log(1 + \Delta h_1) & \text{for } h_1 > h_r \\ 0 & \text{for } h_1 \leq h_r \end{cases} \quad (3.8.1)$$

and

$$k_a = \begin{cases} 71.4 & \text{for } h_1 > h_r \text{ and } f > 2000MHz \\ 73 - 0.8\Delta h_1 & \text{for } h_1 \leq h_r, f > 2000MHz \text{ and } d \geq 500m \\ 73 - 1.6\Delta h_1 \frac{d}{1000} & \text{for } h_1 \leq h_r, f > 2000MHz \text{ and } d < 500m \\ 54 & \text{for } h_1 > h_r \text{ and } f \leq 2000MHz \\ 54 - 0.8\Delta h_1 & \text{for } h_1 \leq h_r, f \leq 2000MHz \text{ and } d \geq 500m \\ 54 - 1.6\Delta h_1 \frac{d}{1000} & \text{for } h_1 \leq h_r, f \leq 2000MHz \text{ and } d < 500m \end{cases} \quad (3.8.2)$$

$$k_d = \begin{cases} 18 & \text{for } h_1 > h_r \\ 18 - 15\frac{\Delta h_1}{h_r} & \text{for } h_1 \leq h_r \end{cases} \quad (3.8.3)$$

$$k_f = \begin{cases} -8 & \text{for } f > 2000MHz \\ -4 + 0.7\left(\frac{f}{925} - 1\right) & \text{for medium sized city and suburban centers with medium tree density and } f \leq 2000MHz \\ -4 + 1.5\left(\frac{f}{925} - 1\right) & \text{for metropolitan centers and } f \leq 2000MHz \end{cases} \quad (3.8.4)$$

- Calculation of $L2_{msd}$ for $l<d_s$ (in this it is necessary to make a further distinction according to the relative heights of the antenna and the roof-tops)

$$L2_{msd}(d) = -10\log(Q_M^2) \quad (3.9)$$

where

$$Q_M = \begin{cases} 2.35\left(\frac{\Delta h_1}{d}\sqrt{\frac{b}{\lambda}}\right)^{0.9} & \text{for } h_1 > h_r + \delta h_u \\ \frac{b}{d} & \text{for } h_1 \leq h_r + \delta h_u \text{ and } h_1 \geq h_r + \delta h_l \\ \frac{b}{2\pi d}\sqrt{\frac{\lambda}{\rho}}\left(\frac{1}{\theta} - \frac{1}{2\pi+\theta}\right) & \text{for } h_1 < h_r + \delta h_l \end{cases} \quad (3.9.1)$$

and

$$\theta = \arctan\left(\frac{\Delta h_1}{b}\right)$$

$$\rho = \sqrt{\Delta h_1^2 + b^2}$$

$$\delta h_u = 10^{-log\left(\sqrt{\frac{b}{\lambda}}\right) - \frac{log(d)}{9} + \frac{10}{9}log\left(\frac{b}{2.35}\right)}$$

$$\delta h_l = \frac{0.00023b^2 - 0.1827b - 9.4978}{(\log f)^{2.938}} + 0.000781b + 0.06923$$

where b is the average building separation in meters.

Additional losses are introduced by the presence of vegetation. Two major mechanism can be identified:

- Propagation through trees;
- Propagation over trees.

The first mechanism predominates when the antennas are below tree-tops, while the latter is more significant for geometries where one antenna is located much higher than the others. Then, we are more interested in the second case, which is also the simplest: in fact, this propagation mode can be modeled by using an ideal knife-edge diffraction model as reported in ITU-R P.526.

The whole model is a function of two random variables, then it can be described as a random variable itself. Since the variables are independent it is possible to analyze each contribution to the total path loss separately. First, we provide a brief theory recall.

Given a random variable x, with density function $f_X(x)$, let $y=g(x)$ be its correspondence. Now, we want to determine the probability distribution $f_Y(y)$. If g is a monotonically increasing (or decreasing) and differentiable function we have

$$f_y(y)dy = f_x(x)dx \tag{3.10}$$

and for differentiability hypothesis we can write

$$dy = g'(x)dx \tag{3.11}$$

so that we finally have

$$f_y(y)g'(x)dx = f_x(x)dx$$

$$f_y(y) = \frac{f_x(x)}{g'(x)} \tag{3.12}$$

So, we divide the terms depending on distance d, L_{bf} and L_{msd}, from that depending on the orientation φ, L_{rts}.

First, we study this last:

$$L_{rts} = -8.2 - 10\log(w) + 10\log(f) + 20\log(\Delta h_2) + L_{ori}$$

$$L_{ori} = \begin{cases} -10 + 0.354\varphi & for\ 0^\circ < \varphi < 35^\circ \\ 2.5 + 0.075(\varphi - 35) & for\ 35^\circ \le \varphi \le 55^\circ \\ 4.0 - 0.114(\varphi - 55) & for\ 55^\circ < \varphi \le 90^\circ \end{cases}$$

From these formulas, we can see that the only term depending on φ is L_{ori}. Since it is a piecewise function, we need to analyze each sub-term. First, we linearize L_{rts}:

$$\mathcal{L}_{rts} = 10^{-\frac{8.2}{10}} \frac{f}{w} \Delta h_2^2\, 10^{\frac{L_{ori}}{10}} = T\, 10^{\frac{L_{ori}}{10}} \tag{3.13}$$

where:

$$T = 10^{-\frac{8.2}{10}} \frac{f}{w} \Delta h_2^2$$

To evaluate the overall probability density function $f_{\mathcal{L}_{rts}}(\mathcal{L}_{rts})$ we have to verify that the integral of the probability density function (pdf) over the considered range $\varphi = [-60^\circ; +60^\circ]$ is one. Then the sum of the pdf integrals corresponding to each sub-term must be one.

The first sub-term is defined for $0^\circ < \varphi < 35^\circ$ and the corresponding probability density function is

$$f_{\varphi}(\varphi) = \frac{1}{\varphi_{\max 1} - \varphi_{\min 1}} = \frac{1}{35} \tag{3.14}$$

and, from (3.5) we have

$$L_{ori} = -10 + 0.354\varphi$$

then

$$\mathcal{L}_{rts} = T\ 10^{-1}\ 10^{0.0354\varphi} = T' 10^{0.0354\varphi} \tag{3.15}$$

from here, we get:

$$\varphi = \frac{\log\left(\frac{\mathcal{L}_{rts}}{T'}\right)}{0.0354} = \frac{\log(\mathcal{L}_{rts}) - \log(T')}{0.0354} \tag{3.15.1}$$

so, from (3.11) we need to evaluate

$$g'(\varphi) = \frac{d\varphi}{d\mathcal{L}_{rts}} \stackrel{\text{def}}{=} g'(\mathcal{L}_{rts})$$

$$g'(\mathcal{L}_{rts}) = \frac{1}{0.0354}\ \frac{\log(e)}{\mathcal{L}_{rts}} \tag{3.16}$$

and then:

$$f_{\mathcal{L}_{rts}}(\mathcal{L}_{rts}) = \beta_1 \frac{1}{35}\ \frac{0.0354}{\log(e)}\ \mathcal{L}_{rts} = \beta_1 \gamma_1 \mathcal{L}_{rts} \tag{3.17}$$

where:

$$\gamma_1 = \frac{1}{35}\ \frac{0.0354}{\log(e)}$$

β_1 is a normalization term that we have to introduce since the original pdf is uniform: in this way, we force the integral of $f_{\mathcal{L}_{rts}}(\mathcal{L}_{rts})$ to be equal to the corresponding sub-range

$$\int_{\mathcal{L}_{rts\,\min 1}}^{\mathcal{L}_{rts\,\max 1}} f_{\mathcal{L}_{rts}}(\mathcal{L}_{rts})\, d\mathcal{L}_{rts} = \frac{35}{120} \tag{3.18}$$

$$\mathcal{L}_{rts\,\min 1} = \mathcal{L}_{rts}|_{\varphi=0^\circ} = 10^{-\frac{8.2}{10}}\ \frac{f}{w}\ \Delta h_2^2\ 10^{\frac{-10+0.354\varphi}{10}}\Big|_{\varphi=0^\circ} = 10^{-1.82}\ \frac{f}{w}\ \Delta h_2^2$$

$$\mathcal{L}_{rts\,\max 1} = \mathcal{L}_{rts}|_{\varphi=35^\circ} = 10^{-\frac{8.2}{10}}\ \frac{f}{w}\ \Delta h_2^2\ 10^{\frac{-10+0.354\varphi}{10}}\Big|_{\varphi=35^\circ} = 10^{-0.581}\ \frac{f}{w}\ \Delta h_2^2$$

then, substituting them into (3.18):

$$\int_{\mathcal{L}_{rts\,\min 1}}^{\mathcal{L}_{rts\,\max 1}} \beta_1\gamma_1\mathcal{L}_{rts}\,d\mathcal{L}_{rts} = \frac{1}{2}\beta_1\gamma_1\left[{\mathcal{L}_{rts}}^2\right]_{\mathcal{L}_{rts\,\min 1}}^{\mathcal{L}_{rts\,\max 1}}$$

$$= \beta_1 \frac{1}{70}\,\frac{0.0354}{\log(e)}\left[\left(\frac{10^{-0.581} f\,\Delta h_2^2}{w}\right)^2 - \left(\frac{10^{-1.82} f\,\Delta h_2^2}{w}\right)^2\right]$$

$$= \beta_1 \frac{1}{70}\,\frac{0.0354}{\log(e)}\frac{f^2\,\Delta h_2^4}{w^2}\;0.0386 = \beta_1 \frac{4.494}{10^5}\,\frac{f^2\,\Delta h_2^4}{w^2} \triangleq \frac{35}{120}$$

$$\Rightarrow \beta_1 = \frac{35}{120}\frac{10^5}{4.494}\,\frac{w^2}{f^2\,\Delta h_2^4} \cong 6.5\cdot 10^3\,\frac{w^2}{f^2\,\Delta h_2^4} \tag{3.19}$$

$$\Rightarrow f_{\mathcal{L}_{rts}}(\mathcal{L}_{rts}) = 6.5\cdot 10^3\,\frac{w^2}{f^2\,\Delta h_2^4}\,\frac{1}{35}\,\frac{0.0354}{\log(e)}\,\mathcal{L}_{rts} \cong 15.14\frac{w^2}{f^2\,\Delta h_2^4}\mathcal{L}_{rts} \tag{3.20}$$

The second sub-term is defined for $35^\circ < \varphi < 55^\circ$ and the corresponding probability density function is:

$$f_\varphi(\varphi) = \frac{1}{\varphi_{\max 2} - \varphi_{\min 2}} = \frac{1}{20} \tag{3.21}$$

And, from (3.5)

$$L_{ori} = 2.5 + 0.075(\varphi - 35) = 0.075\varphi - 0.0125$$

then

$$\mathcal{L}_{rts} = T\;10^{-0.00125}\;10^{0.0075\varphi} = T''10^{0.0075\varphi} \tag{3.22}$$

From here, we get:

$$\varphi = \frac{\log\left(\frac{\mathcal{L}_{rts}}{T''}\right)}{0.0075} = \frac{\log(\mathcal{L}_{rts}) - \log(T'')}{0.0075} \tag{3.22.1}$$

$$g'(\mathcal{L}_{rts}) = \frac{1}{0.0075}\,\frac{\log(e)}{\mathcal{L}_{rts}} \tag{3.23}$$

and then:

$$f_{\mathcal{L}_{rts}}(\mathcal{L}_{rts}) = \beta_2\frac{1}{20}\,\frac{0.0075}{\log(e)}\,\mathcal{L}_{rts} = \beta_2\gamma_2\mathcal{L}_{rts} \tag{3.24}$$

where:

$$\gamma_2 = \frac{1}{20}\,\frac{0.0075}{\log(e)}$$

β_2 is the normalization term.

$$\int_{\mathcal{L}_{rts\,\min 2}}^{\mathcal{L}_{rts\,\max 2}} f_{\mathcal{L}_{rts}}(\mathcal{L}_{rts})\,d\mathcal{L}_{rts} = \frac{20}{120} = \frac{1}{6} \tag{3.25}$$

$$\mathcal{L}_{rts\,\min 2} = \mathcal{L}_{rts}|_{\varphi=35^\circ} = 10^{-\frac{8.2}{10}}\,\frac{f}{w}\,\Delta h_2^2\;10^{\frac{0.075\varphi-0.0125}{10}}\Big|_{\varphi=35^\circ} = 10^{-0.559}\,\frac{f}{w}\,\Delta h_2^2$$

$$\mathcal{L}_{rts\,\max 2} = \mathcal{L}_{rts}|_{\varphi=55^\circ} = 10^{-\frac{8.2}{10}}\,\frac{f}{w}\,\Delta h_2^2\;10^{\frac{0.075\varphi-0.0125}{10}}\Big|_{\varphi=55^\circ} = 10^{-0.409}\,\frac{f}{w}\,\Delta h_2^2$$

then, from (3.25):

$$\int_{\mathcal{L}_{rts\,\min 2}}^{\mathcal{L}_{rts\,\max 2}} \beta_2\gamma_2\mathcal{L}_{rts}\,d\mathcal{L}_{rts} = \frac{1}{2}\beta_2\gamma_2\left[{\mathcal{L}_{rts}}^2\right]_{\mathcal{L}_{rts\,\min 2}}^{\mathcal{L}_{rts\,\max 2}} = \beta_2\frac{1}{40}\frac{0.0075}{\log(e)}\frac{f^2\,\Delta h_2^4}{w^2}\,0.704$$

$$= \beta_2\frac{3.04}{10^4}\frac{f^2\,\Delta h_2^4}{w^2} \triangleq \frac{1}{6}$$

$$\Rightarrow \beta_2 = \frac{1}{6}\frac{10^4}{3.04}\frac{w^2}{f^2\,\Delta h_2^4} \cong 548.25\frac{w^2}{f^2\,\Delta h_2^4} \tag{3.26}$$

$$\Rightarrow f_{\mathcal{L}_{rts}}(\mathcal{L}_{rts}) = 548.25\frac{w^2}{f^2\,\Delta h_2^4}\frac{1}{20}\frac{0.0075}{\log(e)}\,\mathcal{L}_{rts} \cong 0.47\frac{w^2}{f^2\,\Delta h_2^4}\mathcal{L}_{rts} \tag{3.27}$$

The last sub-term is defined for $55^\circ < \varphi < 60^\circ$ and the corresponding probability density function is:

$$f_\varphi(\varphi) = \frac{1}{\varphi_{\max 3} - \varphi_{\min 3}} = \frac{1}{5} \tag{3.28}$$

From (3.5)

$$L_{ori} = 4.0 - 0.114(\varphi - 55) = 10.27 - 0.114\varphi$$

then

$$\mathcal{L}_{rts} = T\;10^{1.027}\;10^{-0.0114\varphi} = T'''10^{-0.0114\varphi} \tag{3.29}$$

$$\varphi = -\frac{\log\left(\frac{\mathcal{L}_{rts}}{T'''}\right)}{0.0114} = \frac{\log(T''') - \log(\mathcal{L}_{rts})}{0.0114} \tag{3.29.1}$$

In this case, since the function is decreasing, we have to consider in $g'(x)$ the modulus of $\frac{dy}{dx}$:

$$g'(\mathcal{L}_{rts}) = \frac{1}{0.0114}\frac{\log(e)}{\mathcal{L}_{rts}} \tag{3.30}$$

and then:

$$f_{\mathcal{L}_{rts}}(\mathcal{L}_{rts}) = \beta_3\frac{1}{5}\frac{0.0114}{\log(e)}\,\mathcal{L}_{rts} = \beta_3\gamma_3\mathcal{L}_{rts} \tag{3.31}$$

where:

$$\gamma_3 = \frac{1}{5}\frac{0.0114}{\log(e)}$$

β_3 is the normalization term.

$$\int_{\mathcal{L}_{rts\,\min 3}}^{\mathcal{L}_{rts\,\max 3}} f_{\mathcal{L}_{rts}}(\mathcal{L}_{rts})\,d\mathcal{L}_{rts} = \frac{5}{120} \tag{3.32}$$

$$\mathcal{L}_{rts\,\min 3} = \mathcal{L}_{rts}|_{\varphi=60^\circ} = 10^{-\frac{8.2}{10}}\frac{f}{w}\Delta h_2^2\,10^{\frac{10.27-0.114\varphi}{10}}\Big|_{\varphi=60^\circ} = 10^{-0.48}\frac{f}{w}\Delta h_2^2$$

$$\mathcal{L}_{rts\,\max 3} = \mathcal{L}_{rts}|_{\varphi=55^\circ} = 10^{-\frac{8.2}{10}}\frac{f}{w}\Delta h_2^2\,10^{\frac{10.27-0.114\varphi}{10}}\Big|_{\varphi=55^\circ} = 10^{-0.42}\frac{f}{w}\Delta h_2^2$$

$$\int_{\mathcal{L}_{rts\min 3}}^{\mathcal{L}_{rts\max 3}} \beta_3\gamma_3\mathcal{L}_{rts}\,d\mathcal{L}_{rts} = \frac{1}{2}\beta_3\gamma_3\left[{\mathcal{L}_{rts}}^2\right]_{\mathcal{L}_{rts\min 3}}^{\mathcal{L}_{rts\max 3}} = \beta_3\frac{1}{10}\frac{0.0114}{\log(e)}\frac{f^2\,\Delta h_2^4}{w^2} \quad (0.035)$$

$$= \beta_3\frac{9.18}{10^5}\frac{f^2\,\Delta h_2^4}{w^2} \triangleq \frac{5}{120}$$

$$\Rightarrow \beta_3 = \frac{5}{120}\frac{10^5}{9.18}\frac{w^2}{f^2\,\Delta h_2^4} \cong 453.89\frac{w^2}{f^2\,\Delta h_2^4} \quad (3.33)$$

$$\Rightarrow f_{\mathcal{L}_{rts}}(\mathcal{L}_{rts}) = 453.89\frac{w^2}{f^2\,\Delta h_2^4}\frac{1}{5}\frac{0.0114}{\log(e)}\,\mathcal{L}_{rts} \cong 2.38\frac{w^2}{f^2\,\Delta h_2^4}\mathcal{L}_{rts} \quad (3.34)$$

Finally, since we are working only on a range of 60°, the sum of the three pdf integrals will be equal to $\frac{1}{2}$:

$$\int_{\mathcal{L}_{rts\min 1}}^{\mathcal{L}_{rts\max 1}} 15.14\frac{w^2}{f^2\,\Delta h_2^4}\mathcal{L}_{rts}\,d\mathcal{L}_{rts} + \int_{\mathcal{L}_{rts\min 2}}^{\mathcal{L}_{rts\max 2}} 0.47\frac{w^2}{f^2\,\Delta h_2^4}\mathcal{L}_{rts}\,d\mathcal{L}_{rts}$$
$$+ \int_{\mathcal{L}_{rts\min 3}}^{\mathcal{L}_{rts\max 3}} 2.38\frac{w^2}{f^2\,\Delta h_2^4}\mathcal{L}_{rts}\,d\mathcal{L}_{rts} \triangleq \frac{1}{2}$$

Now, we take in account the pathloss terms depending on the distance d, from (3.3) and (3.7):

$$L_{bf} = 32.4 + 20\log\left(\frac{d}{1000}\right) + 20\log(f)$$

$$L_{msd} = \begin{cases} -\tanh\left(\frac{\log(d)-\log(d_{bp})}{\chi}\right)(L1_{msd}(d) - L_{mid}) + L_{mid} & \text{for } l > d_s \text{ and } dh_{bp} > 0 \\ L2_{msd}(d) & \text{for } dh_{bp} = 0 \\ L1_{msd}(d) - \tanh\left(\frac{\log(d)-\log(d_{bp})}{\zeta}\right)\cdot\left(L_{upp} - L_{mid}\right) - L_{upp} + L_{mid} & \text{for } l > d_s \text{ and } dh_{bp} < 0 \end{cases}$$

In particular, we are interested only in the sub-terms of L_{msd} where $l > d_s$, since we can consider the building extension infinite. First, we linearize both functions:

$$\mathcal{L}_{bf} = \left(\frac{4\pi}{c}df\right)^2 = Kd^2$$

where:

$$K = \left(\frac{4\pi}{c}f\right)^2$$

and:

$$\mathcal{L}_{msd} = \begin{cases} 10^{\frac{-\tanh\left(\frac{\log(d)-\log(d_{bp})}{\chi}\right)(L1_{msd}(d)-L_{mid})}{10}}10^{\frac{L_{mid}}{10}} & \text{for } dh_{bp} > 0 \\ 10^{\frac{L2_{msd}(d)}{10}} & \text{for } dh_{bp} = 0 \\ 10^{\frac{L1_{msd}(d)}{10}}10^{\frac{-\tanh\left(\frac{\log(d)-\log\left(d_{bp}\right)}{\zeta}\right)(L_{upp}-L_{mid})}{10}}10^{\frac{-L_{upp}}{10}}10^{\frac{L_{mid}}{10}} & \text{for } dh_{bp} < 0 \end{cases}$$

The whole pathloss term depending on d is:

$$\mathcal{L}_d(d) = \mathcal{L}_{msd}\mathcal{L}_{bf} \tag{3.35}$$

In order to give a numerical example as well as an approximated study of this function we plot it with the following fixed parameters:

- Frequency: *f=800MHz*
- Average building level: *b=30m*
- Distance between the average building level and the eNB: Δh_1*=2m*

Then, the (3.7) becomes:

$$L_d(d) = 32.4 + 20\log(d) + 20\log(800) - \tanh\left(\frac{\log(d) - 0.51}{0.1}\right)(19.9 + 18\log(d) + 3.7) - 3.7$$

and its logarithmic and linear behavior for $dh_{bp} > 0$ are shown in figure 3.5. Note that for $dh_{bp} < 0$ the behavior is the same.

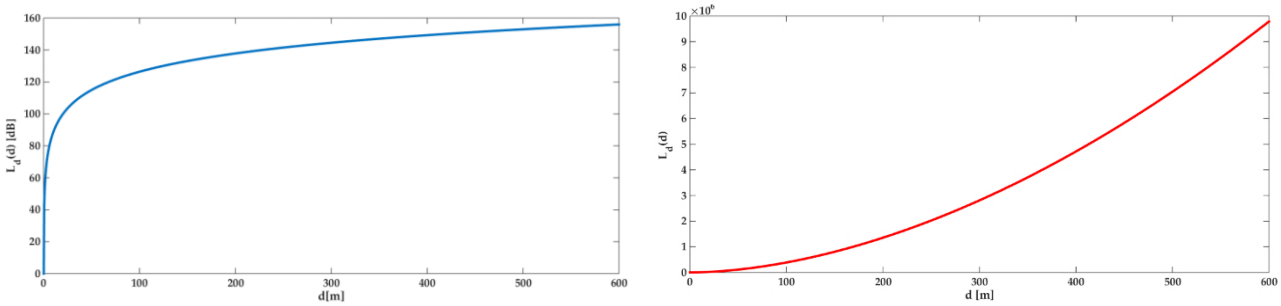

Figure 3.5 Qualitative behavior in log scale (left) and in linear scale (right) for $dh_{bp}>0$

As we can see in the figures, both in logarithmic and linear behaviors, the dominant term is the one referring to the free-space loss. It is impossible to make the calculus to get the pdf of this function in closed form, due to the high complexity in evaluating the inverse function of the pathloss. For this reason, we need to approximate it with an even function like the one we propose (in linear scale):

$$\hat{\mathcal{L}}_d(d) = Ad^4 + Bd^2$$

where A and B are constants that include all the constant terms in $\mathcal{L}_d(d)$. Once the constants are determined, it is possible to develop the same calculus made for the pathloss term depending on the orientation and to obtain a qualitative probability density function $f_{\hat{\mathcal{L}}_d}(\hat{\mathcal{L}}_d)$. The calculus is based on (3.10-12)

$$f_d(d) = \frac{1}{d_{max} - d_{min}}$$

$$g(\hat{\mathcal{L}}_d) = \frac{1}{\sqrt{2}}\left[\frac{B\sqrt{4A\hat{\mathcal{L}}_d + B^2} - 2A\hat{\mathcal{L}}_d - B^2}{2\hat{\mathcal{L}}_d{}^2\sqrt{4A\hat{\mathcal{L}}_d + B^2}\sqrt{\frac{\sqrt{4A\hat{\mathcal{L}}_d+B^2}-B}{\hat{\mathcal{L}}_d}}}\right]$$

$$f_{\hat{\mathcal{L}}_d}(\hat{\mathcal{L}}_d) = \frac{\sqrt{2}}{d_{max} - d_{min}} \frac{2\hat{\mathcal{L}}_d{}^2\sqrt{4A\hat{\mathcal{L}}_d + B^2}\sqrt{\frac{\sqrt{4A\hat{\mathcal{L}}_d+B^2}-B}{\hat{\mathcal{L}}_d}}}{B\sqrt{4A\hat{\mathcal{L}}_d + B^2} - 2A\hat{\mathcal{L}}_d - B^2}$$

The overall pathloss $\mathcal{L}_{NLoS}(d, \varphi)$ is

$$\mathcal{L}_{NLoS}(d, \varphi) = \mathcal{L}_d(d)\mathcal{L}_{rts}(\varphi) \tag{3.38}$$

This term is the product of two independent random process and we need to evaluate its pdf. To do it, we follow the theory:

If X and Y are two random variables, let Z be their product $Z=XY$. Then, we may find the product distribution as follows:

$$f_Z(z) = \int_{-\infty}^{\infty} \frac{1}{|u|} f_X(u) f_Y\left(\frac{z}{u}\right) du \tag{3.39}$$

To demonstrate it, we need to suppose that the distribution of X is continuous in the origin

$$P(Z \le z) = P(XY \le z) = P\left(Y \le \tfrac{z}{X} \middle| X > 0\right) P(X > 0) + P\left(Y \ge \tfrac{z}{X} \middle| X > 0\right) P(X > 0)$$

$$= \int_0^{\infty} P\left(Y \le \frac{z}{u}\right) f_X(u) du + \int_{-\infty}^{0} P\left(Y \ge \frac{z}{u}\right) f_X(u) du$$

Then, to get the pdf, we need to derivate

$$f_Z(z) = \int_0^{\infty} \frac{1}{u} f_Y\left(\frac{z}{u}\right) f_X(u) du + \int_{-\infty}^{0} -\frac{1}{u} f_Y\left(\frac{z}{u}\right) f_X(u) du = \int_{-\infty}^{\infty} \frac{1}{|u|} f_X(u) f_Y\left(\frac{z}{u}\right) du$$

obtaining (3.39).

In our case, we have

$$f_{\mathcal{L}_{NLoS}}(\mathcal{L}_{NLoS}) = \int_{-\infty}^{\infty} \frac{1}{|u|} f_{\mathcal{L}_d}(u) f_{\mathcal{L}_{rts}}\left(\frac{\mathcal{L}_{NLoS}}{u}\right) du \tag{3.40}$$

Once the propagation loss is determined, we can get the received power for every single point of the site we are considering. Along with noise power and interference, it is one of the factors characterizing the Signal-To-Interference-Plus-Noise-Ratio:

$$SINR(x) = \frac{P_R(x)}{I + N}$$

SINR, as we know from the theory, is the fundamental parameter for the Channel Quality Indicator (CQI) which is determined by each vendor in its own way.

Now, once the CQI is evaluated, we can get the correspondent spectral efficiency, as shown in table 3.1 in the following page which refers to 3GPP TS 36.213 Release 13.

CQI index	CQI index in previous table	Modulation	Code rate x 1024	Spectral efficiency
0	0	out of range		
1	1	QPSK	78	0,1523
2	2	QPSK	120	0,2344
3	4	QPSK	308	0,6016
4	6	QPSK	602	1,1758
5	8	16QAM	490	1,9141
6	9	16QAM	616	2,4063
7	10	64QAM	466	2,7305
8	11	64QAM	567	3,3223
9	12	64QAM	666	3,9023
10	13	64QAM	772	4,5234
11	14	64QAM	873	5,1152
12	15	256QAM	711	5,5547
13	-	256QAM	790	6,1719
14	-	256QAM	869	6,7891
15	-	256QAM	948	7,4063

Table 3.1 CQI vs. Spectral Efficiency

Once the spectral efficiency is determined, the Modulation and Coding Scheme assignation depends on the vendor. In fact, it is not standardized by 3GPP and each vendor can propose its own process. So far, there are no proposals, so we proposed ours and integrated it into the code, as we will present later.

The last parameter we are interested in to evaluate the overall throughput is the number of Physical Resource Blocks (PRB) that each device is capable to aggregate. It depends merely on the category and then on carrier aggregation capability. Once again, everything will depend on the position of the UE: for instance, if a Cat16 device is located where all the 4 bands are disposable, it will reach the maximum throughput, whilst if it is located away from the cell, it will not use the highest bands and will not take advantage of its features.

This can be described as well as a random process, as long as we make a further assumption: if we had the (3.40) in closed form we would be able to describe accurately the distribution of the received power and consequently of the SINR. To characterize the

site according to the MCS indices we assume the respective areas to be annular rings as shown in figure 3.6.

Note that ρ_{min} and ρ_{max} are the radii corresponding to the minimum and maximum power associated to the i-th MCS index. Then, the probability that a given user equipment is located into the i-th MCS index area is:

$$P(\rho_{min} \leq d_i \leq \rho_{max}) = \frac{A_{MCS_i}}{A_{tot}} = \frac{\pi(\rho_{max}^2 - \rho_{min}^2)}{\pi(d_{max}^2 - d_{min}^2)} \tag{3.41}$$

From here we can evaluate the probability that a device belonging to a certain category is located in the i-th MCS area:

$$P(UE_k \in A_{MCS_i}) = N_k \frac{A_{MCS_i}}{A_{tot}} = N_k \frac{\rho_{max}^2 - \rho_{min}^2}{d_{max}^2 - d_{min}^2} \tag{3.42}$$

where N_k is the number of devices belonging to Category k (i.e. N_{16} is the number of Cat16 devices). Then, from (3.43) we can get the number of PRBs that can be assigned to the device taken into account.

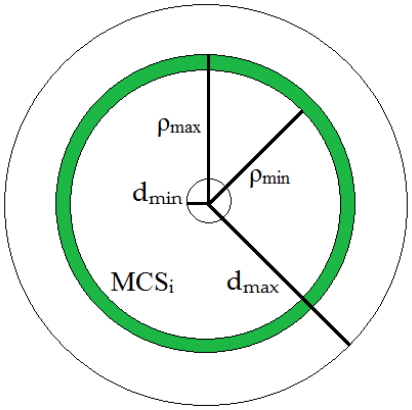

Figure 3.6 MCS_i area

Finally, we can describe the single user throughput as a function of the terms evaluated so far:

$$T_i = F[x_i(t), y_i(t), NPRB_i, \eta_i] \tag{3.43}$$

and the overall throughput is given by

$$T_{tot} = \sum_i T_i(t) \tag{3.44}$$

4 NS-3 Simulator

4.1 Architecture and features

The ns-3 simulator is a discrete-event network simulator whose main target are research and education. It has been developed in an open-source project and provides models of how packet data networks perform. Differently from other simulation tools, it is designed as a set of libraries that can be combined together also with external software libraries. Moreover, there are several animators and data analysis tools that can be used. User programs are mainly written in C++ even if Python can be used as well.

Figure 4.1 Software organization of ns-3 (*nsnam.org*)

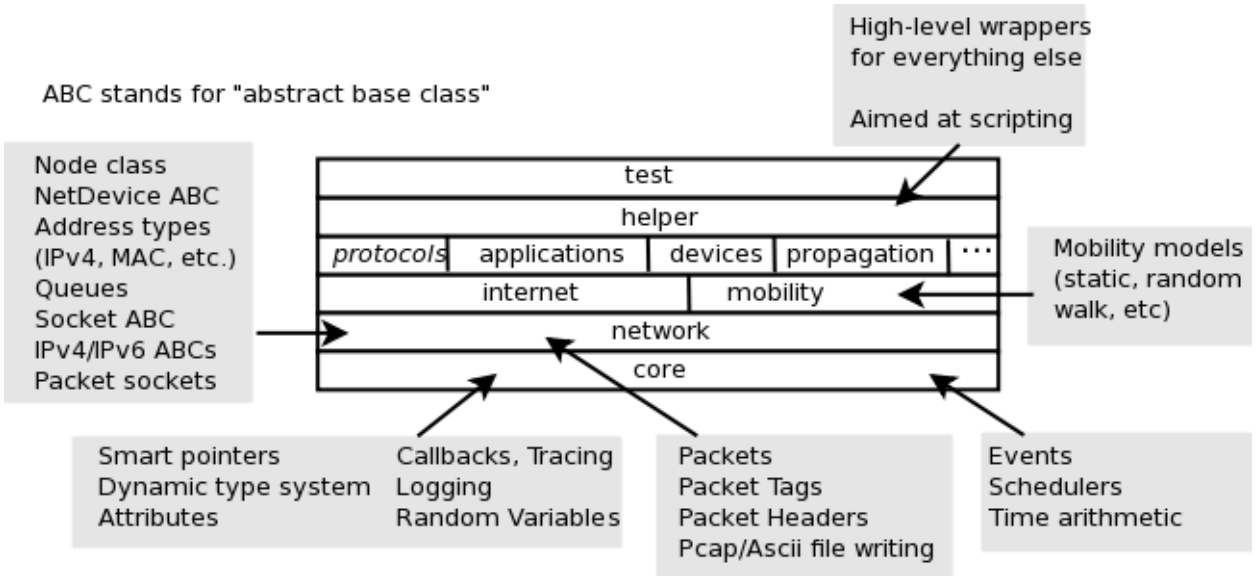

The source code of ns-3 is mostly organized in the directory `src` and is described by fig. 4.1. in general, modules have dependencies only on those beneath them in the figure.

The core of the simulator includes all those components that are common across all protocol, hardware and environmental models. It is implemented in `src/core` while `src/network` contains packets, that are fundamental objects in a network simulator and are independent of specific networks and device models.

From an abstract point of view, the simulation is a sequence of events, sequentially executed; each event can schedule new events, leading to a continuous time flow. Since it is a discrete event simulator, the simulation time advances only when the scheduled event is completed, then it is important to avoid concurrent events.

The main concepts in this simulator are:

- Event
- Node
- NetDevice
- Channel
- Protocol
- Application

Now we will give a brief description of each of the these.

An *event* is something scheduled to happen at a given time. It has a target function and can have parameters. A simulation-wise scheduler takes care of ordering the events and executing them sequentially.

A *node* is an object used to aggregate other objects. It is the representation of a device connected to a network.

A *NetDevice* is the logical representation of a Layer2 communication interface. In ns-3, NetDevice design and functionality are kept as close as possible to the reality by replicating the interface described in the standards.

Channels are the abstract representation of the effect of a given medium on the signal, including the propagation loss and the interference from other sources. The most advanced channels are based on the propagation module that we will describe later.

Protocols represent specific high-level protocol (i.e. IPv6, ICMP). Each protocol is modelled following the standards, so that there should not be differences between the implemented and the real ones.

Applications are simply used to generate traffic according to specific statistical distributions and/or reacting to data reception.

Each ns-3 element can be configured with the *Attributes*, which are the way to change an object property. We can modify both the default behavior of a class or of a single instance.

The simulator is organized in modules, each providing a single functionality or layer. In our case, we are mainly interested in the followings:

- LTE
- Internet

- Application
- Mobility
- Propagation
- FlowMonitor

4.1.1 LTE Module

This module is based on two models, LTE and EPC, as shown in figure 4.2. the first one manages the Radio Protocol stack, while the latter includes core network interfaces, protocols and entities.

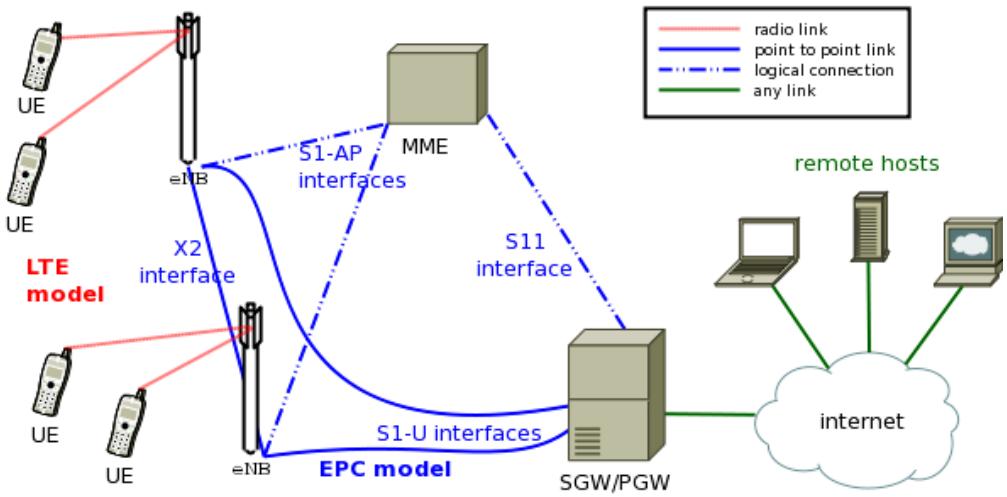

Figure 4.2 Overview of the LTE-EPC simulation model (*nsnam.org*)

The LTE module is definitely the most complex among those implemented in ns-3, so we will give a brief summary of the main functions and of the architecture.

The LTE model is designed to provide the evaluation of the following aspects of LTE systems:

- Radio Resource Management
- QoS-aware Packet Scheduling
- Inter-cell Interference Coordination
- Dynamic Spectrum Access

At the radio level, the granularity of the model is that of the Resource Block which is the minimum level of granularity that must be granted to ensure a correct simulation; in this way, it is possible to model accurately packet scheduling and inter-cell-interference.

The simulator can handle up to tens of eNBs and hundreds of User Equipment and it can configure different cells so that they can use different carrier frequencies and system bandwidths.

The aim of the EPC model is to provide a mean for the simulation of end-to-end IP connectivity over the LTE model. Note that the only Packet Data Network type supported is IPv4 and that the SGW and the PGW functional entities are implemented within a single node. This model must simulate end-to-end performance of realistic applications. Hence, it is possible to use regular applications working both with TCP or UDP. Finally, the model allows the possibility to perform an X2-based handover between two eNBs.

Figure 4.3 represents the end-to-end LTE-EPC data plane protocol stack as it is modeled in the simulator. From here, it is clear that the biggest simplification is the inclusion of the SGW and PGW functionalities within a single node; this leads to the removal of the S5 or S8 interfaces specified by 3GPP. On the other hand, it is evident the presence of both the S1-U and LTE radio protocol stacks as specified by the standard.

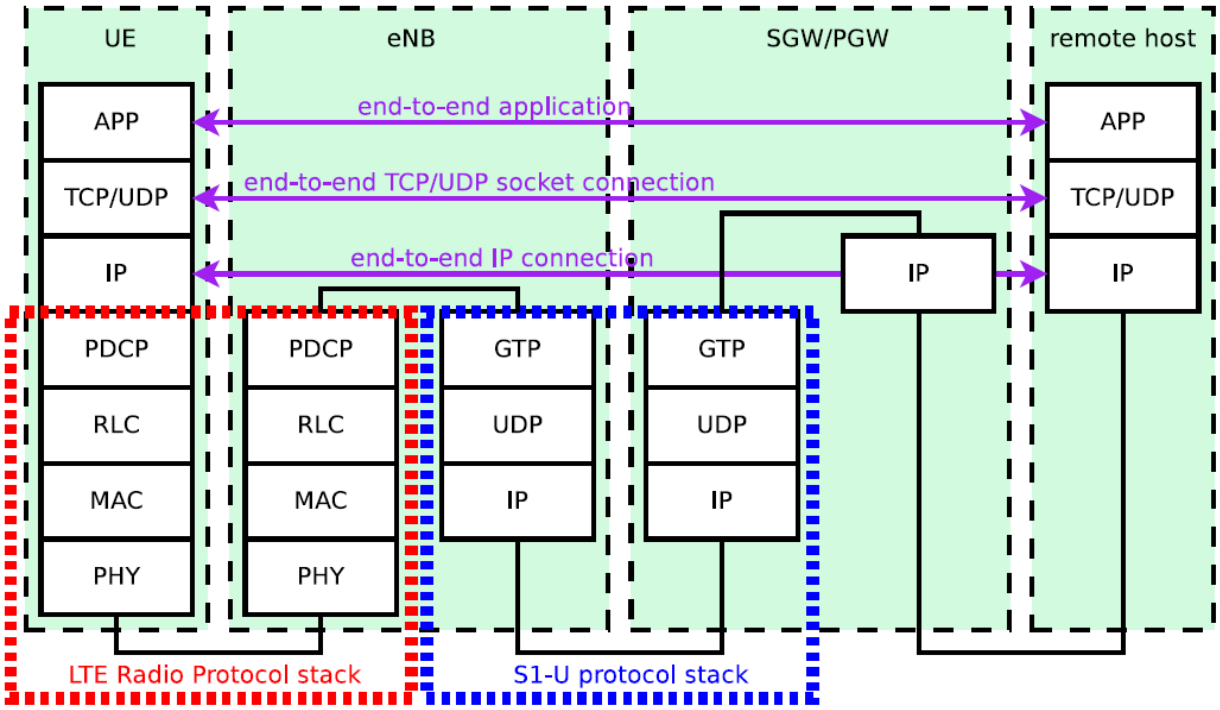

Figure 4.3 LTE-EPC data plane protocol stack (*nsnam.org*)

The physical layer model is very similar to the reality. In our case study, we are interested in the Data PHY Error Model above the others implemented in the LTE Module.

The simulator includes an error model of the data plane (i.e. PDSCH and PUSCH) according to the standard link-to-system mapping (LSM) techniques. The choice is aligned with the standard system simulation methodology of OFDMA radio transmission technology. Thanks to this technique it is possible to maintain a satisfactory level of accuracy and at the same time to limit the computational complexity increase. In particular, the specific LSM method adopted is the one based on the usage of a mutual information metric known as Mutual Information Effective SINR Mapping (MIESM). LSM allows the usage of the Code Block Error Rate curves as the parameter to analyze the performance of a single link. To do this the Vienna LTE Simulator has been used for what concerns the extraction of the link layer and the MIESM.

Note that the module provides the link performance only for what concerns the MCSs, assuming the Effective Code Rate as fixed.

Another model in which we are interested is the Medium Access Control model which is responsible for the Adaptive Modulation and Coding (AMC) and resource allocation.

The simulator provides two AMC models: one is a version proposed by the simulator authors themselves and one based on the physical error model described in the standards. The former is described as follows: let i be a generic user and γ_i be its SINR. The spectral efficiency η_i is evaluated according to:

$$\eta_i = \log_2\left(1 + \frac{\gamma_i}{\Gamma}\right)$$
$$\Gamma = \frac{-\ln(5 \cdot BER)}{1.5}$$
$$BER = 0.00005$$

The spectral efficiency is quantized based on the channel quality indicator (CQI), rounding to the lowest value, and is mapped to the corresponding MCS scheme.

The alternative model is based on the physical error model that adapts the MCS selection to the actual PHY layer performance according to specific CQI report.

The resource allocation in the simulator is managed by the MAC scheduler interface: ns-3 provides several types of scheduler as a set of abstract classes. As we said in Chapter 1, we use the Proportional Fair (PF) Scheduler.

It works by scheduling user when its instantaneous channel quality is high relatively to its own average channel condition over time. Let *i*, *j* denote generic users; let *t* be the subframe index and *k* be the resource block index; let $M_{i,k}(t)$ be MCS usable by user *i* on resource block *k* according to what reported by the AMC model; finally, let *S(M,B)* be the TB size in bits for the case where a number *B* of resource blocks is used. The achievable rate $R_i(k, t)$ in bit/s for user *i* on resource block group *k* at subframe *t* is defined as

$$R_i(k,t) = \frac{S(M_{i,k}(t), 1)}{\tau}$$

where τ is the TTI duration.

Then, the index $\hat{\imath}_k(t)$ to which RBG *k* is assigned at time *t* is determine as follows

$$\hat{\imath}_k(t) = \underset{j=1,\dots,N}{\operatorname{argmax}} \left(\frac{R_j(k,t)}{T_j(t)} \right)$$

where $T_j(t)$ is the past throughput performance perceived by the user *j*. According to the above scheduling algorithm, a user can be allocated to different RBGs, which can be either adjacent or not, depending on the current condition of the channel and the past throughput performance $T_j(t)$ which is determined at the end of the subframe *t* in this way

$$T_j(t) = \left(1 - \frac{1}{\alpha}\right) T_j(t-1) + \frac{1}{\alpha} \hat{T}_j(t)$$

where α is the time constant of the exponential moving average and $\hat{T}_j(t)$ is the actual throughput achieved by the user *i* in the subframe *t*.

4.1.2 Internet Module

The internet module offers several functionalities belonging to the TCP/IP stack. As an example, available models are:

- IP (v4 and v6)
- ICMP (v4 and v6)
- UDP
- TCP (NewReno, Westwood, Westwood+, with more being developed)

Moreover, some routing protocols are included in this module like RIPng or Static Routing. We use this module to configure the IP addresses of the core network and of the devices. The internet module must work in combination with the application module.

4.1.3 Application Module

This module provides the base class for ns-3 applications. They are associated with individual nodes. Each node holds a list of references (smart pointers) to its applications. To create an API, it is necessary to define a socket, that can be both TCP or UDP, in accordance with the transport protocol. The socket is selected by modifying the `PacketSink` module. Then, there are client classes that are used to define the data flow.

4.1.4 Mobility Module

This module includes:

- a set of mobility models used to track and/or maintain the position and speed of an object
- several helper classes which are used to set the position and the mobility of a node.

The initial position of objects is typically set with a `PositionAllocator`. These types of objects will lay out the position on a notional canvas. The `MobilityHelper` combines a mobility model and position allocator, and can be used with a node container to install mobility capability on a set of nodes.

The position of a node can be assigned either randomly or assigning precisely the coordinates. Both these assignations are made with one of the following position allocators:

- ListPositionAllocator
- GridPositionAllocator
- RandomRectanglePositionAllocator
- RandomBoxPositionAllocator
- RandomDiscPositionAllocator
- UniformDiscPositionAllocator

The mobility of a node is described with one the following subclasses:

- ConstantPosition
- ConstantVelocity

- ConstantAcceleration
- GaussMarkov
- Hierarchical
- RandomDirection2D
- RandomWalk2D
- RandomWaypoint
- SteadyStateRandomWaypoint
- Waypoint

4.1.5 Propagation Module

This module defines the interface to model the propagation loss. It calculates the received signal power considering the transmitted power and the mutual positions of the antennas. Several models are implemented, from the simplest ones (free space loss model) to the most complex. Some of these refer to propagation loss models that have been described by ITU, like the one we used for the simulation: `ItuR1411NlosOverRooftopPropagationLossModel`.

Models can be chained in order to combine, for instance, different fading effects. The accurate description of the model will be given later.

4.1.6 Flow Monitor Module

The aim of this module is to provide a flexible system to measure the performance of network protocols. This module can track the packets exchanged by the nodes and can measure several parameters. The statistics collected for each data flow can be exported in XML format. At the moment of writing, this module works only at IP level and can give as output the transmitted and received bytes and packets, the lost packets, the duration of the transmission and the throughput.

4.2 Assumptions and settings

This paragraph is focused on the description of the implementation choices that have been made when simulating, both to lighten the simulation and to face some limitations of the simulator. In fact, the simulator is continuously renewing and enhancing its

features but it doesn't provide the whole LTE-A functionalities. The introduction of 256QAM will be presented in next paragraph, while here we present our implementation of MIMO 4x4 and Carrier Aggregation.

Since we are describing a high dense urban environment, there should be around 500/1000 users per site leading to thousands of UE (considering the five sites). This would lead to a too heavy simulation. In a real network, not all devices transmit data simultaneously, then we can consider a lower number of UE.

As we said in the Introduction, we focus the study on the video streaming application that must grant a minimum data rate of 12Mbps. In real networks, there is a bottleneck at core level in terms of data flow: in fact, for each site there is a limitation at 1Gbps. Then, to further reduce the number of devices to simulate, we augmented the transmitted flow up to 40 Mbps and considered 20 users per site leading to an average maximum system throughput of 800Mbps, which is comparable to the real limit. Note that it is just an average value: most of the users move around the scenario and cannot achieve the maximum data rate.

To set up this data flow we modified some of the Attributes in `udp-client`:

- "`PacketSize`" = 500B
- "`Interval`" = 100μs

Then we have:

$$\frac{500 \cdot 8}{10^{-4}}\left[\frac{b}{s}\right] = 40Mbps$$

which is the data flow we want to transmit.

With this assumption, the simulation doesn't lose in generality: in fact, we are interested in the peak performance of the system and this can be achieved also in this way.

We had to deal with a limitation due to the UDP traffic as implemented in the simulator. In fact, UDP traffic saturates whit data rates higher than 75Mbps. Since there are three eNBs per site, the input data flow would have been 225Mbps which is far away from the 800Mbps that we want to guarantee for each site. The solution of this problem came along with the implementation of carrier aggregation described later.

In *ns-3*, MIMO is not implemented as the use of multiple antennas in transmission and reception. The model is obtained considering the gain that MIMO schemes bring in the system from a statistical point of view. This solution is based on a study conducted by Severine Catreaux et al. in "*Some Results and Insights on the Performance Gains of MIMO Systems*". In the work, the gain is presented as the cumulative distribution function (CDF) of the output SINR for what concerns both SISO and MIMO 2x2 schemes. Then, they compared the output SINR distribution in terms of mean and variance. Therefore, the simulator implements the MIMO model as the gain perceived by the receiver when using a MIMO scheme with respect to the one obtained using SISO one. In this way, the simulation is not very accurate and, above all, there is not the possibility to exploit MIMO 4x4 schemes. In fact, the simulator provides only the following transmission modes:

- Transmission Mode 1: SISO.
- Transmission Mode 2: MIMO Tx Diversity.
- Transmission Mode 3: MIMO Spatial Multiplexity Open Loop.

Then, we propose another technique to implement MIMO, either with 2 or 4 layers. As 3GPP shows in TS 36.213, there are precise translation table when we switch from a single layer to multiple ones. In particular, we focused our attention on tables 7.1.7.2.2-1 and 7.1.7.2.5-1. The former refers to the translation from one-layer to two-layer while the latter refers to the translation to four-layer. Just to give an example, we report an excerpt of the first one.

TBS_L1	**TBS_L2**	**TBS_L1**	**TBS_L2**	**TBS_L1**	**TBS_L2**	**TBS_L1**	**TBS_L2**
1544	3112	2024	4008	2536	5160	3240	6456
1608	3240	2088	4136	2600	5160	3368	6712
1672	3368	2152	4264	2664	5352	3496	6968
1736	3496	2216	4392	2728	5544	3624	7224
1800	3624	2280	4584	2792	5544	3752	7480
1864	3752	2344	4776	2856	5736	3880	7736
1928	3880	2408	4776	2984	5992	4008	7992
1992	4008	2472	4968	3112	6200	4136	8248

Table 4.1 Excerpt of table 7.1.7.2.2-1 from 3GPP TS 36.213

From here, it is evident that the usage of MIMO 2x2 leads to an average doubling of the TBS. Equally, the TBS is quadrupled in presence of MIMO 4x4. This observation of this relationship between the transport block size and the number of layer led us to implement MIMO schemes as the multiplication of the TBS. We adapted the function `GetTbSizeFromMcs` in `LteAmc` so that it returns the TBS doubled (or quadrupled) depending on the MIMO scheme.

As seen in Chapter 2, the four-layer technology is more sensitive to SINR with respect to the two-layer scheme. To regard this aspect, it is useful to evaluate the CQI of each transmission and decide whether to allow the adoption of MIMO 4x4. To do this, we made an *if-clause* inside the function mentioned above.

Our proposal for implementing the Carrier Aggregation is simple: we locate multiple devices or eNBs in the same place and, if necessary, we make them move jointly. This follows the reality: in fact, a device has an antenna for each frequency used to received and/or transmit. One problem would be the unawareness when scheduling resources. Actually, there are two kinds of scheduling procedure: Single-Carrier Scheduler and Cross-Carrier Scheduler. The former is the one used nowadays in real networks and doesn't imply each frequency receiver to be aware one another.

A second problem was the mobility of co-located devices: in fact, we wanted them to move randomly across the scenario. We would have used the `RandomDirection2D` mobility model but in this way the devices wouldn't have moved jointly. The we decided to use the `GaussMarkov` mobility model.

Unlike the other mobility models in ns-3, which are memoryless, the Gauss Markov model has both memory and variability. The tunable alpha parameter determines the amount of memory and randomness in the model. Each object starts with a specific velocity, direction (radians), and pitch angle (radians) equivalent to the mean velocity, direction, and pitch. At each timestep, a new velocity, direction, and pitch angle are generated based upon the previous value, the mean value, and a gaussian random variable. Then, applying this model contemporaneously to the "carrier" devices, we obtain co-located entities that move jointly with a certain randomness.

To be thorough, we report that Carrier Aggregation has been recently introduced in *ns-3* and can be enabled with the command `ns3::LteHelper::UseCa`. The number of component carriers to be used in carrier aggregation can be configured by setting the attribute `NumberOfComponentCarriers`. We decided to implement our proposal in order to solve the problem coming from the saturation of the UDP. In fact, if we use four antennas per sector we have 12 co-located antennas per site each of which can guarantee 75Mbps. Hence, the entire site can provide a 900Mbps data rate, which is enough to satisfy the simulation requirement.

4.3 Changes applied

Three libraries have been modified to adapt the simulator to our needs: `LteEnbRrc`, `LtePhy` and `LteAmc`. The first couple was modified to be able to simulate a higher number of UE, while the last was edited to introduce 256QAM.

In LTE-A real networks, eNBs use Sounding Reference Signals sent by the UE to figure out the channel quality of the uplink path. These signals are sent with a certain periodicity that can be 2, 5, 10, 20, 40, 80, 160, 320ms in accordance with Table 8.2-1 of 3GPP TS 36.213. Furthermore, there is an option in which UE does not transmit SRS at all.

In the simulator, the periodicity affects the maximum number of devices that can be simulated; for instance, with a SRS periodicity fixed at 80ms, the maximum number of allowed UE is 69. This is due to the fact that during the Random-Access Procedure for the attachment, many RNTIs to be assigned to UEs are generated and then never used due to collisions. Moreover, in *ns-3* we cannot disable the send of SRS periodicity.

Now, we want to simulate 100 UE that can be equivalent to up to 400 entities because of the way we implement the carrier aggregation. Then, the maximum value of SRS periodicity isn't enough and we would like to disable it even because our study is centered on the downlink performance. Since SRS transmission cannot be disabled, we edited the related libraries to increase the transmission period to 640ms. In addition to the periodicity, we had to change also the SRS Configuration Indices. Here you can find the changes applied to `lte-phy`; the same has been done on `lte-enb-rrc`:

```
uint16_t
LtePhy::GetSrsPeriodicity (uint16_t srcCi) const
{
  // from 3GPP TS 36.213 table 8.2-1 UE Specific SRS Periodicity
  uint16_t SrsPeriodicity[10]={0, 2, 5, 10, 20, 40, 80, 160, 320, 640};
  uint16_t SrsCiLow[10] = {0, 0, 2, 7, 17, 37, 77, 157, 317, 637};
  uint16_t SrsCiHigh[10] = {0, 1, 6, 16, 36, 76, 156, 316, 636, 1276};
  uint8_t i;
  for (i = 10; i > 0; i --)
    {
      if ((srcCi>=SrsCiLow[i])&&(srcCi<=SrsCiHigh[i]))
        {
          break;
        }
    }
  return SrsPeriodicity[i];
}
```

In this simulator, the tables referred to spectral efficiency, CQI, MCS and TBS are referred to Release 8. Then, to introduce the 256QAM, we modified them in `lte-amc` with those referred to Release 13. First, we modified `SpectralEfficiencyForCqi` with Table 7.2.3-2 from 3GPP TS 36.213, already shown in Chapter 2. Then we updated the table `SpectralEfficiencyForMcs`; its original version was proposed by Qualcomm in 2008 and links the MCS index to the spectral efficiency. Unfortunately, there aren't proposals made so fare by any company, then we introduced ours, following the previous one's construction.

MCS Index	Modulation Order	TBS Index	CQI index	Spectral efficiency
0	2	0	2	0,2344
1	2	2		0,3057
2	2	4	3	0,6016
3	2	6		0,7393
4	2	8	4	1,1758
5	4	10		1,4766
6	4	12		1,69535
7	4	13	5	1,9141
8	4	14		2,1602
9	4	15	6	2,4063
10	6	15		2,5684
11	6	16	7	2,7305

12	6	17		3,0264
13	6	18	8	3,3223
14	6	19		3,6123
15	6	20	9	3,9023
16	6	21		4,21285
17	6	22	10	4,5234
18	6	23		4,8193
19	6	24	11	5,1152
20	6	25		5,335
21	8	27	12	5,5547
22	8	28		5,8633
23	8	29	13	6,1719
24	8	30		6,4805
25	8	31	14	6,7891
26	8	32		7,0977
27	8	33	15	7,4063
28	2	reserved		
29	4	reserved		
30	6	reserved		
31	8	reserved		

Table 4.2 MCS vs Spectral Efficiency

We also changed the `McsToItbs` table substituting it with table 7.1.7.1-1A from TS 36.213:

MCS Index	MCS Index in current table	Modulation Order	TBS Index
0	0	2	0
1	2	2	2
2	4	2	4
3	6	2	6
4	8	2	8
5	11	4	10
6	13	4	12
7	14	4	13
8	15	4	14
9	16	4	15
10	17	6	15
11	18	6	16
12	19	6	17
13	20	6	18

14	21	6	19
15	22	6	20
16	23	6	21
17	24	6	22
18	25	6	23
19	26	6	24
20	27	6	25
21	-	8	27
22	-	8	28
23	-	8	29
24	-	8	30
25	-	8	31
26	-	8	32
27	-	8	33
28	29	2	reserved
29	30	4	
30	31	6	
31	-	8	

Table 4.3 MCS vs TBS Indices

Finally, we added the new lines of the transport block size Table 7.1.7.2.1-1, always belonging to TS 36.213, to the relative table in the library, TransportBlockSizeTable.

5 Simulations

5.1 Preliminary Simulations

To analyze the assumptions and the changes described in the previous Chapter we made some simple simulations: we compared how the MIMO and Carrier Aggregation implementations in the simulator work with respect to ours and we controlled the effective contribution of the 256QAM in terms of throughput increase. Here, we give a brief description of them.

5.1.1 MIMO Simulations

As presented in 4.2, the simulator implements MIMO technique as an additional gain in transmission. This can be set with a command to modify the library that controls the RRC, `lte-enb-rrc`:

```
Config::SetDefault("ns3::LteEnbRrc::DefaultTransmissionMode",
UintegerValue (0));
```

The value *0* stands for SISO, while *2* stands for MIMO 2x2. To experiment the validity of our implementation, based on doubling (or quadrupling) the TBS, we described a scenario with a single user moving around an antenna. Note that since MIMO 4x4 is not implemented within the simulator, we provide on the results relative to our technique.

	SISO	**SIMULATOR MIMO**	**IMPLEMENTED MIMO 2x2**	**IMPLEMENTED MIMO 4x4**
THROUGHPUT	6.35 Mbps	12.46 Mbps	12.38 Mbps	21.05Mbps

Table 5.1 Results of the MIMO Simulations

Note that results relative to MIMO 4x4 reflect the real nature of this technique: in fact, it requires an appropriate level of channel quality and if SINR is below a given threshold it cannot be activated. To implement this condition, we allow the activation of MIMO 4x4 only when CQI is greater than 14. Then, since the UE is moving around the antenna, the quality indicator varies and the usage of 4 layer is not always allowed, leading to a throughput lower than the expected.

5.1.2 Carrier Aggregation Simulations

Starting from an input data flow of about 20Mbps, we added co-located nodes to carry out our implementation of carrier aggregation. Results show that it works properly: in fact, there is no interference among the carriers and each node works independently of the others.

	SINGLE CARRIER	2-CARRIER AGGREGATION	3-CARRIER AGGREGATION	4-CARRIER AGGREGATION
THROUGHPUT	21.12Mbps	42.23Mbps	59.37Mbps	79.64Mbps

Table 5.2 Results of the Carrier Aggregation Simulations

Note that the UE are co-located at a certain distance from the eNBs and the flows on the higher frequencies (1800MHz and 2600MHz) are affected by some losses, as we expected from the theory.

5.1.3 Tri-Sector Antenna and Handover Implementation

In this simulator, the tri-sector antenna is not implemented as a single entity. Then, it was necessary to create three antennas with beam directions shifted on three directions. To do this, we needed to characterize the antenna model attributes in `LteHelper`:

```
lteHelper->SetEnbAntennaModelType ("ns3::CosineAntennaModel");
lteHelper->SetEnbAntennaModelAttribute ("Orientation",
            DoubleValue (120)); //angle with respect to the x axis
lteHelper->SetEnbAntennaModelAttribute ("Beamwidth",
            DoubleValue (60));
lteHelper->SetEnbAntennaModelAttribute ("MaxGain",
            DoubleValue (15.0));
```

We configured the antennas' beams with a 120° shift angle and 60° beamwidth to maximize the coverage. Then, to allow the UE to switch from an antenna to another we configured the X2 interface that manages the handover algorithms. Specifically, we used the *Strongest Cell Handover Algorithm* which was developed using the description made by Konstantinos Dimou et al. in "*Handover within 3GPP LTE: Design Principles and Performance*". The result of this implementation is the `A3RsrpHandoverAlgorithm` class. According to 3GPP TS36.331, the parameters `Hysteresis` and `TimeToTrigger` are configured:

```
lteHelper->SetHandoverAlgorithmType("ns3::A3RsrpHandoverAlgorithm");
lteHelper->SetHandoverAlgorithmAttribute ("Hysteresis",
                                          DoubleValue (2.0));
lteHelper->SetHandoverAlgorithmAttribute ("TimeToTrigger",
                                         TimeValue(MilliSeconds (64)));
```

To ensure the correct operation of this code, we analyzed the statistics provided by the flow monitor and verified that the UE switched among the three antennas when moving around the scenario.

5.2 Complete Simulations

The scenario to describe is depicted in figure 3.1. We made some simulations to study the behavior of the network with the deploying of devices belonging to dissimilar categories and, thereby, with different capabilities:

- Category 6 devices: 2 Carrier Aggregation (800 + 1800 MHz or 800 + 2600 MHz), MIMO 2x2 and 64QAM
- Category 11 devices: 3 Carrier Aggregation (800 + 1800 + 1500 MHz or 800 + 1800 + 2600 MHz), MIMO 2x2, 256QAM
- Category 16 devices:
  - 2 Carrier Aggregation (800 + 1800 MHz or 800 + 1500 MHz), MIMO 4x4, 256QAM
  - 4 Carrier Aggregation (800 + 1800 + 1500 + 2600 MHz), MIMO 2x2, 256QAM

We also placed the eNBs and set the frequencies at which each one works and the pathloss model with commands below:

```
lteHelper->SetEnbDeviceAttribute ("DlEarfcn", UintegerValue (2400));
lteHelper->SetAttribute("PathlossModel",StringValue
                ("ns3::ItuR1411NlosOverRooftopPropagationLossModel"));
lteHelper->SetPathlossModelAttribute ("Frequency",DoubleValue(800e6));
```

We got the overall throughput and, in particular, we were interested in comparing the results of the two simulations for Category 16 devices. In fact, the principal aim of this study is to compare the deployment strategies in order to give the estimation of the best one.

5.2.1 Coverage Analysis

To design the scenario within the simulator we set the positions of the antennas and the directions of the respective beams to maximize the coverage. The simulator provides with a tool to analyze the SINR levels over the considered area, the *Radio Environment Map Helper*. The output is a list of the positions of eNBs, UE and the level of SINR for each point of the map. Then, we used the program *gnuplot* to obtain the SINR maps for each frequency. Unluckily, it is impossible to obtain a general map including simultaneously the contributions of each frequency: in fact, the helper works only at a given frequency for each simulation and can be set as follows:

```
remHelper->SetAttribute ("Earfcn", Uinteger (2400)); //800 MHz
```

The frequencies are set using the equivalent EARFCN values described in TS 36.101 Section 5.7.3:

E-UTRA Operating Band	Downlink			Uplink		
	F_{DL_low} (MHz)	$N_{Offs-DL}$	Range of N_{DL}	F_{UL_low} (MHz)	$N_{Offs-UL}$	Range of N_{UL}
1	2110	0	0 – 599	1920	18000	18000 – 18599
2	1930	600	600 - 1199	1850	18600	18600 – 19199
3	1805	1200	1200 – 1949	1710	19200	19200 – 19949
4	2110	1950	1950 – 2399	1710	19950	19950 – 20399
5	869	2400	2400 – 2649	824	20400	20400 – 20649
6	875	2650	2650 – 2749	830	20650	20650 – 20749
7	2620	2750	2750 – 3449	2500	20750	20750 – 21449
8	925	3450	3450 – 3799	880	21450	21450 – 21799
9	1844.9	3800	3800 – 4149	1749.9	21800	21800 – 22149
10	2110	4150	4150 – 4749	1710	22150	22150 – 22749
11	1475.9	4750	4750 – 4949	1427.9	22750	22750 – 22949
12	729	5010	5010 – 5179	699	23010	23010 – 23179
13	746	5180	5180 – 5279	777	23180	23180 – 23279
14	758	5280	5280 – 5379	788	23280	23280 – 23379
…						
17	734	5730	5730 – 5849	704	23730	23730 – 23849
18	860	5850	5850 – 5999	815	23850	23850 – 23999
19	875	6000	6000 – 6149	830	24000	24000 – 24149
20	791	6150	6150 – 6449	832	24150	24150 – 24449
21	1495.9	6450	6450 – 6599	1447.9	24450	24450 – 24599

22	3510	6600	6600 – 7399	3410	24600	24600 – 25399
23	2180	7500	7500 – 7699	2000	25500	25500 – 25699
24	1525	7700	7700 – 8039	1626.5	25700	25700 – 26039
25	1930	8040	8040 – 8689	1850	26040	26040 – 26689
26	859	8690	8690 – 9039	814	26690	26690 – 27039
27	852	9040	9040 – 9209	807	27040	27040 – 27209
28	758	9210	9210 – 9659	703	27210	27210 – 27659
29	717	9660	9660 – 9769	N/A		
30	2350	9770	9770 – 9869	2305	27660	27660 – 27759
31	462.5	9870	9870 – 9919	452.5	27760	27760 – 27809
32	1452	9920	9920 – 10359	N/A		
33	1900	36000	36000 – 36199	1900	36000	36000 – 36199
34	2010	36200	36200 – 36349	2010	36200	36200 – 36349
35	1850	36350	36350 – 36949	1850	36350	36350 – 36949
36	1930	36950	36950 – 37549	1930	36950	36950 – 37549
37	1910	37550	37550 – 37749	1910	37550	37550 – 37749
38	2570	37750	37750 – 38249	2570	37750	37750 – 38249
39	1880	38250	38250 – 38649	1880	38250	38250 – 38649
40	2300	38650	38650 – 39649	2300	38650	38650 – 39649
41	2496	39650	39650 –41589	2496	39650	39650 –41589
42	3400	41590	41590 – 43589	3400	41590	41590 – 43589
43	3600	43590	43590 – 45589	3600	43590	43590 – 45589
44	703	45590	45590 – 46589	703	45590	45590 – 46589
45	1447	46590	46590 – 46789	1447	46590	46590 – 46789
46	5150	46790	46790 – 54539	5150	46790	46790 – 54539
47	5855	54540	54540 - 55239	5855	54540	54540 – 55239
48	3550	55240	55240 – 56739	3550	55240	55240 – 56739
…						
64	Reserved					
65	2110	65536	65536 – 66435	1920	131072	131072 – 131971
66	2110	66436	66436 – 67335	1710	131972	131972 – 132671
67	738	67336	67336 – 67535	N/A		
68	753	67536	67536 - 67835	698	132672	132672 - 132971
69	2570	67836	67836 - 68335	N/A		
70	1995	68336	68336 - 68585	1695	132972	132972 - 133121

Table 5.3 E-UTRA Channel Numbers from 3GPP 36.101 Table 5.7.3-1

Below, we present the results of the coverage analysis. Note that the higher the frequency, the worse is the coverage. In all the images, one can distinguish a circular area which becomes more marked whit higher frequencies. It corresponds to the settled field distance d_s, as described in (3.6): in fact, as you can see in (3.7) this is the distance at which the propagation model equation changes.

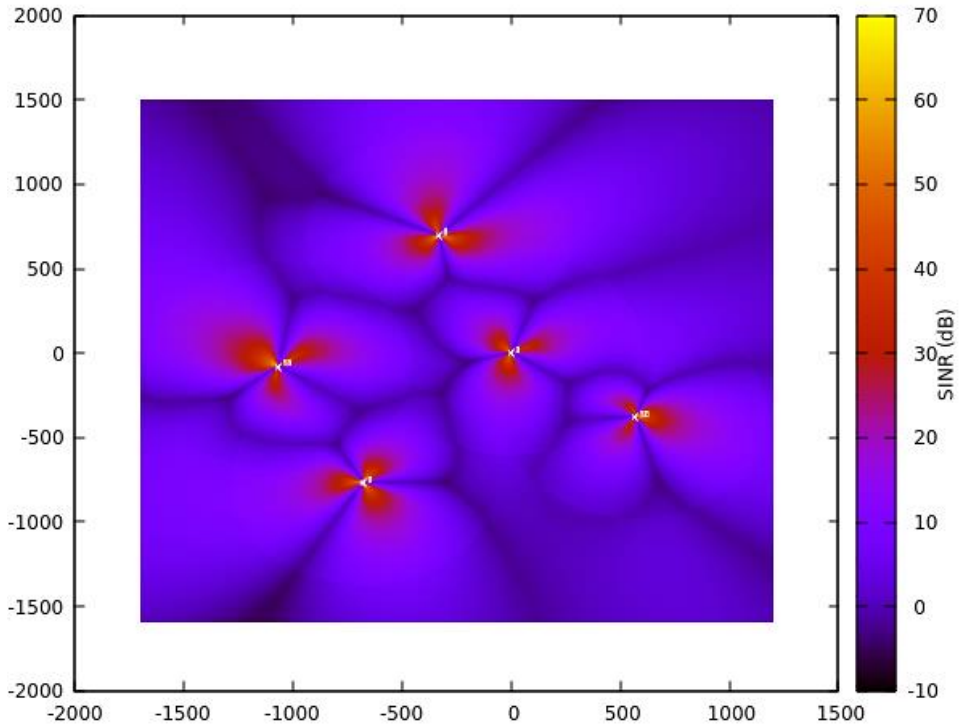

Figure 5.1 Coverage at 800MHz

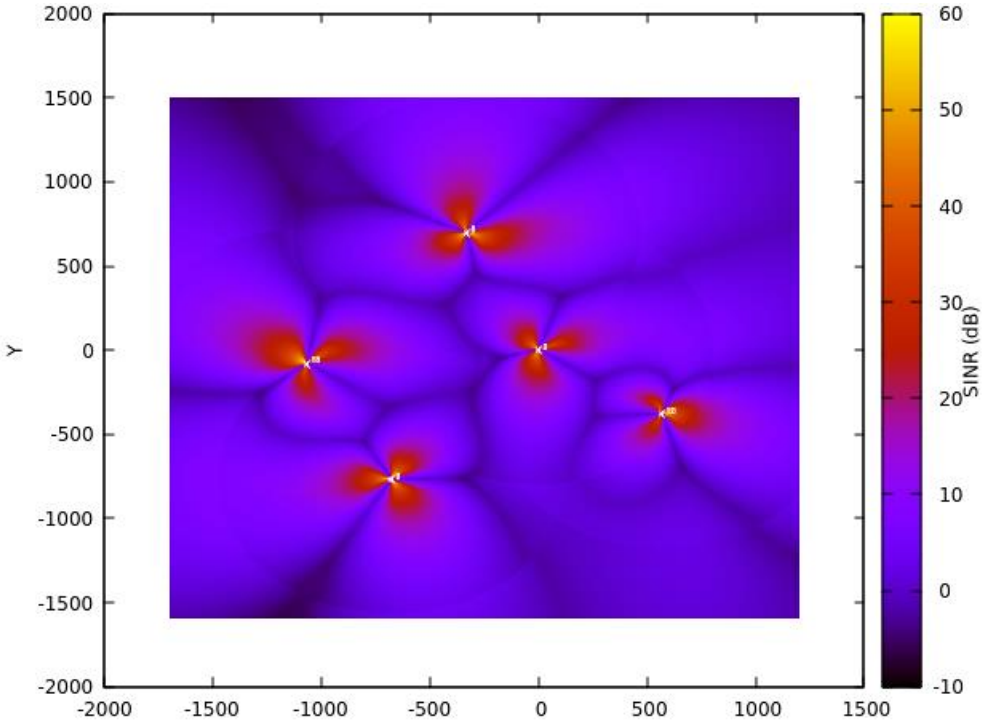

Figure 5.2 Coverage at 1500MHz

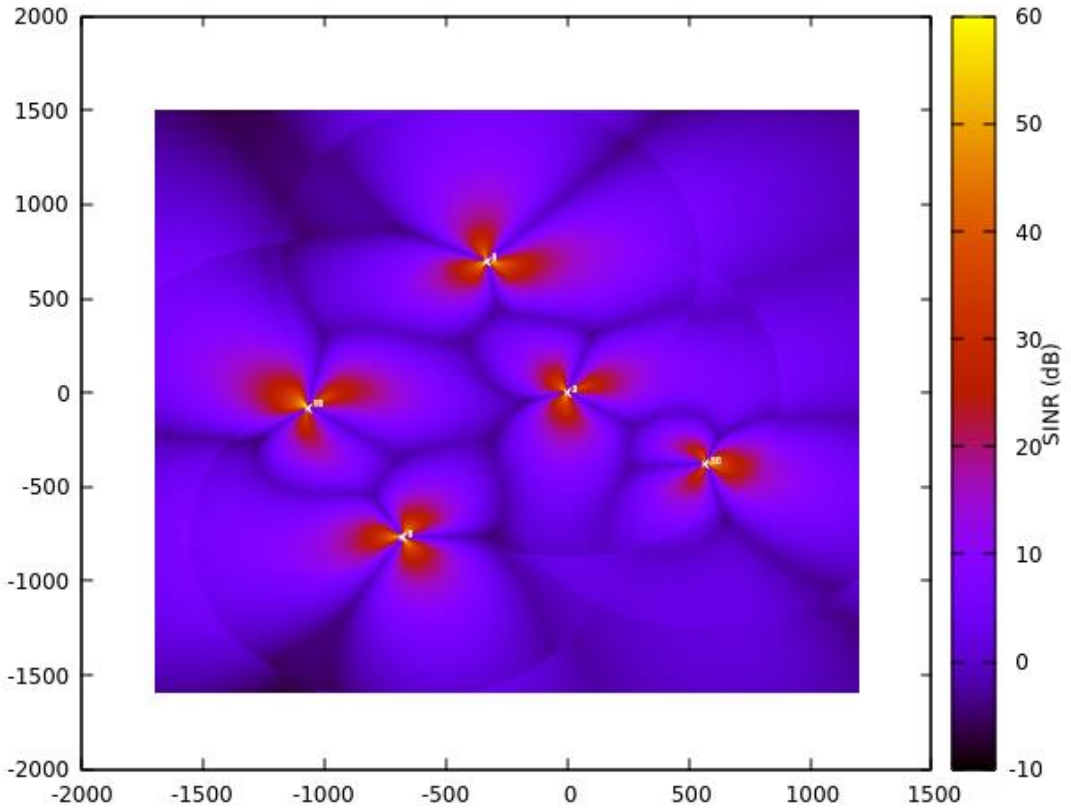

Figure 5.3 Coverage at 1800MHz

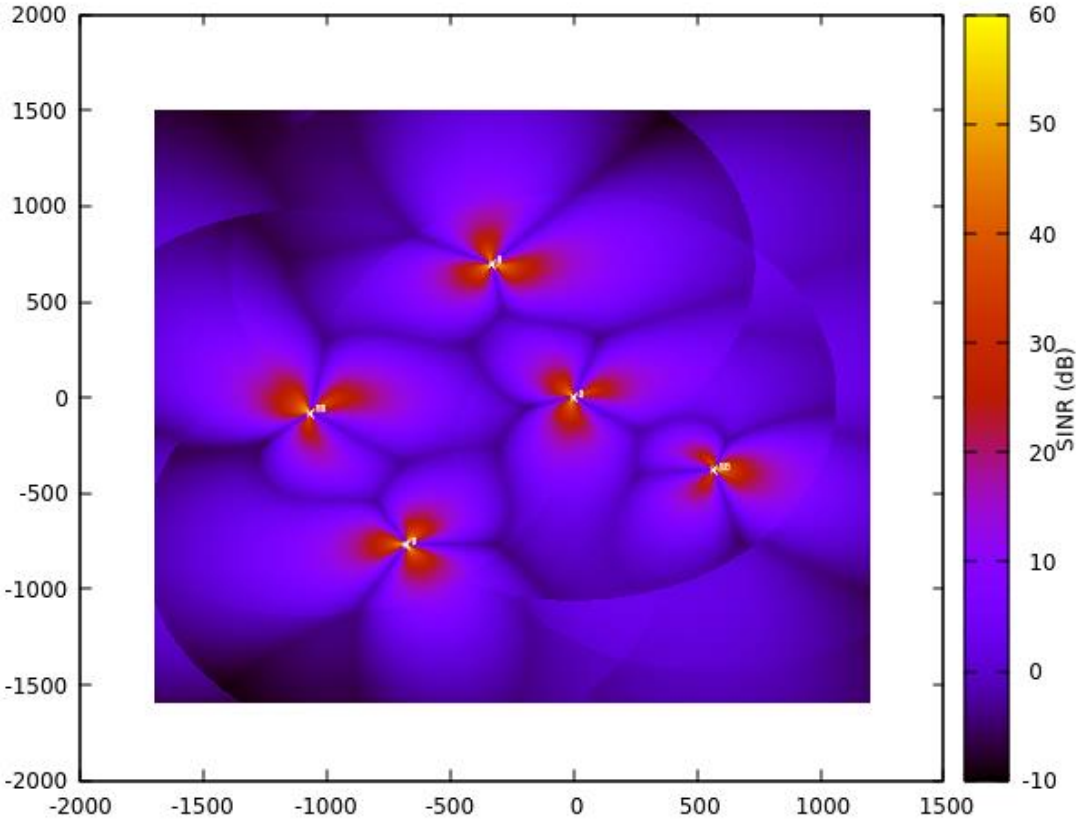

Figure 5.4 Coverage at 2600MHz

5.2.2 Category 6 Deployment

First of all, to implement a Cat6 device we created two distinct entities to configure the 2 Carrier Aggregation. Since the modulation for these devices is the 64QAM, we used the `LteAmc` file as it was first intended by the simulators developers, without updating the TBS tables. Then, after the configuration of the IP addresses, we attached the devices to the eNBs with the proper frequencies using "*for cycles*" where the fundamental command is:

```
lteHelper->AttachToClosestEnb (ueDevs_cat6.Get(i), enbDevs_800);
```

Note that we used the `AttachToClosestEnb` instead of the more common `Attach` function because the former allows to link a single user to multiple eNBs at the same time so that the UE can do the handover among them.

The peak data rate for a single Cat6 UE is 300Mbps. This comes from the following considerations: the 64QAM uses 6 bits per symbol. In each symbol there are 12 subframes. Moreover, we need to consider the number of Sub-Carriers: with a 20MHz bandwidth, there are 1200 Sub-Carriers. Then, considering that the duration of a TTI is 1ms the peak data rate with SISO and 64QAM is:

$$\frac{\text{Number of bits/symbol} \cdot \text{Number of symbols/subframe} \cdot \text{Number of Sub-Carriers}}{\text{TTI}} =$$

$$\frac{6 \cdot 12 \cdot 1200}{10^{-3}} = 86.4\text{Mbps}$$

This is what we obtain at PHY layer. The peak data rate should be evaluated at the MAC layer and one should consider the overheads introduced, e.g. for signaling. Hence, we consider that for 20MHz with 64QAM and SISO transmission the peak data rate is 75Mbps.

The best configuration to employ MIMO 2x2 as well was given by the usage of 1500 and 1800MHz to aggregate 35MHz and the peak throughput is:

$$(75 + 75) \cdot 2 = 300\text{Mbps}$$

Of course, this value is only a theoretical one and cannot be achieved in a dense urban scenario, with many devices transmitting simultaneously. Moreover, the peak data rate

is evaluated with the best bandwidth configuration. If the 800MHz is used, there are less resources and the data rate is lower.

From the simulation we can evaluate the performances of the network in terms of throughput: in fact, it returns this value both at IP and at RLC level. Morevoer, we can also evaluate the robustness of the modulation and of the 2-layer transmission from the MAC statistics. We omit the full statistics since they are composed of tens of thousands rows; we only provide with few rows in order to give an example.

% start	end	CellId	IMSI	RNTI	nTxPDUs	TxBytes	nRxPDUs	RxBytes
…	…	…	…	…	…	…	…	…
0	00:25:00	37	74	5	4	40152	3	30114
0	00:25:00	37	79	15	9	35850	9	35850
0	00:25:00	37	80	1	4	37432	4	37432
0	00:25:00	37	63	4	4	40152	4	40152
0	00:25:00	37	85	8	19	45656	17	44958
0	00:25:00	38	3	1	106	45482	106	45482
…	…	…	…	…	…	…	…	…

Table 5.4 Extract of DL RLC Statistics

From these data we analyzed the correct dialogue between the eNBs and the UE. Moreover, we could evaluate the throughput on the RLC level.

The throughput in the air, at IP level, was obtained from the Flow Monitor. Here, we give an example of its structure:

Flow ID : 7 ; 1.0.0.2 -----> 7.0.0.8
Tx Packets = 299339
Rx Packets = 134497
Duration : 29.9318
Last Received Packet : 29.998 Seconds
Throughput: 18.101 Mbps

In the first row there are the IP address of the transmitter (which is always the same, since it is the core network) and the IP address of the UE, that varies from flow to flow. Then, there is also the number of the transmitted and received packets, as well as the duration of the transmission. Finally, the throughput of the single flow is evaluated. The UE with the best throughput are those closer to an eNB and with a constant position. Summing the contributions from the two carriers, they can achieve up to 80Mbps (since we designed each flow to transmit up to 40Mbps). Although, some of them do not succeed to attach to an eNB and do not start a trasnsmission.

The overall system througput was obtained as the sum of the rates of each UE. For the deployment of only Cat6 UE the evaluated system throughput is around 470Mbps.

5.2.3 Category 11 Deployment

This category supports the 3-Carrier Aggregation, then we needed to co-locate three entities per each UE. Moreover, we modified the `LteAmc` library as described in the previous Chapter, to include the 256QAM. The attach procedure is the same described for Cat6 simulation.

The peak throughput for a Cat11 UE is about 600Mbps. Following the considerations made in the previous chapter, we start from 86.4Mbps on 20MHz with SISO. In the best configuration, t-he aggregated bands are 20MHz @1500MHz, 20 MHz @1800MHz and 15MHz @2600MHz, for a 55MHz overall bandwidth. MIMO 2x2 can be used on all these three bands. The inclusion of 256QAM leads to a further 33% increase of the data rate. Hence, the theoretical throughput is

$$\left[\left(75+75+75\cdot\frac{15}{20}\right)\cdot 2\right]\cdot\frac{4}{3}\cong 550\text{Mbps}$$

As we already pointed out before, thi data rate cannot be achieved in real networks, a fortiori if the device aggregates the 800MHz carrier, which has a narrower spectrum bandwidth and thereby less resources. Note that, in case of its utilization, the peak data rate decreases by 100Mbps. In this simulation, apart from evaluating the system throughput, we wanted to evaluate the robustness of 256QAM. This can be done reading the MAC statistics and the transport block size on both layers.

time	cellId	IMSI	RNTI	mcsTb1	sizeTb1	mcsTb2	sizeTb2
0.77	1	13	1	27	12237	27	12237
0.77	13	18	3	19	7708	19	7708
0.77	14	22	6	17	6882	17	6882
0.77	15	17	1	27	12237	27	12237
0.77	25	7	1	27	12237	27	12237
0.77	26	6	1	15	5861	15	5861
0.77	27	2	1	17	6882	17	6882
0.77	37	80	1	27	12237	27	12237
0.77	38	8	2	21	8324	21	8324
0.77	50	11	1	27	12237	27	12237

Table 5.5 Extract of the DL MAC statistics

The TB size on the two layers are expressed in bytes and must be multiplied by 8 to be compared to the ones in `LteAmc`. For instance, the first row takes into account the channel condition of a UE with a fix position, very close to the eNB. In fact, the MCS is the maximum one as well as the TBS that is 97986 bits.

As reported in Table 4.3, the 256QAM can be activated only when the MCS is 21 or more. Then, to evaluate the robustness of this modulation, we read through the complete MAC statistics to evaluate the efficiency as the ratio between the transmission with the 256QAM and the whole transmissions. As result, we obtained a 75% efficiency, which is a very high percentage if we consider the dense urban environment.

As in the previous case, we also evaluated the system throughput. We summed the throughputs of each flow and we obtained about 750Mbps.

5.2.3 Category 16 Simulations

The Cat16 devices can achieve their maximum data rate in the two ways already described and that will be examined in depth below. Since one of them requires the employ of MIMO 4x4, it was necessary to decrease the input flow: in fact, if we used 40Mbps we could not figure out the real adoption because of the 75Mbps limitation introduced by the UDP traffic in this simulator. Then, differently from the simulations made so far, we decreased it to 20Mbps.

The first approach we studied is the one focused on spectrum broadening that provides for 4-Carrier Aggregation that leads to a usage of 65MHz on the four bands 800, 1500, 1800 and 2600MHz. MIMO 4x4 cannot be used since the limitation to 8 Antenna Port due of RF component on the transceivers.

The maximum single user theoretical throughput for this configuration is evaluated in the same way we obtained the previous ones:

$$\left[\left(75 + 75 + 75 \cdot \frac{15}{20} + 75 \cdot \frac{10}{20}\right) \cdot 2\right] \cdot \frac{4}{3} \cong 650\text{Mbps}$$

The overall system throughput, evaluated as the sum of each UE data rate, is about 790Mbps.

The second approach consists in aggregating only two carriers with MIMO 4x4 on both. The best configuration is the one that aggregates 40MHz from 1500 and 1800MHz.

In this way the peak data rate for a single user is

$$[(75 + 75) \cdot 4] \cdot \frac{4}{3} \cong 800\text{Mbps}$$

In case of aggregation of one of the other bands (800 or 2600MHz) that have less frequency resources, the peak throughput would decrease to around 700Mbps.

This simulation is mainly focused on evaluating the robustness of MIMO 4x4 with respect to SINR. The method is the same used to evaluate the robustnes of 256QAM. Though, since MIMO 4x4 feels the effect of noise more than modulation, it can be activated only with a very good channel quality (CQI>14). Then it can be activated only for MCS higher than 24. In case of a lower channel quality, it is permitted to transmit with a lower rank and, thereby, three layers, in order to guarantee however a faster transmission. This can be done for MCS greater than 21. In the code this consideration is made with an *if clause* in function `GetTbSizeFromMcs` within the `LteAmc` library:

```
int
LteAmc::GetTbSizeFromMcs (int mcs, int nprb)
{
  NS_LOG_FUNCTION (mcs);
  NS_ASSERT_MSG (mcs < 28, "MCS=" << mcs);
  NS_ASSERT_MSG (nprb < 111, "NPRB=" << nprb);
  int itbs = McsToItbs[mcs];
  if (mcs > 24) {
      return (4*(TransportBlockSizeTable[nprb - 1][itbs]));
     }
  else if (mcs > 21) {
      return (3*(TransportBlockSizeTable[nprb - 1][itbs]));
     }
  else {
      return (2*(TransportBlockSizeTable[nprb - 1][itbs]));
     }
 }
```

Since the environment we are simulating is characterised by many users transmitting simultaneously and many multipaths and interferences, it is very hard to achieve a high channel quality and the MIMO 4x4 was activated only in the 27% of transmissions.

Hence, the throughput of the overall system is around 630Mbps, lower than the one evaluated in the first configuration.

To achieve better SINR levels in a given region, it is possible to increase the number of cells. It could lead to a higher inter-cells interference and to a worsening of the data rate and it is important to desing the deployment in appropriate manner.

Then, we added another cell to our scenario as shown in figure 5.5.

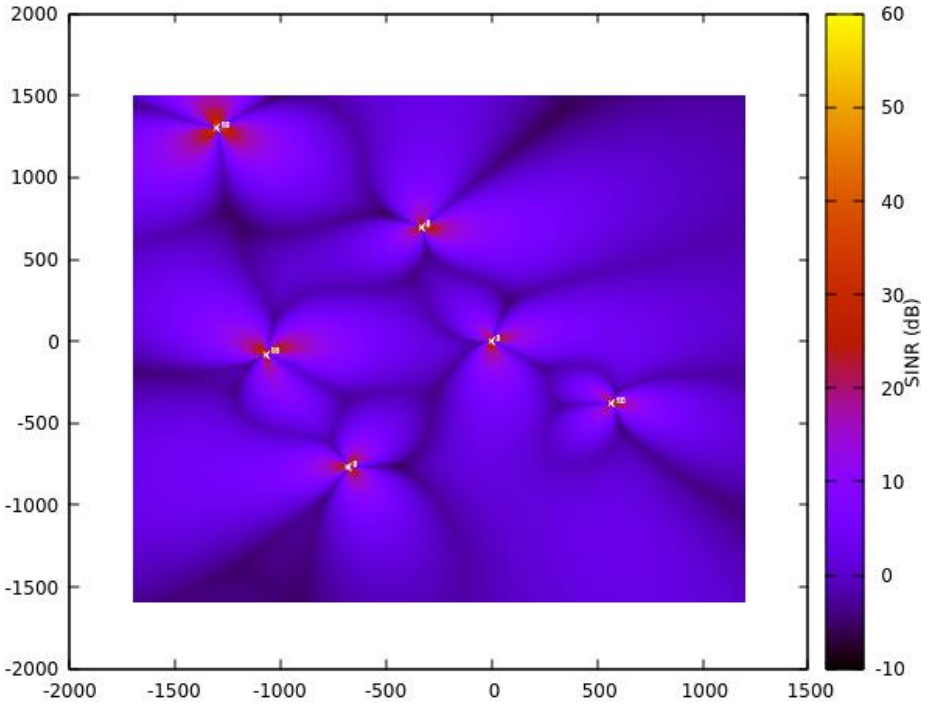

Figure 5.5 Coverage at 800MHz with six cells

In this case, MIMO 4x4 was activated in the 33% of cases and the throughput was around 670Mbps.

It is interesting to highlight that with this configuration only two bands are used (i.e. 1800 and 2600MHz) and the network can manage other devices that aggregate other bands like Category 6 devices. Then, the complexive capacity increases a lot since the two configuration are independent one another and the throughput of each configuration can be summed and the system capacity increases.

Finally, we provide all the results in the table below:

CAT	CONFIGURATION	INPUT FLOW (per UE)	SYSTEM THROUGHPUT	AVERAGE ENB THROUGHPUT	SPECTRAL EFFICIENCY
6	2 CA MIMO 2x2 64 QAM	40 Mbps	470 Mbps	103 Mbps	13.4 bps/Hz
11	3 CA MIMO 2x2 256QAM	40 Mbps	750 Mbps	130 Mbps	13.6 bps/Hz
16	4 CA MIMO 2x2 256QAM	20 Mbps	790 Mbps	158 Mbps	12.15 bps/Hz
16	2 CA MIMO 4x4 256QAM	20 Mbps	630 Mbps (670 Mbps with six sites)	126 Mbps (134 Mbps with six sites	15.75 bps/Hz

Table 5.6 Results of the simulations

The spectral efficiency is evaluated as the overall throughput divided by the used spectrum. Of course, the first two simulations have better efficiencies than the third one because of the limit on the UDP traffic that causes the saturation. Moreover, note that within the simulated environment it was very hard to achieve high SINRs. This is the reason of difference between the two Cat16 configurations.

Below, we report the analysis on the efficieny of the capabilities, evaluated as the percentage of transmissions where they are activated.

CAPABILITY	EFFICIENCY
256QAM	75%
MIMO 4x4	27%
MIMO 4x4 with 6 sites	33%

Table 5.7 Efficiency of the LTE-A capabilities

These results show that the 256QAM is a very robust capability and in fact, it is already widely diffused whereas MIMO 4x4 suffers from low signal levels.

6 Real measures and validation

With the simulations we analyzed the behavior of the overall network. Tools like *ns-3* are fundamental for studies like this one, since it is impossible to make such analysis for a complex scenario. In this chapter we will provide the results of some tests made on Cat11 and Cat16 commercial devices to evaluate the peak and the average data rate in a session. We also focused on the analysis of band L, since it is the last introcuded band to aggregate. Moreover, we also evaluated the performances of MIMO 4x4 and 256QAM in real networks.

6.1 Category 11

Tests on this category can be divided according to the frequncies involved:

- B3 + B7 + B20 (1800 + 2600 + 800MHz)
- B3 + B20 + B32 (1800 + 800 + 1500MHz)

For both tests, a UDP traffic was generated.

The device used in the first test aggregated 45MHz on the TIM spectrum. The peak throughput on the PHY layer was 443.3Mbps while the average throughput was 367.6Mbps. Data were extracted with Qualcomm eXtensible Diagnostic Monitor (QXDM). Below, we report the most significant details of the analysis of throughput and the radio condition during the test.

Aggregated Peak: 443,3 Mbps	**Aggregated Avg: 367,6 Mbps**
Peak PCC (1800) 195,8 Mbps	Avg PCC (1800) 170,6
Peak SCC1 (2600) 149,7 Mbps	Avg SCC1 (2600) 131,1
Peak SCC2 (800) 97,8 Mbps	Avg SCC2 (800) 65,9

Table 6.1 Peak and Average Throughput with B3 + B7 + B20

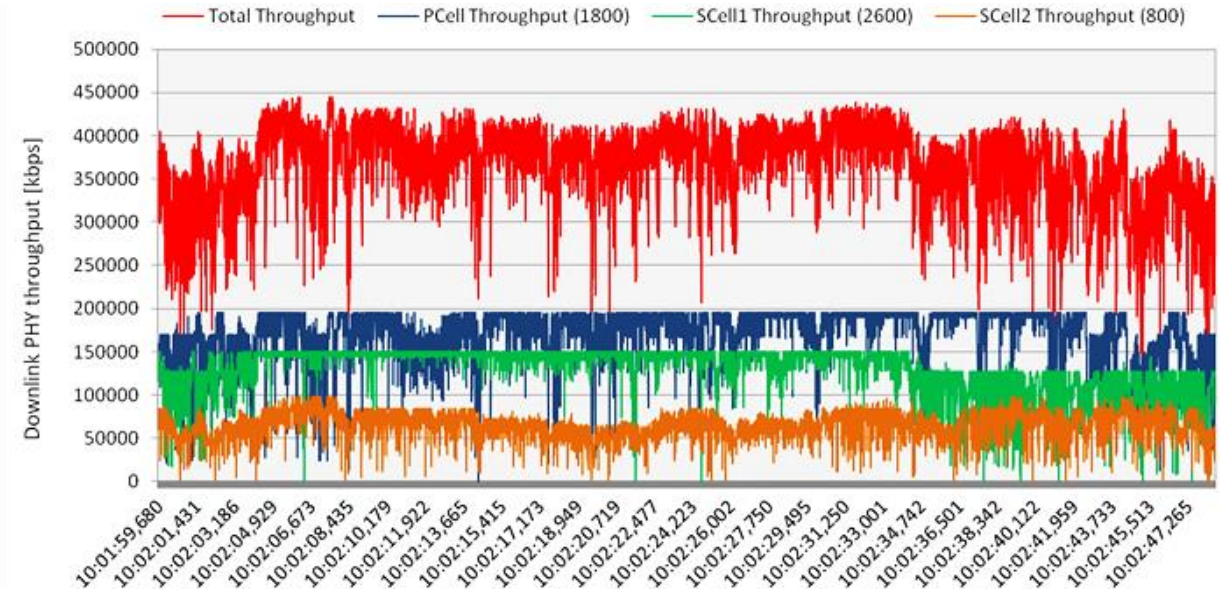

Figure 6.1 Throughput trend with B3 + B7 + B20 on the PHY layer

	EARFCN	**SINR RX0 [dB]**	**SINR RX1 [dB]**
PCC (1800)	1500	28,04	28,23
SCC1 (2600)	3175	29,12	29,31
SCC2 (800)	6300	27,47	28,48

Table 6.2 Radio Condition during the test

Apart from the throughput data, we also evalutaed the performance of the MIMO 2x2 and 256QAM. Because of the optimal channel conditions, both capabilities were used at their maximum: the former was used with rank 2 during most of the transmission and the latter was used next to the whole time on two bands out of three. We also provide the average Modulation and Coding Scheme and number of Resource Blocks

	Scheduling rate	**Spatial Rank**		**Modulation Stream**			**Average MCS**	**Average #RB**
		rank 1	**rank 2**	**256QAM**	64QAM	16QAM		
PCC (1800)	**98,91%**	4,97%	**95,03%**	**99,78%**	0,21%	0,00%	26,65	**98,71**
SCC1 (2600)	**99,58%**	4,03%	**95,97%**	**99,65%**	0,35%	0,00%	26,51	**74,33**
SCC2 (800)	**98,31%**	6,24%	**93,76%**	**91,38%**	8,62%	0,01%	23,66	**48,88**

Table 6.3 PHY layer statistics

We also made some measures with the Speedtest app by OOKLA which returned lower data rates than those evaluated with QXDM. Note that the single carriers peaks were detected at different instants, then the aggregated peak is not given by the arithmetic sum.

Aggregated Peak: 375,8 Mbps	**Aggregated Avg: 296,1 Mbps**
Peak PCC (2600) 118,5 Mbps	Avg PCC (2600) 93,3 Mbps
Peak SCC1 (1800) 169,5 Mbps	Avg SCC1 (1800) 135 Mbps
Peak SCC2 (800) 94,1 Mbps	Avg SCC2 (800) 67,8 Mbps

Table 6.4 Peak and Average Throughput detected with OOKLA Speedtest

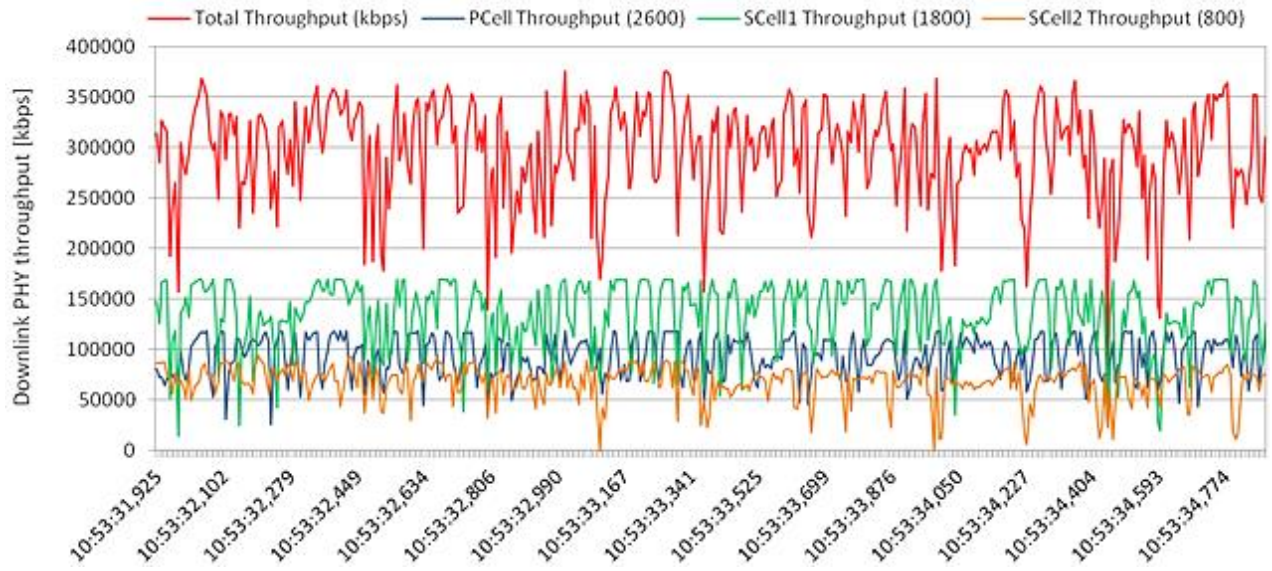

Figure 6.2 OOKLA Speedtest Throughput trend on the PHY layer

From table 6.3 we can see that the 256QAM has a very high efficiency. It was also shown with the simulations: in fact, table 5.7 shows that this modulation was activated in the 75% of the transmissions.

The device used for the second test aggregated 50MHz on the TIM spectrum using the L band. The first measures compare the usage of 64 and 256QAM. With the former the theoretical throughput is 374.93Mbps while with the latter it is 489.5Mbps.

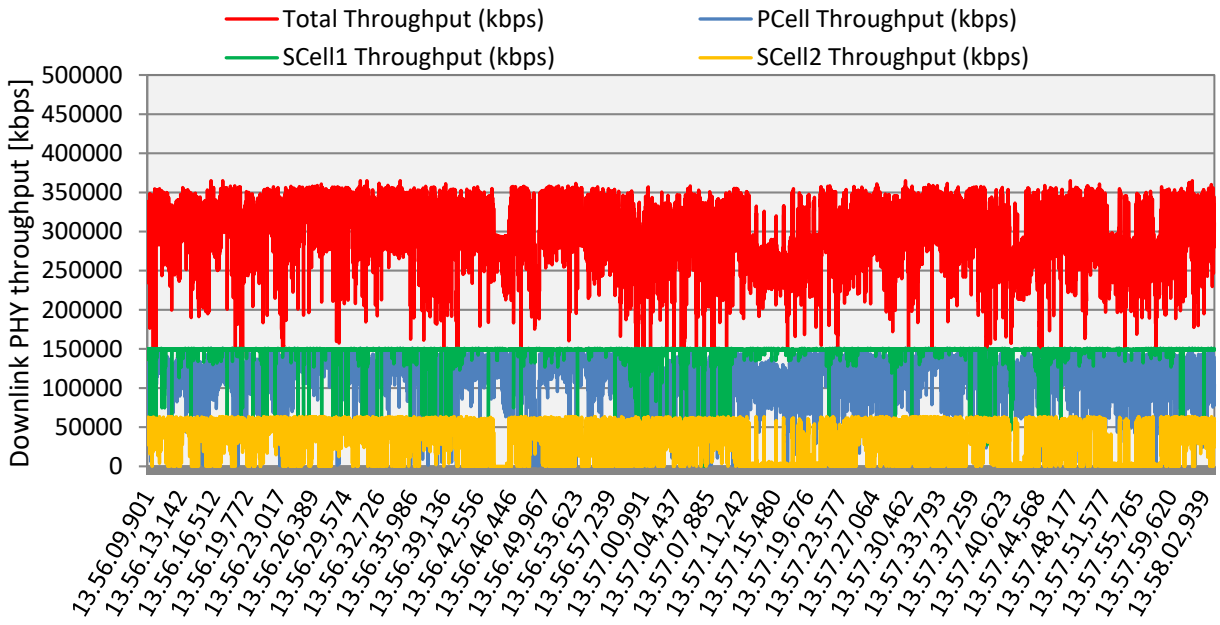

Figure 6.3 Throughput trend with B3 + B20 + B32 and 64QAM

PARAMETER	VALUE
Theoretical TPUT	**374.93 Mbps**
Measured AVG TPUT	**302.2 Mbps**
Measured Peak TPUT	**365 Mbps**
AVG RB PCC (B3)	90.9
AVG RB SCC 1 (B32)	99.2
AVG RB SCC 2 (B20)	41.5
AVG MCS PCC (B3)	27.7
AVG MCS SCC (B32)	27.59
AVG MCS SCC2 (B20)	27.54
64-QAM % PCC (B3)	99.95%
64-QAM % SCC1 (B32)	99.96%
64-QAM % SCC2 (B20)	99.99%

Table 6.5 PHY layer statistics

	Peak TPUT [Mbps]	**AVG TPUT** [Mbps]
Aggregate	365	302.2
PCC (Band 3)	150.7	119.1
SCC1 (Band 32)	150.7	147.1
SCC2 (Band 20)	63.45	36

Table 6.6 Throughput detail on each carrier

PCC [B3]	Avg values
RSRP RX1	-81.71 dBm
RSRP RX2	-84.76 dBm
SINR RX1	22.07 dB
SINR RX2	22.88 dB

SCC1 [B32]	Avg values
RSRP RX1	-85.7 dBm
RSRP RX2	-82.46 dBm
SINR RX1	28.18 dB
SINR RX2	28.87 dB

SCC2 [B20]	Avg values
RSRP RX1	-68.7 dBm
RSRP RX2	-76.67 dBm
SINR RX1	25.3 dB
SINR RX2	24.39 dB

Table 6.7 Radio conditions on the three carriers

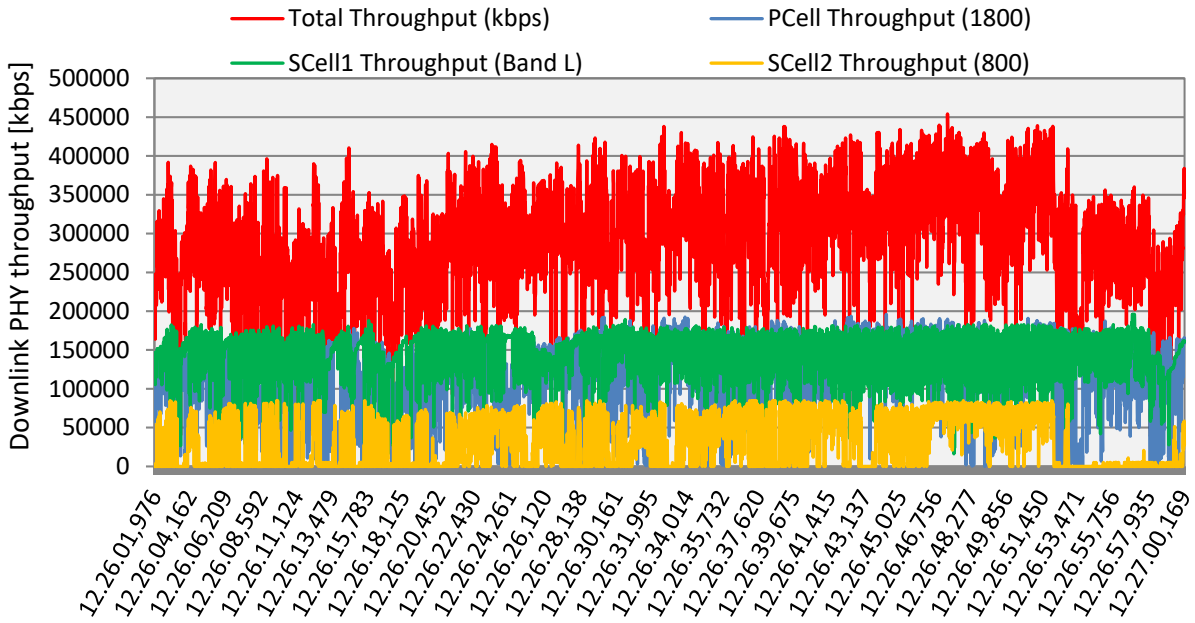

Figure 6.4 Throughput trend with B3 + B20 + B32 and 25QAM

PARAMETER	VALUE
Theoretical TPUT	**489.5 Mbps**
Measured AVG TPUT	**296.9 Mbps**
Measured Peak TPUT	**454.16 Mbps**
AVG RB PCC (B3)	78.29
AVG RB SCC 1 (B32)	99.51
AVG RB SCC 2 (B20)	39.55
AVG MCS PCC (B3)	25.3
AVG MCS SCC (B32)	25.03
AVG MCS SCC2 (B20)	25.5
256-QAM % PCC (B3)	97.80%
256-QAM % SCC1 (B32)	97.88%
256-QAM % SCC2 (B20)	99.10%

Table 6.8 PHY layer statistics

	Peak TPUT [Mbps]	**AVG TPUT** [Mbps]
Aggregate	454.16	296.9
PCC (Band 3)	195.8	115.97
SCC1 (Band 32)	198.5	150.63
SCC2 (Band 20)	84.78	30.3

Table 6.9 Throughput detail on each carrier

PCC [B3]	Avg values
RSRP RX1	-75.01 dBm
RSRP RX2	-74.08 dBm
SINR RX1	22.96 dB
SINR RX2	26.51 dB

SCC1 [B32]	Avg values
RSRP RX1	-83.98 dBm
RSRP RX2	-77.69 dBm
SINR RX1	29.37 dB
SINR RX2	29.68 dB

SCC2 [B20]	Avg values
RSRP RX1	-63.38 dBm
RSRP RX2	-74.3 dBm
SINR RX1	25.3 dB
SINR RX2	23.18 dB

Table 6.10 Radio conditions on the three carriers

If we compare tables 6.3 and 6.8, it is evident that the 256QAM performs better in the first configuration.

Focusing on band L, the advantage of 256QAM compared to 64QAM has not been totally reached in term of average throughput, despite the high robustness of the higher order modulation proved by its percentage of scheduling. According to log analysis, in 256QAM scenario the average MCS index value set by the eNB is lower than the one of 64QAM. This causes lower TBS values.

Band L Parameters	**256-QAM**	**64-QAM**
% Scheduling	95,90%	97,23%
AVG RB	99,5	99,2
AVG CQI	14	14,97
AVG MCS (*)	**25,43**	**27,99**
AVG BLER	**8,90%**	**0,48%**

Band L Throughput	**256-QAM**	**64-QAM**
Theoretical Peak	195,8	150,7
Experienced Peak	**195,8** ✓	**150,7** ✓
Average	**150,6** ✗	**147,1** ✓

Table 6.11 Focus on L band

(*) Max MCS values for 256QAM and 64QAM scenarios are 27 and 28 respectively

On Band L, a higher BLER percentage has been detected in 256QAM scenario compared to that detected in 64QAM.

Another important analysis made with a Cat11 device is the mobility between sectors. We studied both the mobility between different sectors with the same carriers and between sectors with different carriers. Before reporting the data, we need to briefly describe three measurement reports:

- The **LTE Event A3** is triggered when a neighboring cell becomes better than the serving cell by an offset (both intra- and inter-frequency).
- The **LTE Event A4** is triggered when a neighboring cell becomes better than a threshold.
- The **LTE Event A6** was introduced by Release 10 for Carrier aggregation needs. It is triggered when a neighboring cell becomes better than the serving cell by an offset (only intra-frequency).

Below we show the throughput during a session and the measurements and the reports the transmissions between UE and eNB.

The first test describes the behavior in case of mobility between different sectors with 800+1800+L Band. We focused our attention on A6-based SSC change and A3-based intra-frequency handover.

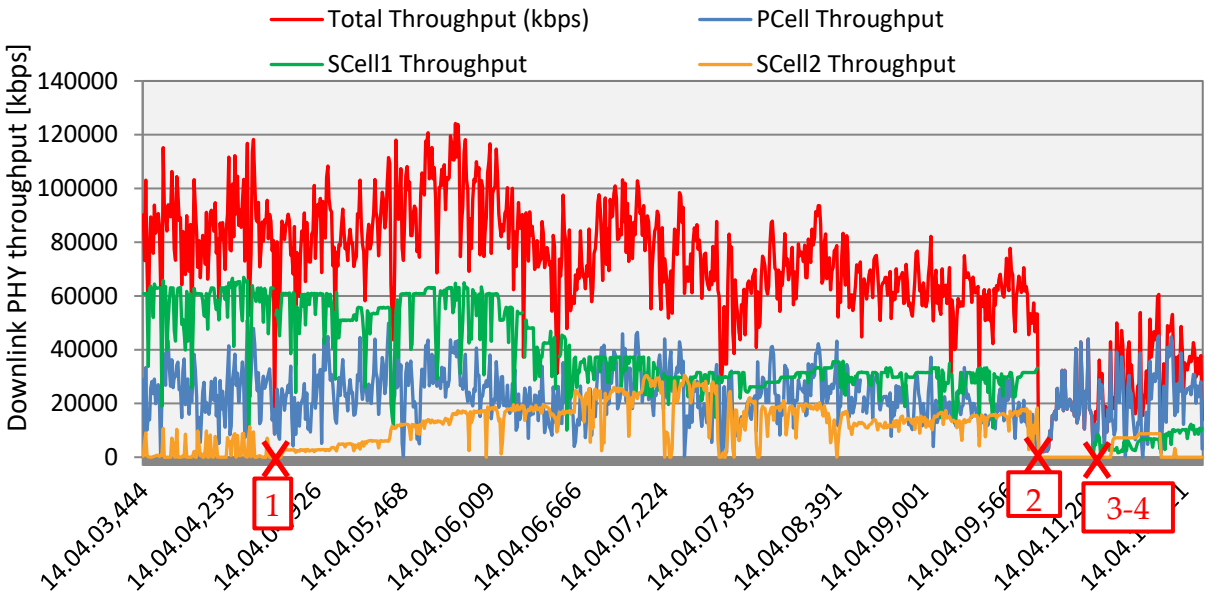

Figure 6.5 Throughput trend with mobility between different sectors with 800+1800+L Band

The highlighted points in this plot correspond to triggered events that we report here:

1 **14:04:04.590**

A6-based SSC2 change (B20)

RRC Connection Reconfiguration:
sCellToReleaseList-r10 { 2
sCellToAddModList-r10 { sCellIndex-r10 3
cellIdentification-r10 {
physCellId-r10 43,
dl-CarrierFreq-r10 6300

2 **14:04:09.745**

A3-based Intra-freq Handover (B3)
From PCC 413 to PCI 411 (sector change)
SCC1 and SSC2 release
RRC Connection Reconfiguration:
sCellToReleaseList-r10 { 1, 3 }

3 **14:04:11.064**

A4-based SCC1 Adding (B20)
(A4-threshold RSRP = -110 dBm)
RRC Connection Reconfiguration
sCellToAddModList-r10 { sCellIndex-r10 1
cellIdentification-r10 {
physCellId-r10 43,
dl-CarrierFreq-r10 6300

4 **14:04:11.332**

A4-based SCC2 Adding (B32)
(A4-threshold RSRP = -110 dBm)
RRC Connection Reconfiguration
sCellToAddModList-r10 { sCellIndex-r10 2
cellIdentification-r10 {
physCellId-r10 5
dl-CarrierFreq-r10 10020

No issues have been detected during these events and the behavior is the one expected: in correspondence of the A3 event, the principal carrier changes and the secondary components are lost so that the throughput goes to zero for some tenths of second.

The second case considers the mobility between sectors with 800+1800+2600 and 800+1800+L Band. The results are those below:

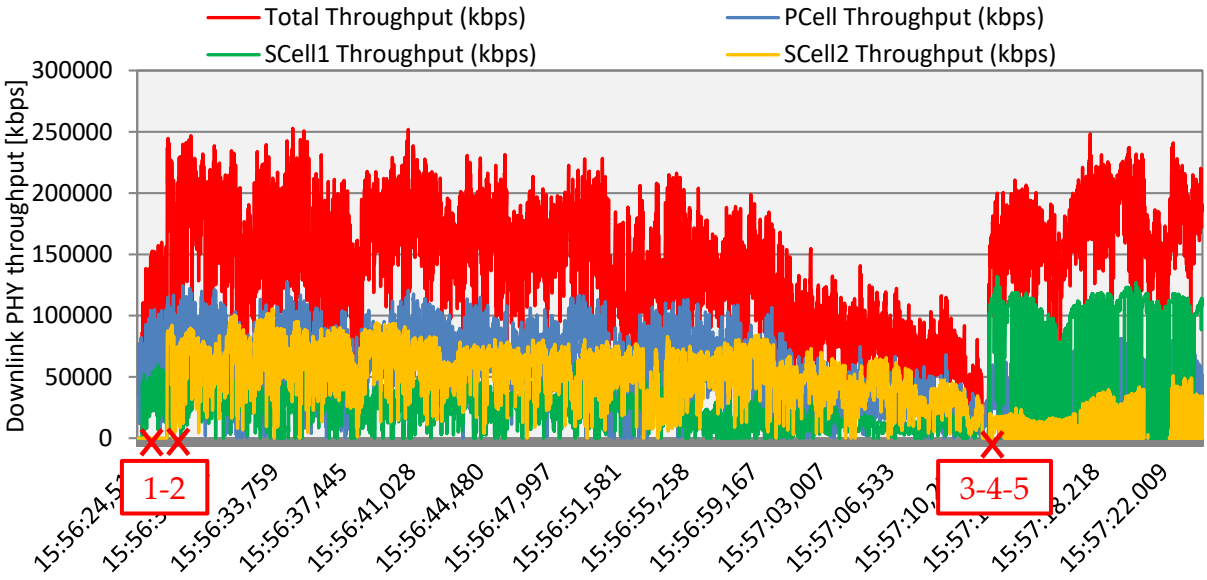

Figure 6.6 Throughput trend with mobility between sectors with 800+1800+L Band and 800+1800+2600

1 **15:56:25.315**
A4-based SCC1 Adding (Band 20)
(A4-threshold RSRP = -110 dBm)
RRC Connection Reconfiguration:
sCellToAddModList-r10 { **sCellIndex-r10 1**
cellIdentification-r10 {
physCellId-r10 44,
dl-CarrierFreq-r10 6300

2 **15:56:27.944**
A4-based SCC2 Adding (Band 7)
(A4-threshold RSRP = -110 dBm)
RRC Connection Reconfiguration
sCellToAddModList-r10 { **sCellIndex-r10 2**
cellIdentification-r10 {
physCellId-r10 16
dl-CarrierFreq-r10 3175

3 **15:57:11.630**
A3-based Intra-freq. Handover
From PCC 412 to PCI 411 (sector change)
SCC1 and SSC2 release
RRC Connection Reconfiguration:
sCellToReleaseList-r10 { 1, 2 }

4 **15:57:12.706**
A4-based SCC1 Adding (Band 32)
(A4-threshold RSRP = -110 dBm)
RRC Connection Reconfiguration
sCellToAddModList-r10 { sCellIndex-r10 1
cellIdentification-r10 {
physCellId-r10 4,
dl-CarrierFreq-r10 10020

5 **15:57:12.925**
A4-based SCC1 Adding (Band 20)
(A4-threshold RSRP = -110 dBm)
RRC Connection Reconfiguration
sCellToAddModList-r10 { sCellIndex-r10 1
cellIdentification-r10 {
physCellId-r10 43,
dl-CarrierFreq-r10 6300

From figure 6.6, it is evident that the throughput on the SCC1 (in green) increases a lot after the frequency change. In fact, at the beginning of the session the first secondary

carrier is the 800MHz while after the frequency change the SCC1 is the L band, as shown in in the fourth box. It depends on the available bandwidth at each carrier: there are 20MHz at 1500MHz with respect to the 10MHz at 800MHz. As we know from the theory, the throughput increases linearly with the bandwidth and these results are the proof of that. The same consideration is worth as well for SCC2: in the first part of the test the second secondary carrier is at 2600MHz – where 15MHz are available – while after the switch, the SCC2 is at 800MHz and the bandwidth decreases to 10MHz.

6.2 Category 16

We simulated two cases with Cat16 devices, one with 4CA with MIMO 2x2 and another with 2CA with MIMO 4x4.

Real measures have been realized only with the second configuration. In fact, the combination of the four LTE carriers available in Italy (bands 3-7-20-32) has been introduced in the 3GPP Standard in July 2017 within TS 36.101 Release 14.4.0. The change request was carried on during the last meeting of the Technical Specifications Group for Radio Access Networks (TSG RAN) held in Hangzhou, China in May 2017.

In particular, the new combinations requirements are in the report R4-1706085, then added to table 5.6A.1-2b "*E-UTRA CA Configuration sets defined for inter-band Carrier Aggregation (four bands)*" in TS 36.101. Here we provide an excerpt:

E-UTRA CA configuration / Bandwidth combination set									
E-UTRA CA Configuration	**E-UTRA Bands**	**1.4 MHz**	**3 MHz**	**5 MHz**	**10 MHz**	**15 MHz**	**20 MHz**	**Maximum aggregated bandwidth**	**Bandwidth combination set**
CA_3A-7A-20A-32A	3			Yes	Yes	Yes	Yes	80	0
	7				Yes	Yes	Yes		
	20			Yes	Yes	Yes	Yes		
	32			Yes	Yes	Yes	Yes		
CA_3A-7A-20A-42A	3			Yes	Yes	Yes	Yes	80	0
	7				Yes	Yes	Yes		
	20			Yes	Yes	Yes	Yes		
	42			Yes	Yes	Yes	Yes		

Table 6.12 Excerpt of table 5.6.1-2b from TS 36.101

Those reported in table 6.12 are not the only additions proposed during the meeting: in fact, 27 four-carrier combinations have been added in Release 14.4.0.

We made measures on a Cat16 commercial device with 2-CA configuration aggregating 35MHz at 1800 and 2600MHz, with MIMO 4x4 on both layers. We measured 15 seconds with a 700Mbps UDP DL traffic. In this case the theoretical throughput is around 700Mbps but the real maximum throughput was 600Mbps because of core network limitations that will be overcome by the end of 2017.

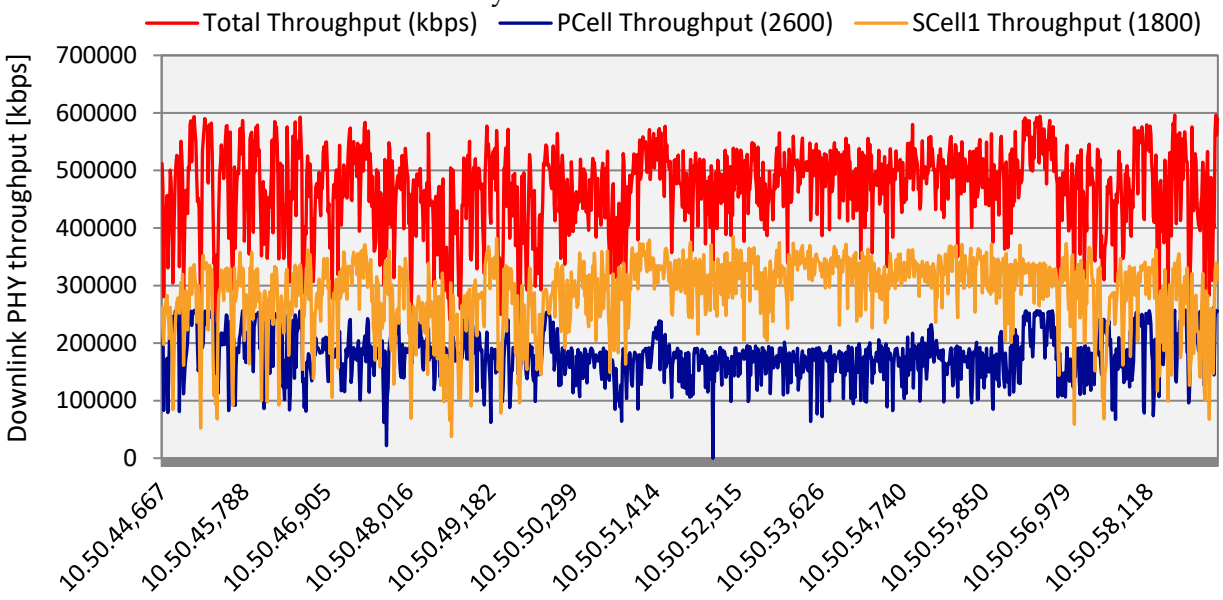

Figure 6.7 Throughput trend with B3+B7, 256QAM and MIMO 4x4

Parameter	Value
Theoretical TPUT	**691,5 Mbps***
Measured Peak TPUT	***596,17 Mbps***
Measured AVG TPUT	***469,83 Mbps***
B7: AVG RB	73,2
B3: AVG RB	95,5
B7: AVG MCS	25,7
B3: AVG MCS	26,2
B7: MIMO4x4 %	**Rank 3: 61,5%**
	Rank4: 36,1 %
B3: MIMO4x4 %	**Rank 3: 54,1%**
	Rank 4: 43,8 %
B7: 256QAM %	**99,82%**
B3: 256QAM %	**99,78%**
B7: SCHEDULING %	93,40%
B3: SCHEDULING %	91,10%

Table 6.13 PHY layer statistics

Component Carrier	AVG Tput [Mbps]
Aggregated PCC + SCC	469,83
PCC (2600 MHz)	180,56
SCC (1800 MHz)	289,27

Table 6.14 Average Throughput on each carrier

PCC [2600 MHz]	Avg values
RSRP RX1	-66,55 dBm
RSRP RX2	-76,33 dBm
RSRP RX3	-88,33 dBm
RSRP RX4	-76,15 dBm
SINR RX1	29,94 dB
SINR RX2	29,27 dB
SINR RX3	29,17 dB
SINR RX4	29,57 dB

SCC [1800 MHz]	Avg values
RSRP RX1	-74,35 dBm
RSRP RX2	-74,47 dBm
RSRP RX3	-76,50 dBm
RSRP RX4	-87,82 dBm
SINR RX1	28,54 dB
SINR RX2	29,79 dB
SINR RX3	29,35 dB
SINR RX4	28,76 dB

Table 6.15 Radio conditions on the two carriers

As you can see from table 6.15, the SINR levels are optimal during the transmission. Despite these values, MIMO 4x4 is activated only in 43,8% of transmissions in B3 and in 36,1% of transmissions in B7. Higher percentages are obtained if we consider the MIMO rank 3 as well. These results correspond to those obtained within the simulations which highlighted the low efficiency of the 4-layers technique. On the contrary, 256QAM turned out to perform well during the whole observation.

We also measured the peak throughput with a prototype device in the same configuration and the very same peak throughput (596,17Mbps) has been reached.

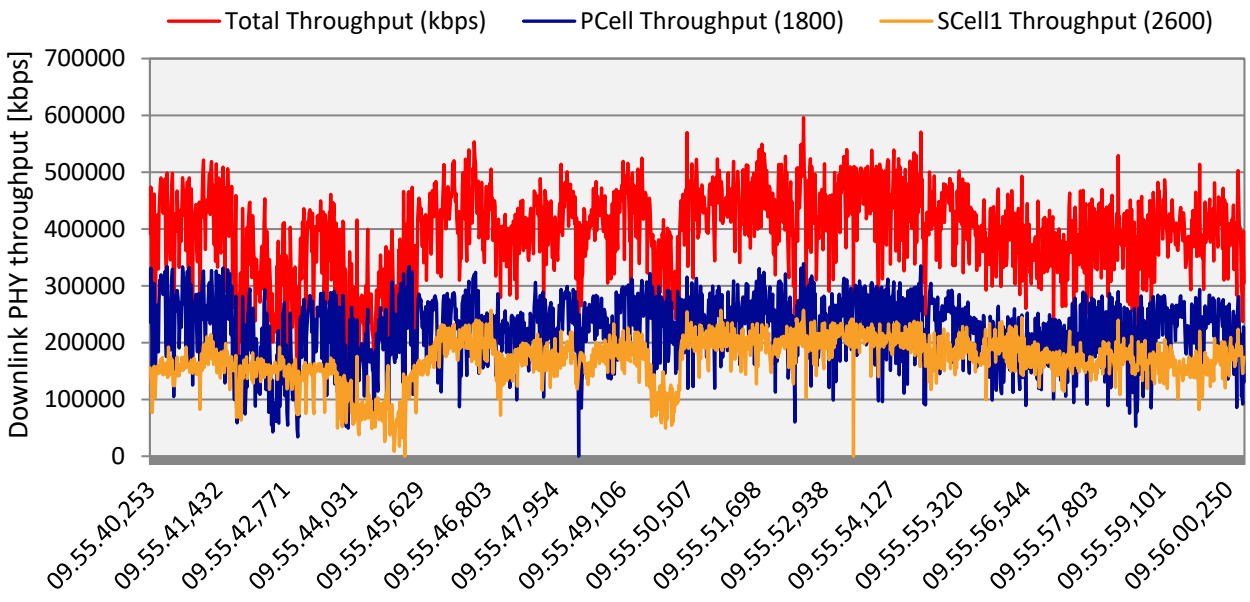

Figure 6.8 Throughput trend with B3+B7, 256QAM and MIMO 4x4 (prototype)

6.3 MIMO 4x4 Downlink performances

MIMO 4x4 is the capability that, in theory, should give the highest contribution to the increase of throughput but both simulations and real measures show the weakness of MIMO 4x4 with respect to noise, even in next to optimal channel condition. Though, neither the simulations nor the real measures were focused only on MIMO 4x4, then we realized a study on its performance in downlink.

First, we analyzed a system with no correlation between each pair of transmit and receive antennas and we compared the throughput with the two highest modulation schemes, 64QAM and 256QAM.

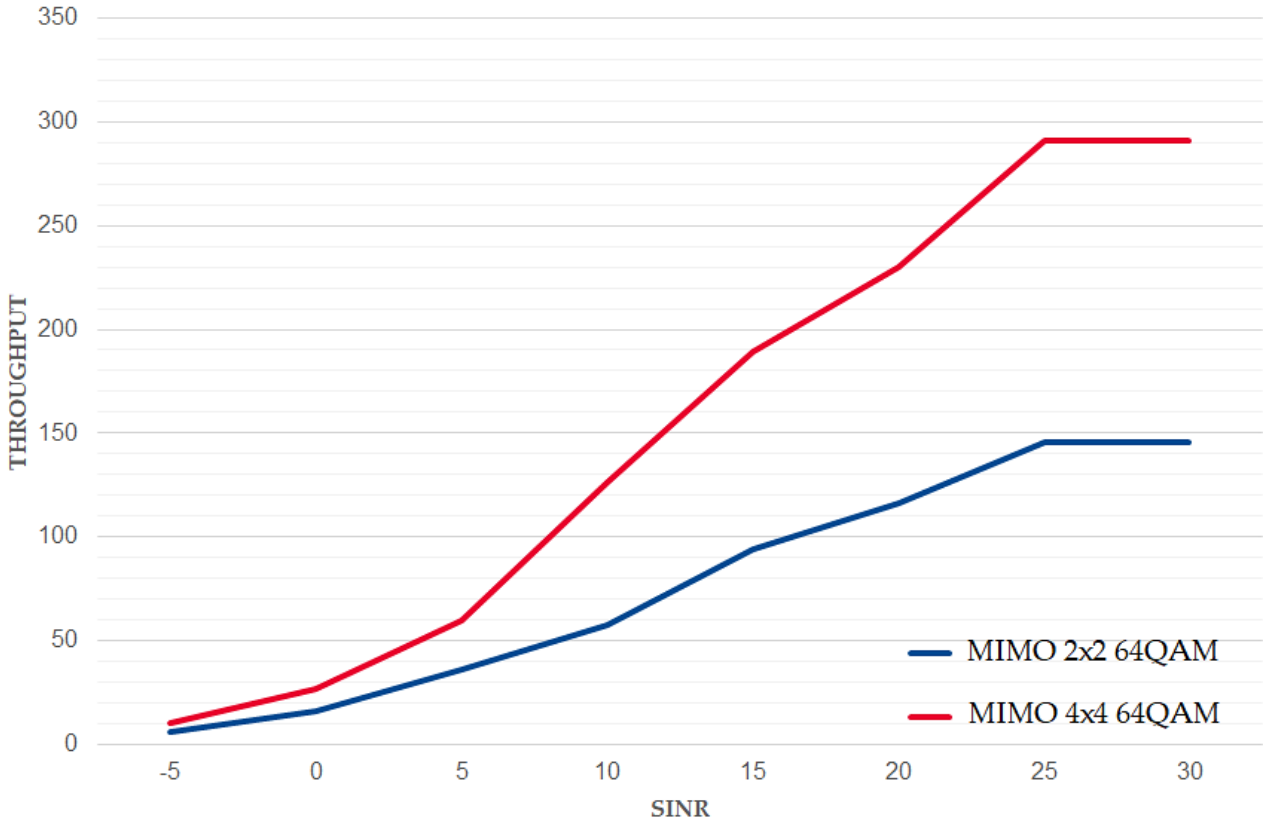

Figure 6.9 MIMO 2x2 vs MIMO 4x4

Here we can see that the 4-layers technology effectively introduces the doubling of the downlink throughput.

A further increment of the data rate is given by the adoption of 256QAM. With this modulation scheme, in fact, the throughput should increase by one third as we can see in figure 6.10.

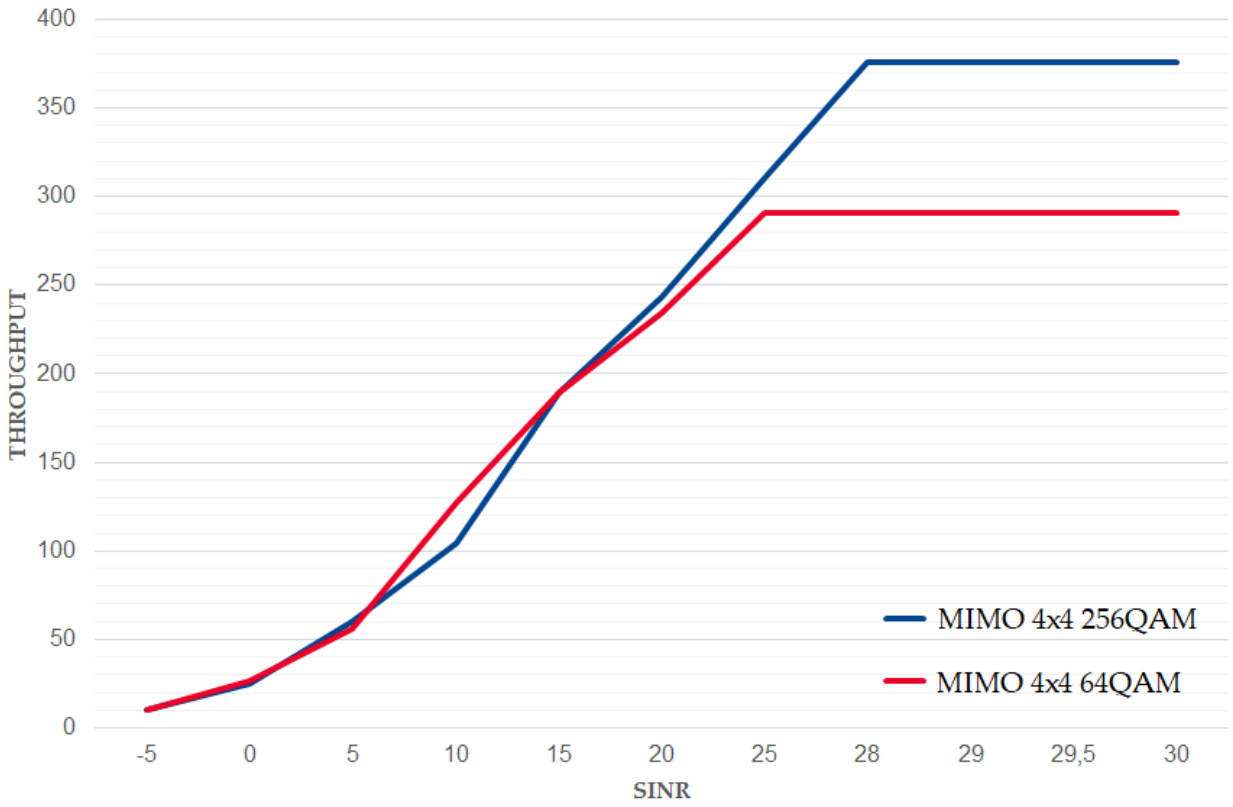

Figure 6.10 64QAM vs 256QAM with MIMO 4x4

These are actually the theoretical behaviors of the multiple-layer transmissions. In fact, if the propagation channels between the antennas can be described as statistically independent and identically distributed, then multiple independent channels can be created by precoding. In practice, this never happens and channels are often correlated and the throughput gain shown in figures above is not achievable.

Then, we made measures in condition of low and medium/high correlation between the paths to reproduce a real radio environment. In fact, in dense urban scenarios like the one we are describing, there are usually many interferences and multipaths. Then, the usage of MIMO 4x4 might increase reflection and refraction phenomena so that there is not the throughput boost expected from the theory and presented in figure 6.9 and 6.10.

Figure 6.11 shows the behavior of MIMO techniques with low correlation between the paths. From here, it becomes evident that MIMO 4x4 does not give the expected contribution a low/medium SINR levels.

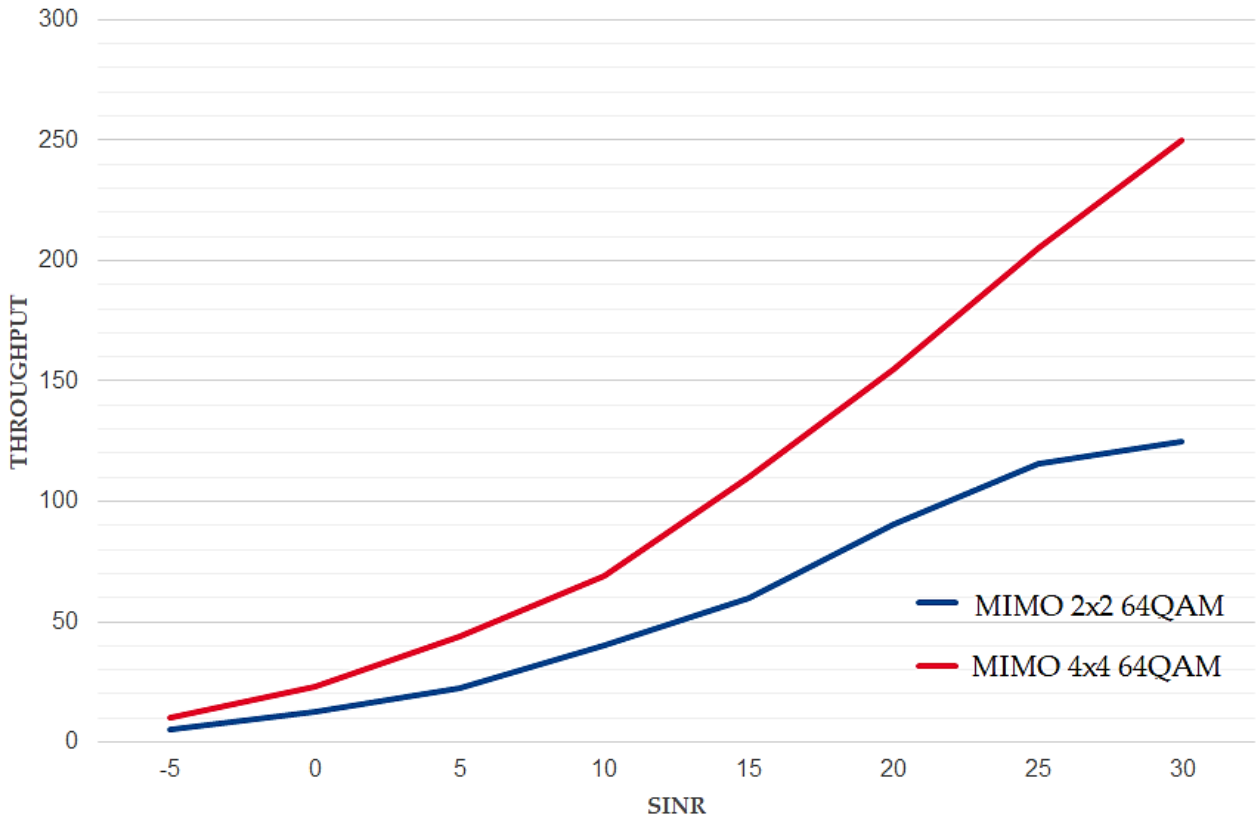

Figure 6.11 MIMO 2x2 vs MIMO 4x4 with low correlation

Finally, we provide the comparison among low, medium and high correlation in case of MIMO 4x4 and 256QAM.

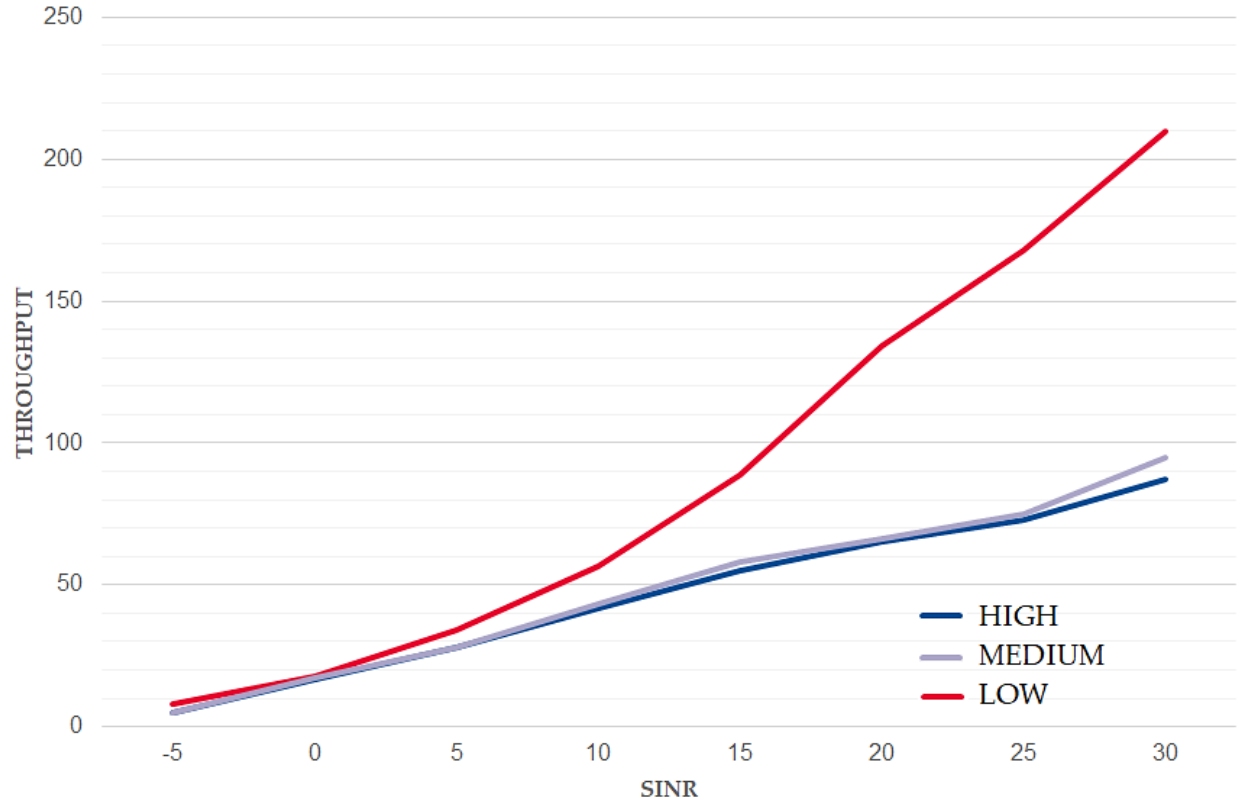

Figure 6.12 Comparison among three correlation levels with MIMO 4x4 and 256QAM

The theoretical limit with MIMO 4x4 and 256QAM is around 400Mbps on 20MHz. In figure 6.12, we can see that this value cannot be reached at all, rather it is very far from being achieved, in particular with medium/high correlation.

Even these measures showed the weakness of MIMO 4x4 in real scenarios with multipaths and low signal levels, as it was already highlighted by the simulations and general measures. However, in case of optimal channel quality, this technology given a huge contribution to throughput, even in case of low correlation.

7 Conclusions and future work

The ever-changing mobile communications market and the request for higher speed rates led to the birth and development of LTE-Advanced which will be the dominant technology in the upcoming years.

In this thesis, we explored the architecture of LTE and LTE-A technologies and studied the last introduced features. We also dealt with Standards and Specifications by 3GPP to fully understand all the processes behind mobile transmissions. The key work was the adaptation of a network simulator with the introduction of Carrier Aggregation, MIMO 4x4 and 256QAM and the simulation of a dense urban scenario to study the overall system in terms of data rate and capacity.

We studied several deployments in order to evaluate the effectiveness of the LTE-A capabilities and compared the results with real measures to figure out the deployment strategies that mobile Operators should implement. In fact, there are two main approaches that they could follow, either the spectrum broadening or the spectral efficiency increase. Each of them has its advantages and disadvantages and we tried to analyze all of them. In particular, we focused our attention on new devices that have just entered the market or will be commercial by the end of 2017.

256QAM is already widely diffused and many devices support it. Our study showed the robustness to noise of this feature and the contribution it gives in terms of data rate.

New devices can support up to 4-Carrier Aggregation over the licensed spectrum and can aggregate also 100MHz. This leads to very high throughputs with a good robustness to noise. But, since mobile Operators have a limited spectrum they are looking for ways not to waste it. Innovative technologies for the forthcoming future will allow to aggregate also unlicensed bands and studies on the coexistence with Wi-Fi are being carried on.

Then, the further enhancement of the spectral efficiency with multiple layers transmissions seems to be the best strategy for mobile Operators: in fact, this would lead to even higher throughputs without using the whole disposable spectrum. On the other hand, this feature is highly affected by noise effects. In fact, our analysis showed the need

for very high SINR levels that are very difficult to achieve in an urban scenario. A solution might be the deployment of small cells that, if well dimensioned, would guarantee a better coverage and better signal levels but it would also entail elevated deploying costs for Operators.

Hence, we suggest deploying MIMO 4x4 – and 8x8 when it will be available – only in those sites where high SINRs are achievable like indoor scenarios or for those applications that require very high data rates and low latency. Massive MIMO will be the dominant technology for 5G communications that will provide for very dense cells and very high SINR levels.

LTE-Advanced target data rate is 3Gbps but as we said in the Introduction it is not achievable because of the limitation on the number of Antenna Port which is 8 nowadays. It is interesting to underline that the peak spectral efficiency in the 800Mbps configuration is 20bps/Hz which is comparable to 30bps/Hz required by the Standard for 5G telecommunications (3GPP TR 38.913), although the restriction of the maximum Antenna Port that will be overcome with the next generation technologies. This to remark that the LTE-A is already near to the best performance that next generation telecommunication networks will fulfill.

Future work will consist in the total adaptation of the *ns-3* simulator to the requirements of LTE-A, in the finalization of Carrier Aggregation and in the implementation of MIMO 4x4 (and above) within it.

Moreover, the limit on UDP traffic shall be overcome in order to completely fulfil the data rate requirements of new devices.

Furthermore, measures on real Cat16 devices with the 4-Carrier Aggregation shall be made as soon as they will be commercialized to compare real data to the results of the simulation.

References

3GPP, “Requirements for Evolved UTRA (E-UTRA) and Evolved UTRAN (E-UTRAN)”, 3rd Generation Partnership Project (3GPP), TR 25.913, v. 7.0.0

3GPP, “Evolved Universal Terrestrial Radio Access (E-UTRA); User Equipment (UE) radio transmission and reception”, 3rd Generation Partnership Project (3GPP), TS 36.101, v. 14.4.0

3GPP, “Evolved Universal Terrestrial Radio Access (E-UTRA); Base Station (BS) radio transmission and reception”, 3rd Generation Partnership Project (3GPP), TS 36.104, v.13.0.0

3GPP, “Evolved Universal Terrestrial Radio Access (E-UTRA); Physical layer procedures”, 3rd Generation Partnership Project (3GPP), TS 36.213, v. 13.0.0

3GPP, “Evolved Universal Terrestrial Radio Access (E-UTRA); User Equipment (UE) radio access capabilities”, 3rd Generation Partnership Project (3GPP), TS 36.306, v.14.1.0

3GPP, “Evolved Universal Terrestrial Radio Access (E-UTRA); Radio Resource Control (RRC); Protocol specification”, 3rd Generation Partnership Project (3GPP), TS 36.331, v. 13.0.0

3GPP, “Requirements for further advancements for Evolved Universal Terrestrial Radio Access (E-UTRA) (LTE-Advanced)”, 3rd Generation Partnership Project (3GPP), TR 36.913, v. 8.0.0

3GPP, “Study on scenarios and requirements for next generation access technologies”, 3rd Generation Partnership Project (3GPP), TR 38.913, v. 14.0.0

Baker M., “LTE-Advanced Physical Layer”, Alcatel-Lucent, 3GPP, December 2009

Castellani A., Angilè F., “Introduzione all’LTE (Long Term Evolution) e alle funzionalità in tecnologia Huawei”, Technical Note, TIM, July 2009

Catreaux S., Erceg V., Greenstein L.J., “Some results and insights on the performance gains of MIMO systems”, *IEEE Journal on Selected Areas in Communications*, vol. 21, n. 5, pp. 839-847, 2003

Ericsson, “Ericsson Mobility Report” Tech. Rep., November 2016

Ferrero U., Gamberini M., “Dal LTE a LTE-Advanced: l’Evoluzione Tecnologica”, Technical Report, February 2013

ITU-R P.526-13, “Propagation by Diffraction”, November 2013

ITU-R P.1411-8, "Propagation data and prediction methods for the planning of short-range outdoor radiocommunication systems and radio local area networks in the frequency range 300 MHz to 100 GHz", July 2015

“ns-3” [Online]. Available: http://www.nsnam.org

Parikh J., Basu A., “Scheduling Schemes for Carrier Aggregation in LTE-Advanced Systems”, *International Journal of Research in Engineering and Technology*, vol. 3, n. 8, pp. 219-223

Qualcomm, “Delivering on the LTE Advanced promise”, March 2016